GEOLOGICAL SURVEY OF CANADA
OPEN FILE 7506

Comparison of commonly used space radiation environment models (highly elliptical high inclination orbit application)

L.Nikitina, L.Trichtchenko

2013

Natural Resources Canada | Ressources naturelles Canada

Canada

GEOLOGICAL SURVEY OF CANADA
OPEN FILE 7506

Comparison of commonly used space radiation environment models (highly elliptical high inclination orbit application)

L.Nikitina, L.Trichtchenko

2013

doi:10.4095/293148

This publication is available for free download through GEOSCAN (http://geoscan.ess.nrcan.gc.ca/).

Recommended citation
Nikitina, L. and Trichtchenko, L., 2013. Comparison of commonly used space radiation environment models (highly elliptical high inclination orbit application); Geological Survey of Canada, Open File 7506, 80 p. doi:10.4095/293148

Publications in this series have not been edited; they are released as submitted by the author

1 Summary

This research was undertaken to provide the radiation hazard assessment for satellites in highly elliptical orbits (HEO) based on available models of the radiation environment. This research gives qualitative and quantitative descriptions of the radiation environment on three HEO orbits. These orbits were selected as candidates for the Polar Communications and Weather mission (PCW) proposal to provide continuous communication and meteorological observations in northern areas of Canada. These orbits are 12-hr Molniya orbit, 16-hr TAP orbit, and 24-hr Tundra orbit. The analyses of the trapped radiation are made by simulations using two basic models for the radiation environment, AE8/AP8 and AE9/AP9. The model AE8/AP8 was implemented in Spenvis and is has been used during the last decades, while the AE9/AP9 model has just been released. The comparison of different models for solar proton fluences and galactic cosmic rays have also been done with use of different models available in SPENVIS tools. Comparison of these different models for the trapped radiation, solar proton fluences, and galactic cosmic rays provides the better understanding for the radiation environment on HEO orbits.

TABLE OF CONTENTS

2 Introduction

This research was undertaken to provide the radiation hazard assessment for satellites in highly elliptical orbits based on available models of the radiation environment. The space radiation environment creates the operating conditions for spacecraft and their on-board electronic systems. The radiation environment is highly dependent on the type of mission, its date, duration and orbit coordinates. Here, three highly elliptical orbits (HEO) will be analyzed to estimate the influence of the radiation environment on a spacecraft in these orbits. This analysis has been done previously in [1] by using SPENVIS tools [2] which included AE8/AP8 models for the trapped radiation. This analysis was made for HEO orbits which provide a very good perspective for monitoring and communication service for northern regions of Canada. The orbits under consideration are 12-hours Molniya orbit, 16-hours Three Apogee orbit ([3], [4]), and 24 hours Tundra orbit [5]. Assessment and comparison of the radiation environment hazard for these three possible highly elliptical orbits and its impact on spacecrafts on these orbits is very important for planning future missions.

This new study was motivated by the appearance of new models of the trapped energetic particles in the magnetosphere, AE9/AP9 [6] .This model was produced by the Air Force Research Laboratory and the National Reconnaissance Office in partnership with MIT Lincoln Laboratory, Aerospace Corporation, Los Alamos National Laboratory, Boston College Institute for Scientific Research, and Atmospheric and Environmental Research, Incorporated ([6], [7]). The beta-version of these models was kindly provided to us by the authors of the models. We were also motivated by our previous study of HEO missions data [8] where the comparison of these data with models AE8/AP8 demonstrated the discrepancy between the model and the observed data.

The models AE9/AP9 are considered as improved models. They are based on a new and larger set of data than the previous AE8/AP8 models. In contrast to this previous model, the AE9/AP9 dataset includes the data provided by several years of missions in highly elliptical orbits, HEO1 and HEO3. So the AE9/AP9 models are expected to provide more accurate description of the radiation environment for these orbits.

In this open file we included analyses of the radiation environment on the HEO orbits which were made based on both the previous and updated models of the trapped radiation (models AE8/AP8 and AE9/AP9). We also included in this study the comparison of different models for solar energetic particle and galactic cosmic rays assessment.

3 Parameters evaluated

The specification of the expected radiation environment on these orbits were made following the assessment of a space hazard items listed in the European Space Agency

Program of Radiation hardness assurance for space systems [9] and in the NASA's Program of Radiation hardness assurance for space systems [10].

The analyses include

External environment

- assessment of fluxes of the trapped radiation (models AE8/AP8 and AE9/AP9),
- assessment of fluences of the trapped radiation (models AE8/AP8 and AE9/AP9),
- spectra of unshielded annual proton and electron fluxes (models AE8/AP8 and AE9/AP9),
- mission dose vs shielding depth (models AE8/AP8 and AE9/AP9),
- influence of long-term solar proton and heavy ions fluences
- influence of galactic cosmic rays,
- influence of short-term solar protons and heavy ions fluxes originated from solar particle events

Environment within the Spacecraft

- damage-equivalent fluences for solar cell damage
- single event upset rate
- total ionizing dose (models AE8/AP8 and AE9/AP9)

4 Orbital Parameters

This section describes orbital parameters of three HEO orbits which could be chosen for the communication and monitoring service for high northern latitudes of Canada. Here we consider

- **12-hr Molniya orbit** which were used for a while for northern communication service in Russia. The Molniya orbit is a highly eccentric orbit with a stable high-latitude apogee, with orbit's inclination of approximately 63.4°. The satellite spends about two thirds of the time near the apogee where it will provide an extension of coverage all the way to the Pole.
- **16-hr TAP orbit** was worked out recently for continuous meteorological imaging of polar regions. This orbit is characterized by three apogees separated by 120^0 . This orbit was chosen as a result of an optimization procedure based on the key requirements such as spatial resolution which depends on the apogee height, minimization of the radiation doze caused by trapped radiation, imaging time over the polar regions, and the stability of the orbit ([3], [4]).
- **24-hr Tundra orbit** is a type of highly elliptical geosynchronous orbit with a high inclination (usually near 63.4°) and an orbital period of one solar day. It also is used for high latitude territories like the Molniya orbit. A satellite placed in this orbit spends most of its time over a chosen area.

Parameters of 12-hr Molniya, 16-hr TAP and 24-hr Tundra orbits are presented in Table 1.

Table 1. Sample of 12-hrs Molniya, 16-hrs TAP and 24-hrs Tundra orbits

Orbit type	**12-hr Molniya**	**16-hr TAP**	**24-hr Tundra**
Apogee:	39380.00 km	43500.14 km	48441.43 km
Perigee:	972.00 km	8107.72 km	23143.38 km
Inclination:	63.40°	63.44°	90.00°
R. A. Ascending Node:	45.00°	212.79°	224.20
Argument of Perigee:	270.00°	270.00°	270.00°
True Anomaly:	0.00°	0.00°	0.00°
Period:	11.96 hr	15.95 hr	23.93 hr
Number of orbits per segment:	4.00	3.00	2.00
Segment Duration:	2.00 days	1.99 days	1.99 days
Semi latus rectum:	12654.90 km	22442.01 km	38368.70 km
Semi major axis:	26547.00 km	32174.93 km	42163.40 km
Eccentricity:	0.72	0.55	0.30
Mean motion:	12.61 rad/day	9.45 rad/day	6.30 rad/day

The altitude of spacecrafts over the Earth's surface plotted by using of SPENVIS tool for different HEO orbits are presented on Figure 1-Figure 3. The time variation for orbital parameters, such as altitude over the Earth's surface, longitude, altitude, and the local time are plotted on Figure 4 - Figure 6.

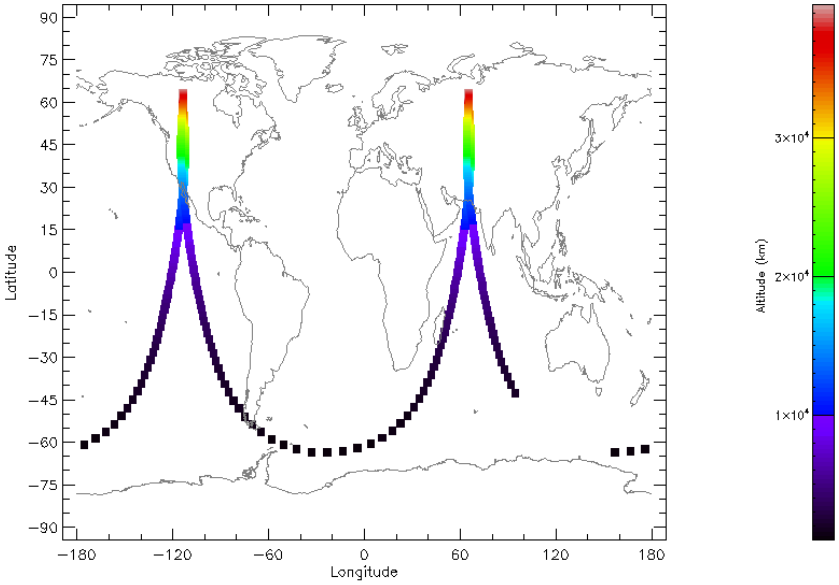

Figure 1. World map of 12-hr Molniya orbit used in space environment analysis

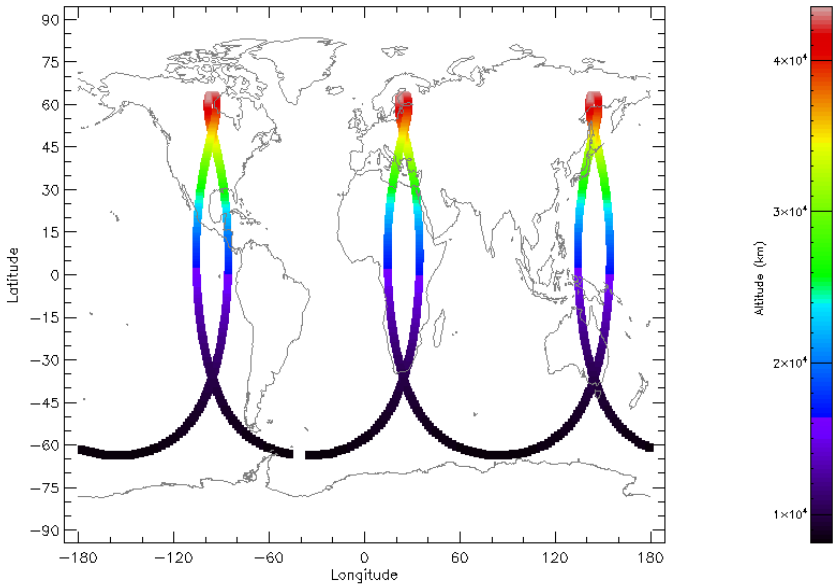

Figure 2. World map of 16-hr TAP orbit used in space environment analysis

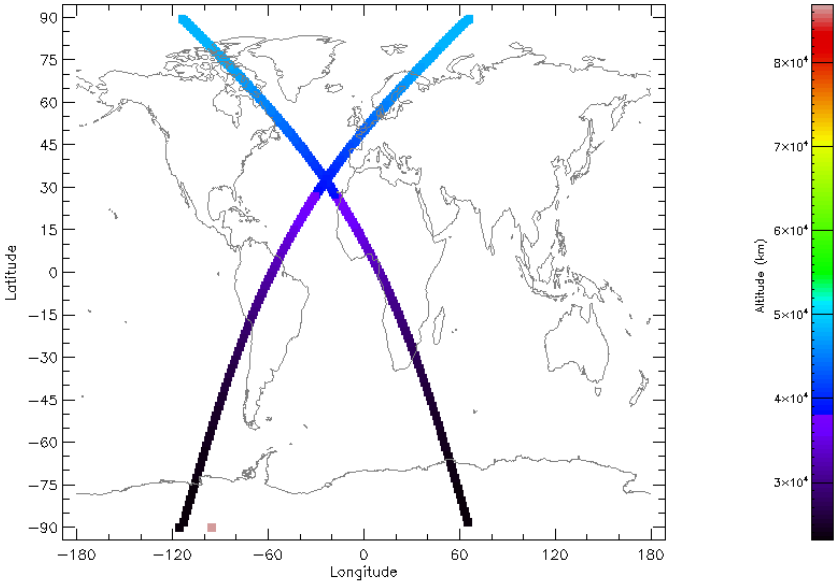

Figure 3. World map of 24-hr Tundra orbit used in space environment analysis

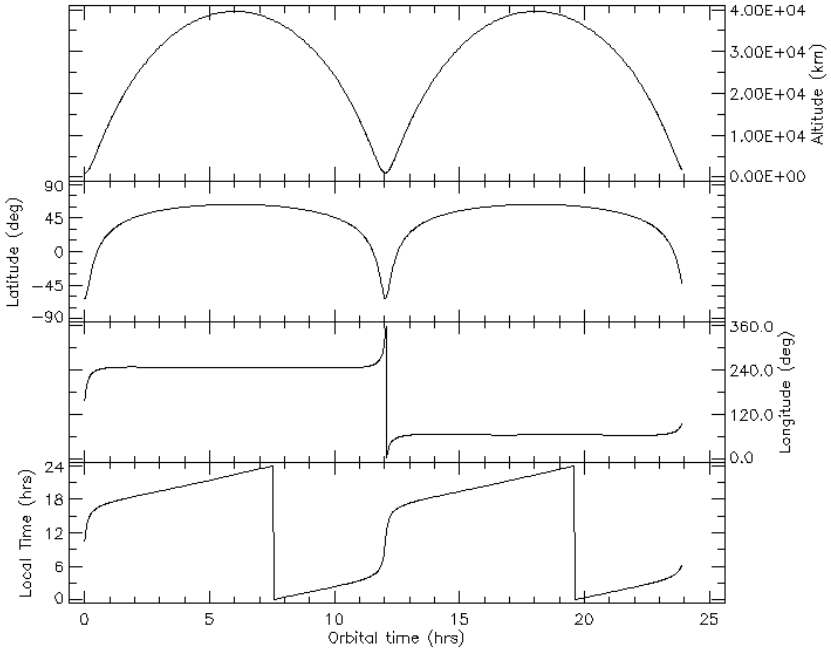

Figure 4. Time variations of Molniya orbital parameters

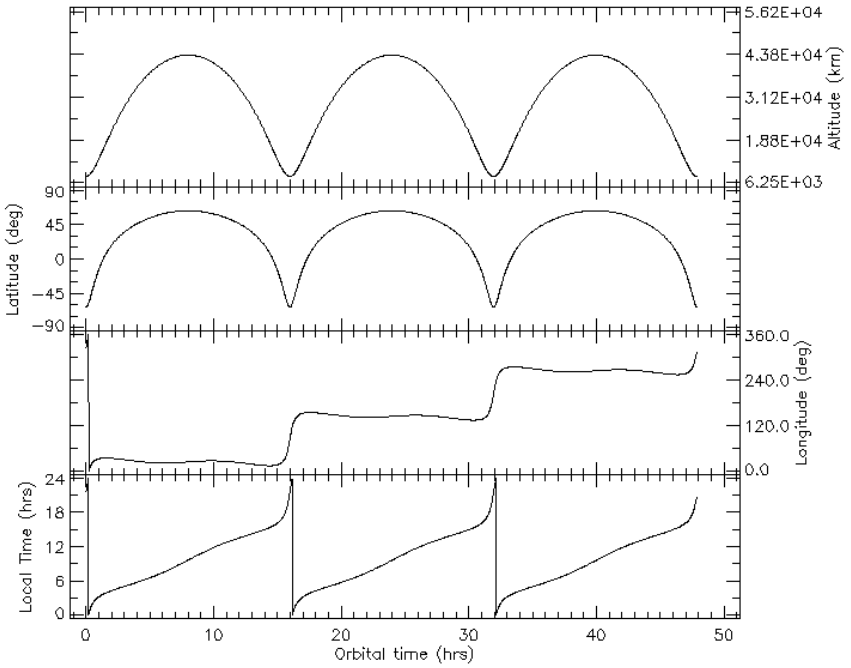

Figure 5. Time variations of TAP orbital parameters

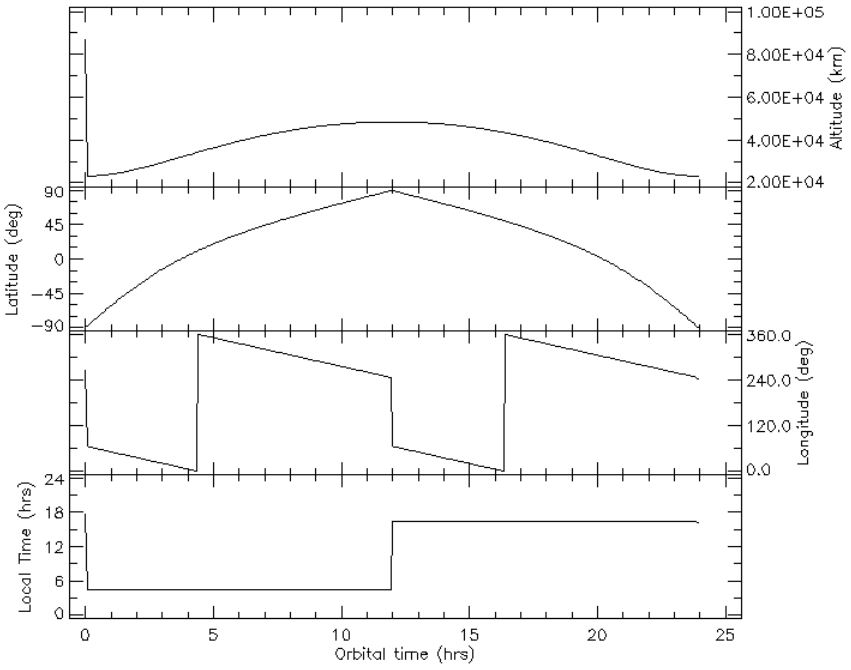

Figure 6. Time variations of Tundra orbital parameters

5 Trapped Radiation

The trapped radiation on the orbits of interest was calculated using two models:

- AE8/AP8 models,
- AE9/AP9 models.

AE8/AP8 models have been widely used for the last several decades. These model are implementations of the first empirical models of radiation belts which were developed in 1960s-1970s. The AP8 model for protons gives proton fluxes from 0.1 to 400 MeV and the AE8 model for electrons covers electrons from 0.04 to7 MeV. This model has two versions, for years with solar maximum and years with solar minimum.

The AE8/AP8 models have some known limitations on their validity (Ginet et al., 2013 [6]). The authors say that there are some discrepancies between the AE8/AP8 models and the radiation data. AE8/AP8 models give (a) over-prediction of dose for Geosynchronous orbits (GEO) and highly elliptical orbits (HEO); (b) under-prediction of dose for orbits in the "slot region", especially dose due to long-lived protons with high energy (> 40 MeV) and electrons (> 1 MeV) injected into the slot region during geomagnetic storms.

Thus, for the HEO orbits of interest in this study the old models AP8/AE8 under-predict the dose in the ‘slot-region’, and they also do not give the reliable prediction of the dose arising from long-lived higher energy protons (>40 MeV) and electrons (>1 MeV) injected during geomagnetic storms.

To overcome issues of AE8/AP8 models and to provide up-to-date estimates of the radiation environment, a new set of models denoted AE9/AP9/SPM have been developed ([6] and [7]). These are assumed to be more accurate for estimation of the radiation environment on HEO orbits. For the analyses made in this paper we used a beta-version of this model which was kindly provided to us by authors of the models.

In the next section the trapped radiation has been analysed for HEO orbits with using of both AE8/AP8 and AE9/AP9 models.

5.1 Variations of the trapped radiation along the orbit (time dependence). Comparison of Molniya, TAP, and Tundra orbits Models A8 and A9.

Trapped particle fluxes and fluences for Molniya, TAP, and Tundra orbits were calculated for solar maximum year 2000 using both AE9/AP9 models and AE8/AP8 models.

This is the year of solar maximum. The model AE8/AP8 has two separate codes, one for years during maximum of solar activity (AE8/AP8 max) and another one for years during minimum of solar activity (AE8/AP8 min). So, for our analyses we use (AE8/AP8 max). For model AE9/AP9 it is enough to specify the year of interest and these models calculate the influence of solar activity on the radiation environment automatically.

Samples of the orbital time variations of the trapped radiation corresponding to 1-2 February 2000 on the considered HEO orbits were calculated for different proton and electron energy levels (above 1MeV, 10 MeV and 50 MeV for protons and above 0.5 MeV, 1 MeV, 4 MeV, and 5 MeV for electrons.) The plots for the daily distribution of the trapped radiation calculated by AE9/AP9 and AE8/AP8 models are shown in Appendix 1.

These figures demonstrate that the AE9 model provides lower values of electron fluxes than AE8 model for energies 0.5 MeV, 1 MeV, and 4 MeV. For energy above 5 MeV, electron fluxes provided by AE9 are higher that the fluxes provided by AE8 model (Figure 77-Figure 82). Developers of AE9/AP9 model pointed out that the old model gave overestimated values for energetic particle fluxes on HEO orbits and their new models are based on the data set provided by HEO1-HEO3 missions and should predict the trapped radiation more accurately than the previous models AE8/AP8. New model also includes high energetic electrons (>1 MeV) and protons (>40 MeV) which were underestimated by AE8/AP8 models. For example, for Tundra orbit the model AP8 predicts no proton fluxes for energies > 4 MeV while the model AP9 gives a small but non-zero amount of the proton fluxes for energy level 4 MeV, approximately 4 orders less than for E>1MeV (see Figure 82).

As can be inferred from the modeling results, there are no protons with energies >10 MeV on Tundra orbit and no protons with energies > 50 MeV on both TAP and Tundra orbits.

Time-distribution of the trapped radiation fluxes provided by both models are presented in Appendix 1 for electron fluxes and fluences and in Appendix 2 for proton fluxes and fluences..

5.2 Comparison of the annual radiation dose on three orbits, Molniya, TAP, and Tundra. Shielded dose.

Here we compared the annual radiation dose depending on the shielding depth for three HEO orbits. Calculations were made using models AE8/AP8 and AE9/AP9 for 1-year missions: for year 2000 as a year of maximum solar activity.

Both models AE8/AP8 and AE9/AP9 demonstrate similar results, that the radiation level on TAP orbit is less than the radiation on Molniya orbit for large shielding levels, > 200 Mils according to AE9/AP9 model, and >300 Mils according to AE8/AP8 model (see Figure 7 and Figure 8). It also can be concluded that the trapped radiation dose on Tundra orbit is less than for TAP and Molniya orbits because the Tundra orbit is located further

from the inner magnetosphere than the other two orbits. Some other plots demonstrating the comparison of annual proton and electron radiation doses for HEO orbits are shown in Appendix 3.

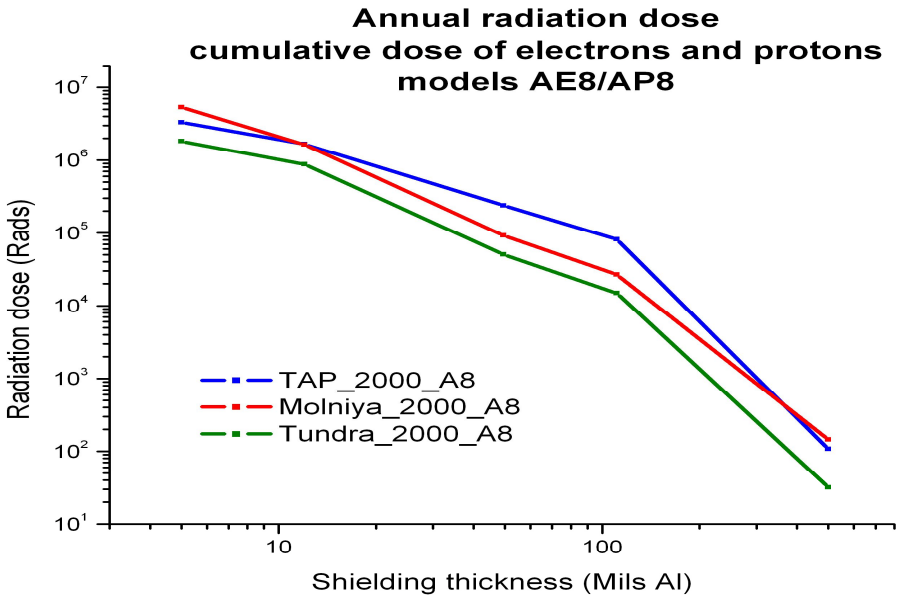

Figure 7. Annual radiation dose, HEO orbits. 2000. Model AE8/AP8 max

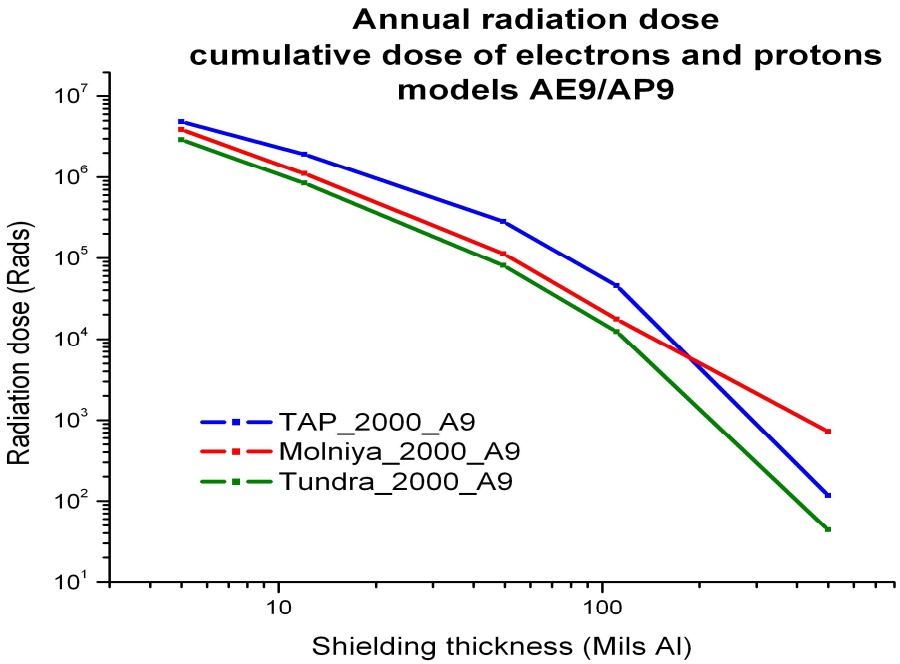

Figure 8. Annual radiation dose, HEO orbits. 2000. Model AE9/AP9

5.3 Unshielded annual proton and electron energy spectra for fluxes of the trapped radiation

In this section both AE8/AP8 models and AE9/AP9 models were used to estimate annual electron and proton fluxes for HEO orbits. Figure 9-Figure 12 demonstrate the spectra of the trapped radiation fluxes. Both models show that the Tundra orbit is not affected by fluxes of protons with energy larger than E> 1 MeV (for AP8 model) and E>8 MeV (for AP9 model).

The trapped proton fluxes for Molniya orbit exceed the proton fluxes for TAP orbit for E>1 MeV for the model AP8 (Figure 10) and E>0.8 MeV for model AP9 (Figure 9). So the influence of high-energetic protons on TAP orbit is less than the influence on Molniya orbit.

Electron fluxes (Figure 11-Figure 12) for all three orbits have similar values for both models, AE8 and AE9. But, according to AE8 model, the electron fluxes for TAP orbit exceeds electron fluxes for Molniya and Tundra orbits for all energy values while AE9 model predicts that fluxes for TAP orbit is less than fluxes on Molniya orbit for energies E>5.5 MeV.

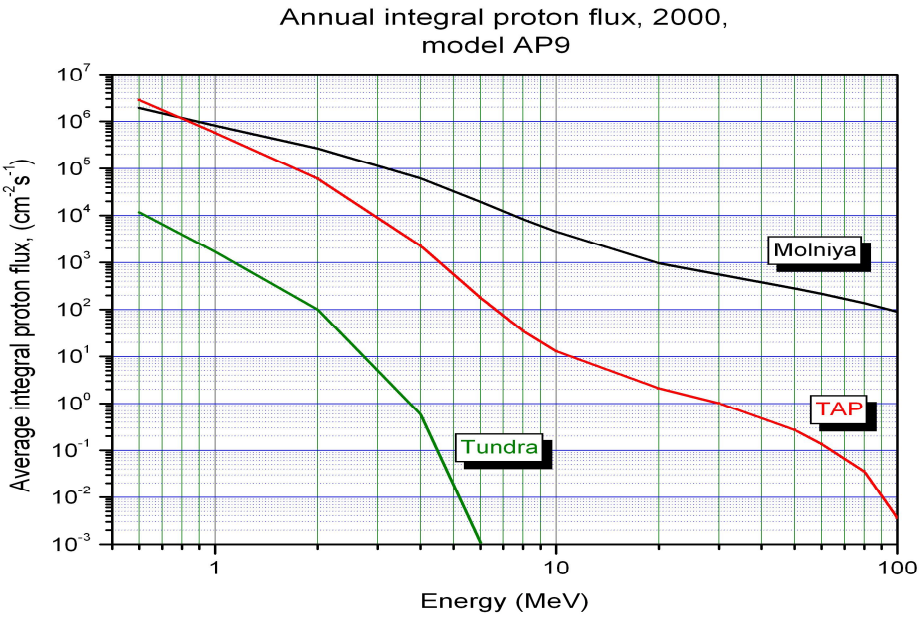

Figure 9. Annual integral proton fluxes on HEO orbits. Model AP9. 2000.

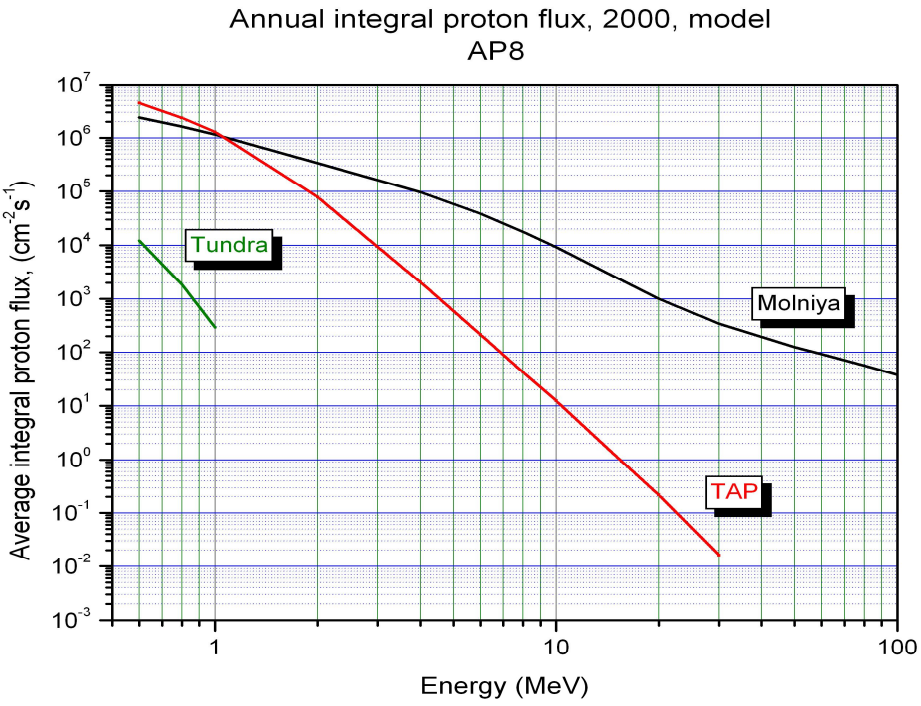

Figure 10. Annual integral proton fluxes on HEO orbits. Model AP8. 2000. Model AP8 does not give any proton fluxes for E>1 MeV for Tundra orbit

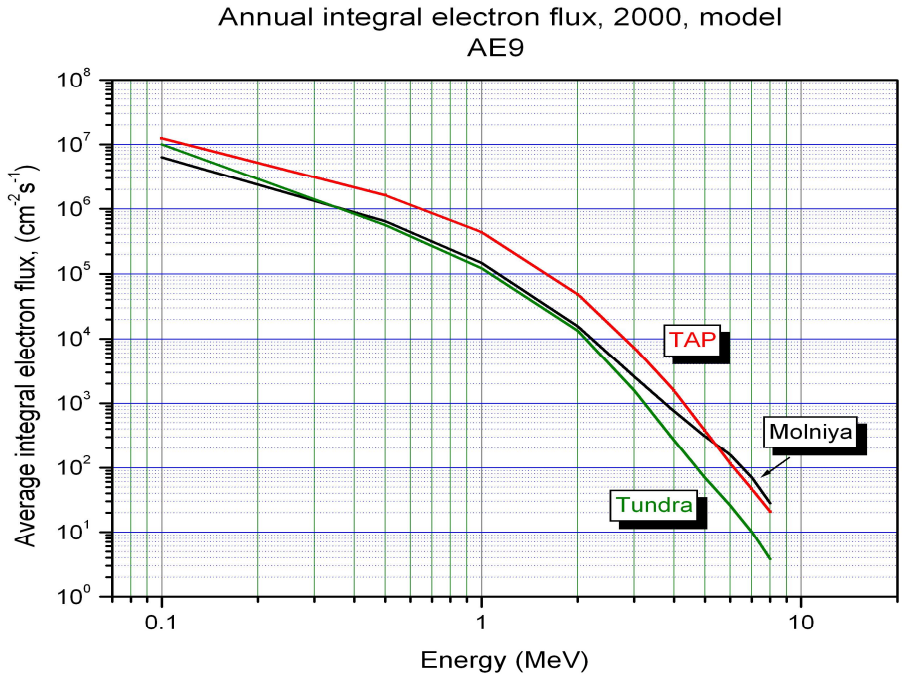

Figure 11. Annual integral electron fluxes on HEO orbits. Model AE9. 2000.

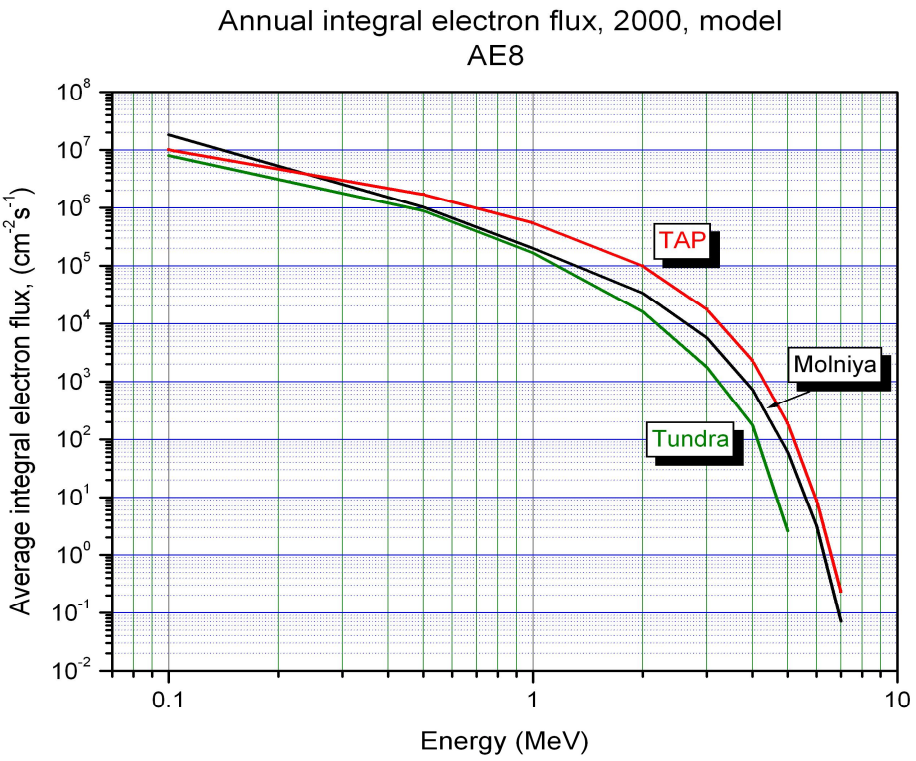

Figure 12. Annual integral electron fluxes on HEO orbits. Model AE8. 2000. Model AE8 does not give electron fluxes for Tundra orbit for energies E>5MeV.

The world map of proton and electron fluxes for E>1 MeV are plotted on Figure 13-Figure 18 with use of SPENVIS tool which is based on AE8/AP8max models.

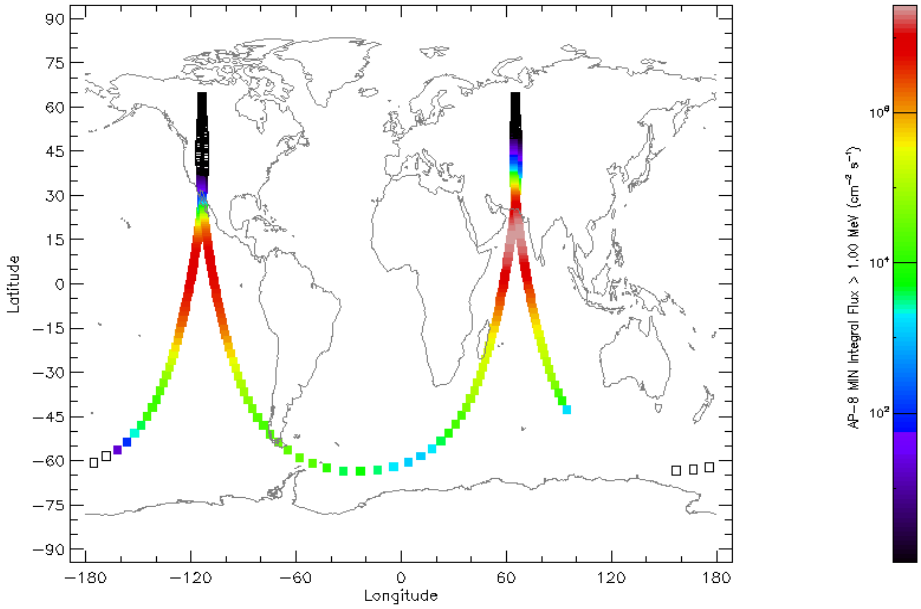

Figure 13. World map of integral flux of protons >1 MeV along Molniya orbit. Model AP8max.

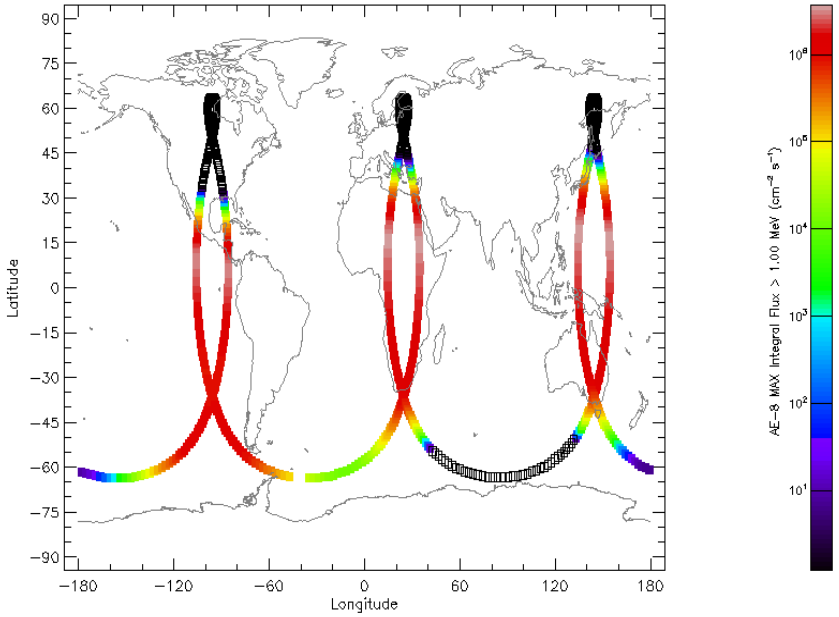

Figure 14. World map of integral flux of protons >1 MeV along TAP orbit. Model AP8MAX.

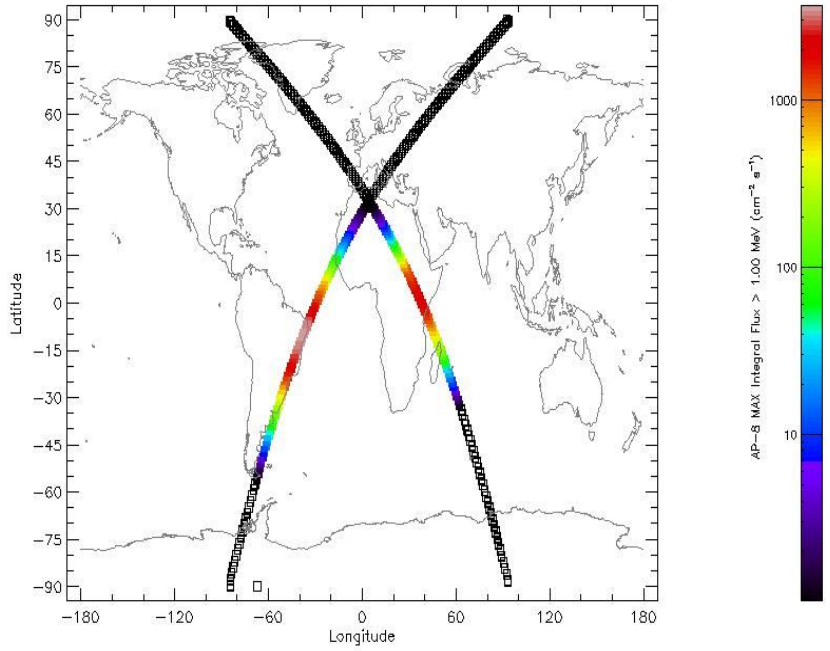

Figure 15. World map of integral flux of protons >1 MeV along Tundra orbit. Model AP8MAX.

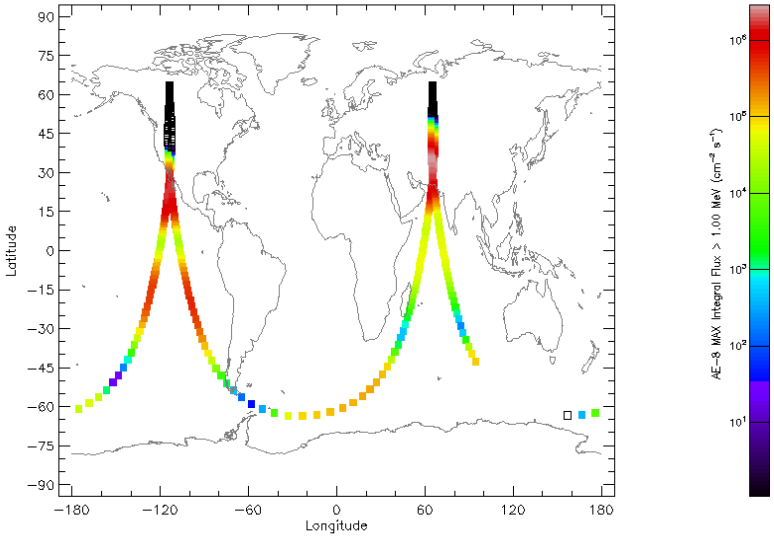

Figure 16. World map of integral flux of electrons >1 MeV along Molniya orbit. Model AE8MAX.

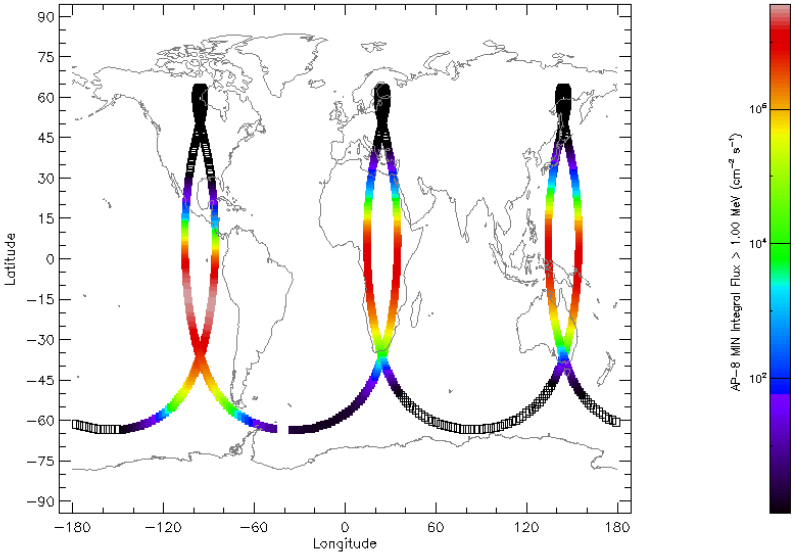

Figure 17. World map of integral flux of electrons >1 MeV along TAP orbit. Model AE8MAX.

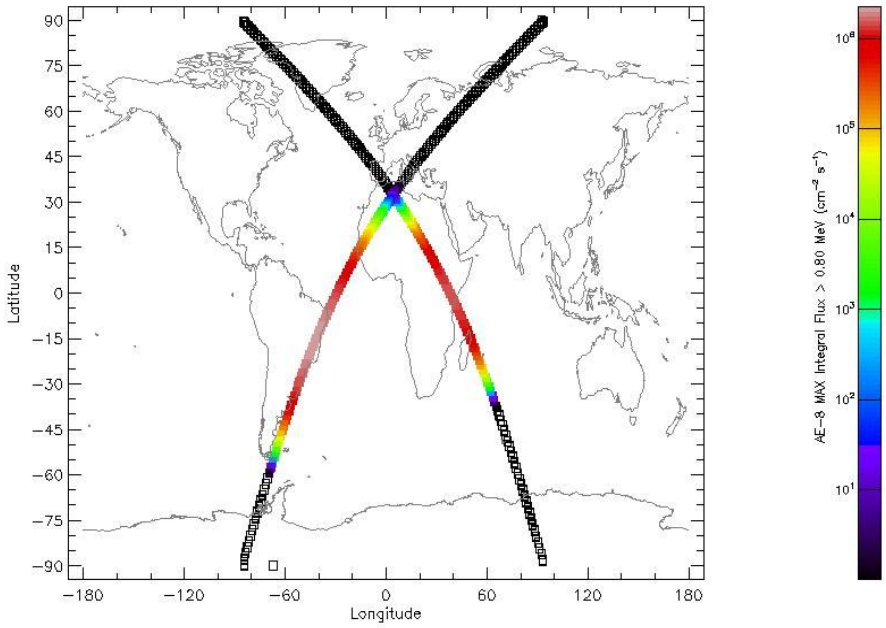

Figure 18. World map of integral flux of electrons >1 MeV alonog Tundra orbit. Model AE8MAX.

5.4 Trapped radiation fluences

In this section integral fluences of trapped electrons and protons accumulated for 48 hours for three HEO orbits were compared using AE8/AP8 and AE9/AP9 models. The electron fluences provided by both models AE8 and AE9 (Figure 19-Figure 24) look similar. The trapped electron fluences on Molniya orbit are less than electron fluences on TAP orbit for energies E=0.5MeV, 1 MeV, and 4 MeV.

According to AP9 model, the trapped proton fluences on Molniya orbit is larger than the fluences on TAP orbit for energies E=1MeV, 10 MeV, and 50MeV while AP8 model demonstrates that the proton fluences on TAP orbit are less than on Molniya orbit for E>1MeV (for E=10 MeV and E=50 MeV) (Figure 25-Figure 30).

The model AP9 was modified comparing to AP8 to provide the better estimation for the trapped radiation on HEO orbits using data of HEO1 and HEO3 missions [6] so we can assume that the conclusions made using AP9 model are more accurate for HEO orbits.

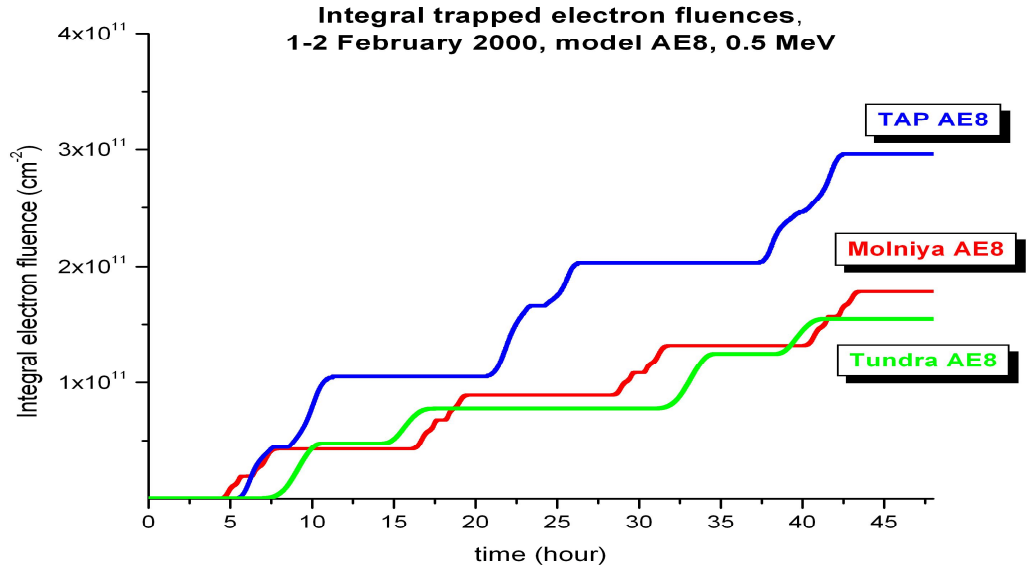

Figure 19. Integral trapped electron fluences on HEO orbits. Model AE8, 0.5 MeV

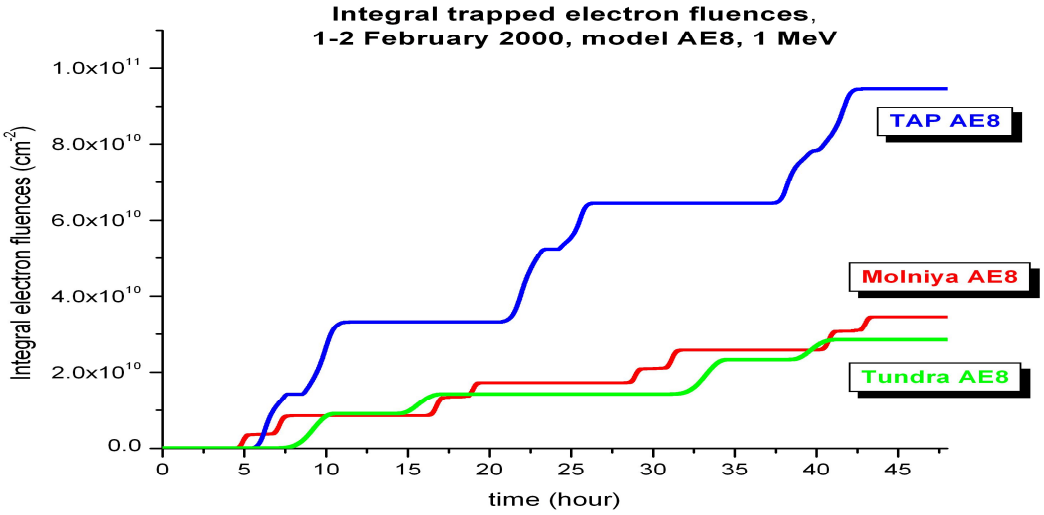

Figure 20 Integral trapped electron fluences on HEO orbits. Model AE8, 1 MeV

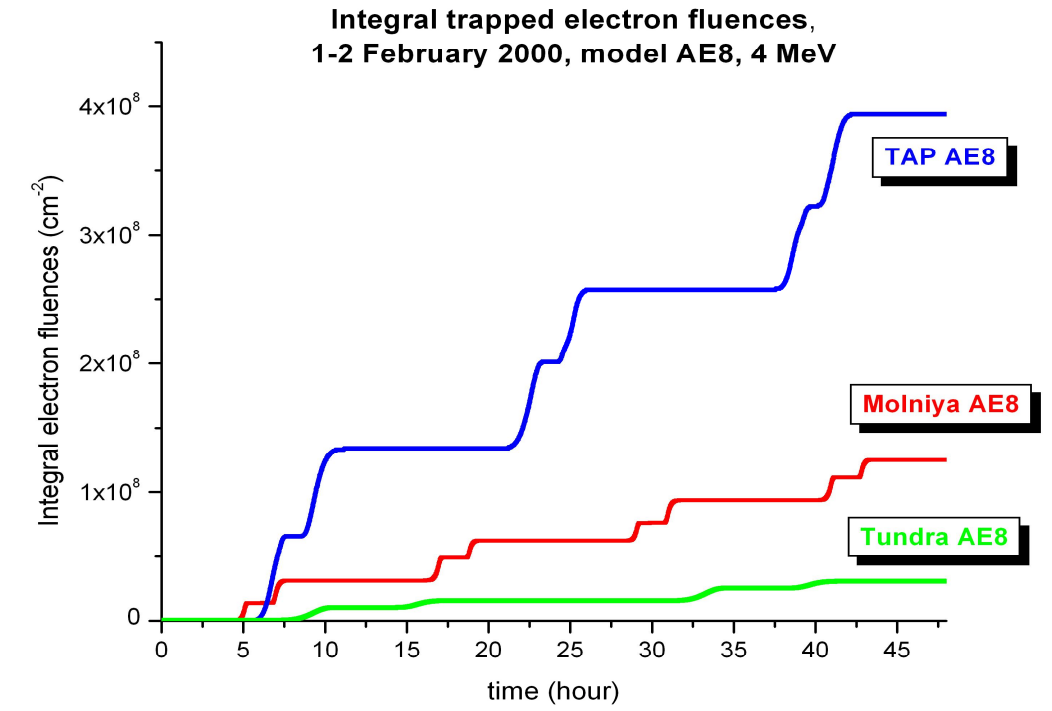

Figure 21. Integral trapped electron fluences on HEO orbits. Model AE8, 4 MeV

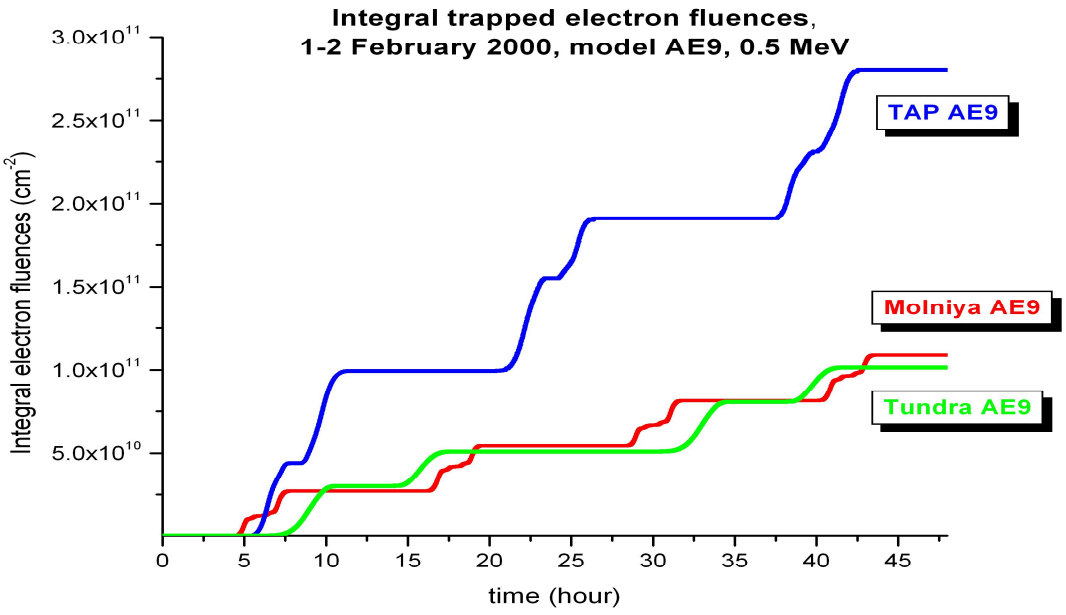

Figure 22. Integral trapped electron fluences on HEO orbits. Model AE9, 0.5 MeV

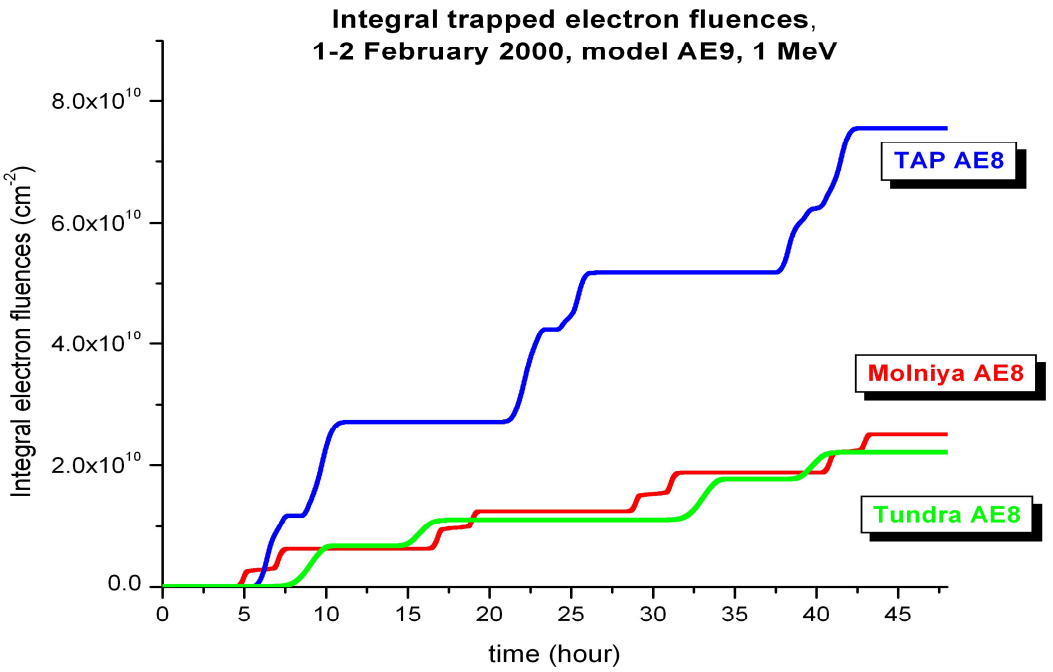

Figure 23. Integral trapped electron fluences on HEO orbits. Model AE9, 1 MeV

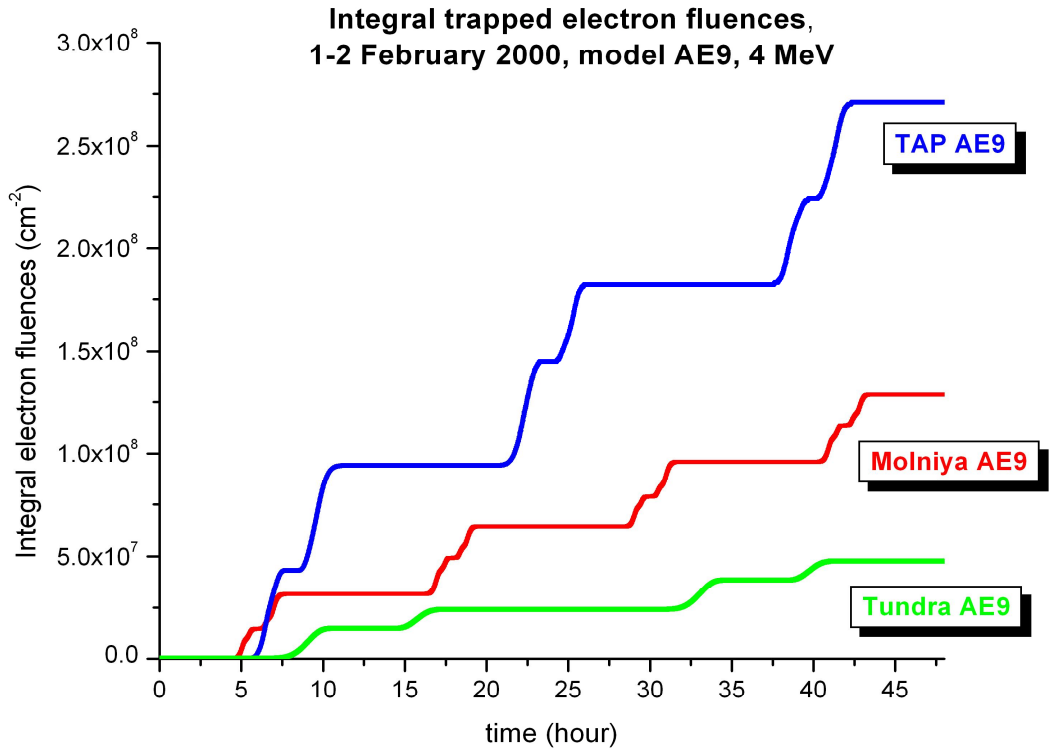

Figure 24. Integral trapped electron fluences on HEO orbits. Model AE9, 4 MeV

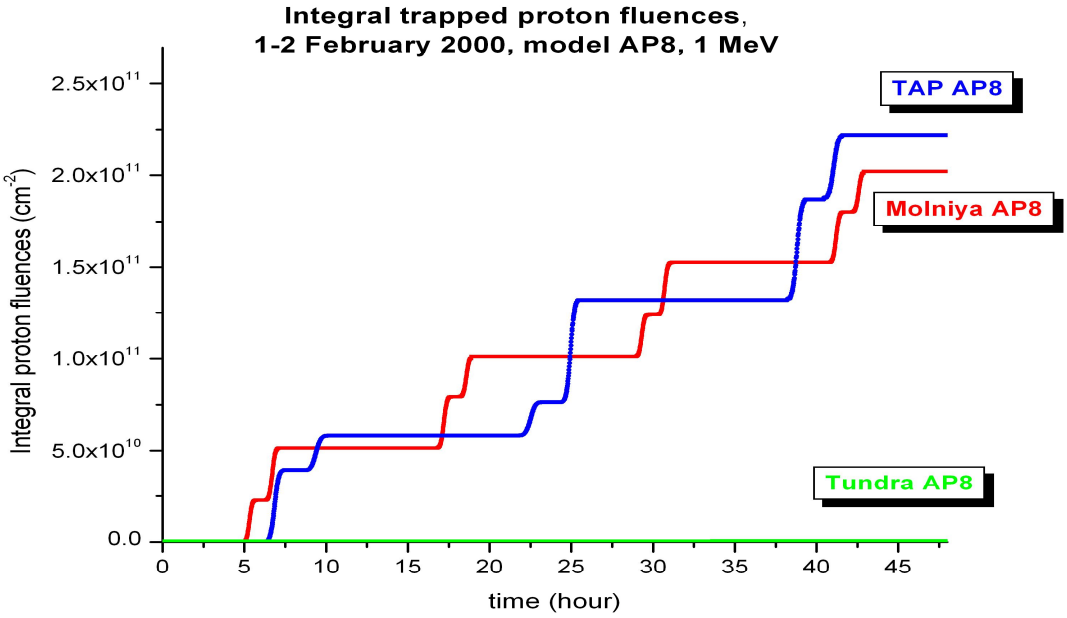

Figure 25. Integral trapped proton fluences on HEO orbits. Model AP8, 1 MeV

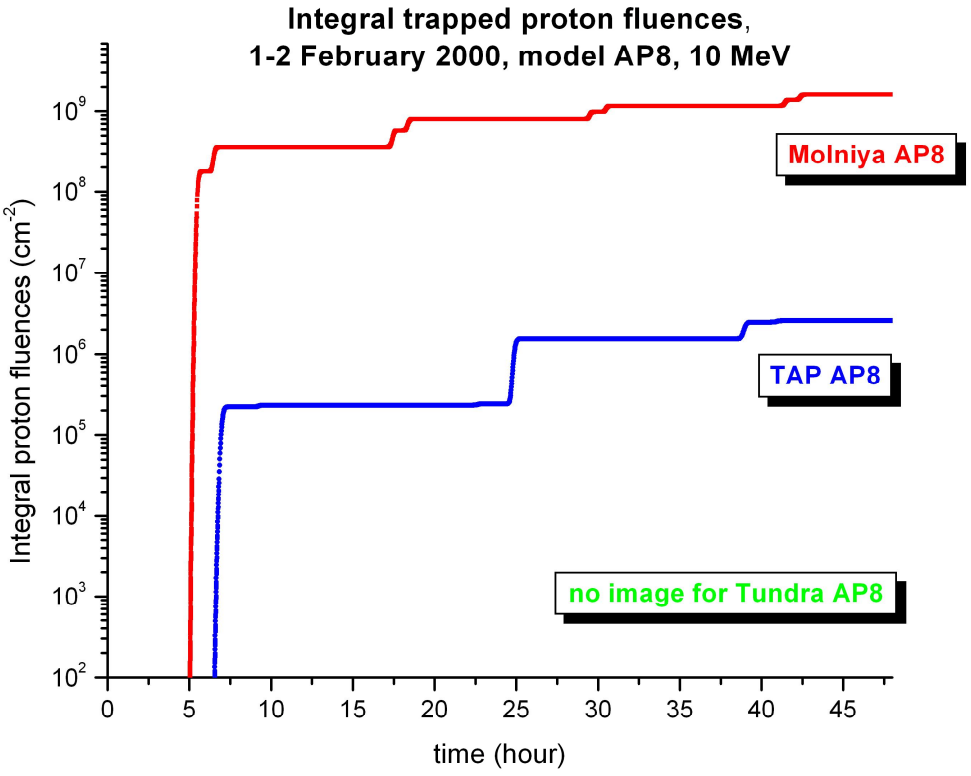

Figure 26. Integral trapped proton fluences on HEO orbits. Model AP8, 10 MeV

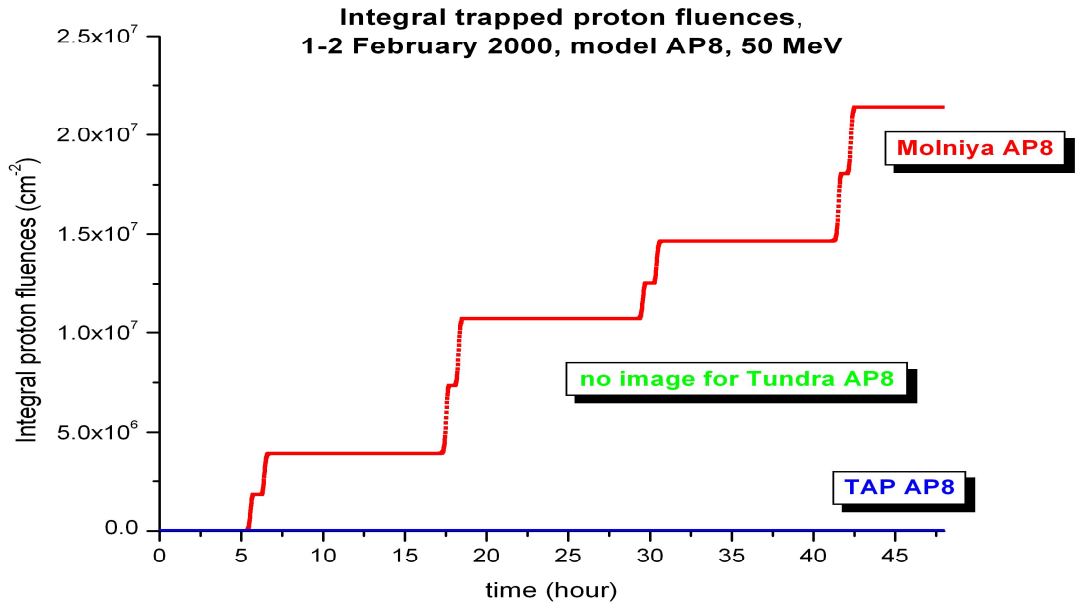

Figure 27. Integral trapped proton fluences on HEO orbits. Model AP8, 50 MeV

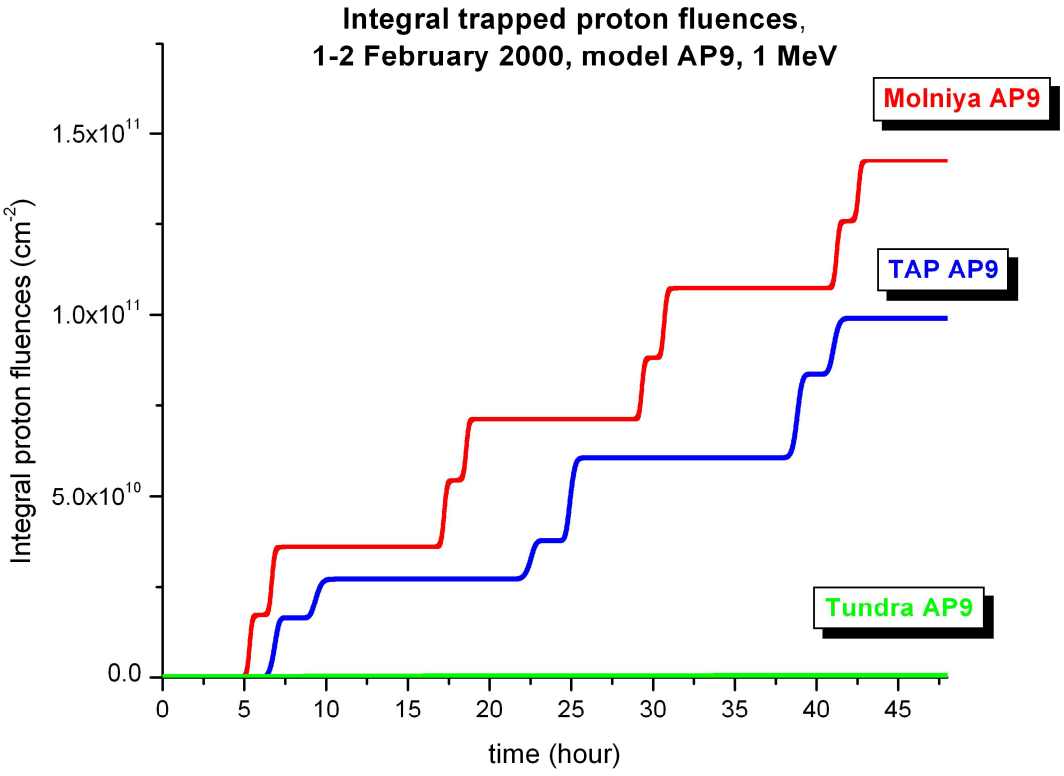

Figure 28. Integral trapped proton fluences on HEO orbits. Model AP9, 1 MeV

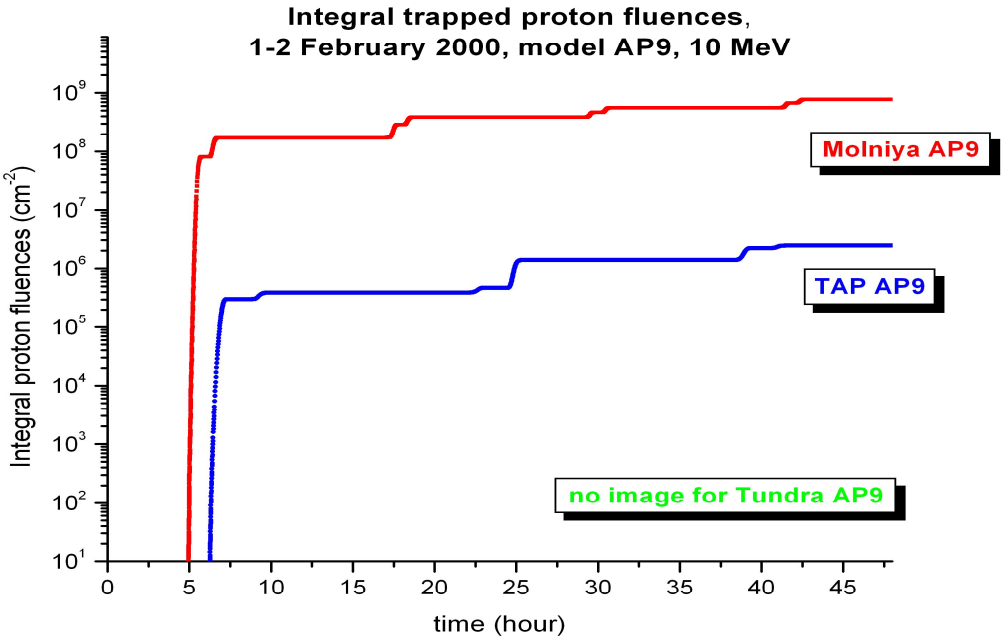

Figure 29. Integral trapped proton fluences on HEO orbits. Model AP9, 10 MeV

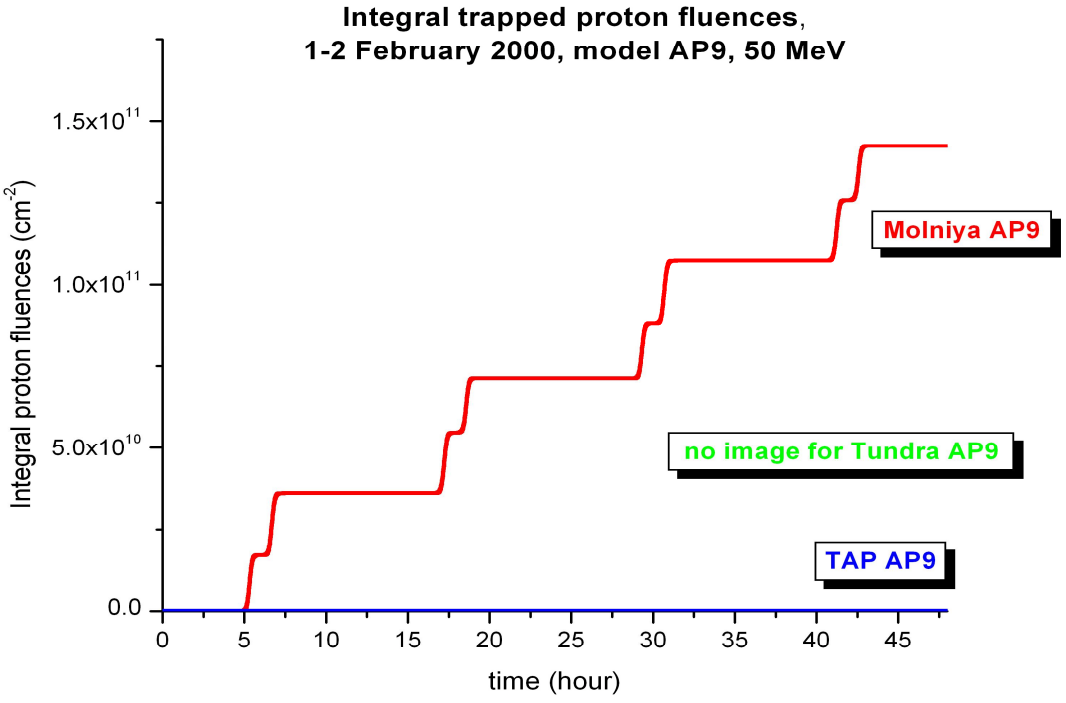

Figure 30. Integral trapped proton fluences on HEO orbits. Model AP9, 50 MeV

6 Long-term Solar Protons and Heavy Ions Environment

6.1 Different models for solar proton fluences calculation

Here the solar proton environment for Molniya, TAP and Tundra orbits was estimated with use of SPENVIS software. We added the comparison of different models for solar energetic particles which are available in SPENVIS.

During solar energetic particles events, large fluxes of energetic protons can reach the Earth. To estimate the fluence value per mission caused by solar events one of the following models can be used. Four solar proton event models are implemented in SPENVIS for predicting long term solar proton fluences:

- the King model [11],
- the JPL-91 model [12],
- the ESP (Emission of Solar Protons) model developed by Xapsos et al. [13], [14] for total fluence and worst event fluence
- Rozenquist model [1514]

The King solar proton model was constructed using data obtained exclusively during the active years of solar cycle 20 (1966-1972). The data set was mainly constructed using proton measurements (in the energy range 10-100 MeV) made by instruments on satellites IMP 4, 5 and 6, which all flew in geocentric, highly elliptical orbits. The data from any individual instrument or satellite were cross-calibrated with independent measurements whenever possible, to check the mutual consistency of the complete data set. There are 25 individual events used in the King data set, including the great proton event of August 1972, which accounted for about 70% of the total >10 MeV fluence for the complete solar cycle. Since this large event made such a dominant contribution to the total solar cycle fluence, King decided to separate it from the remaining 24 events, and to class it as an anomalously large (AL) event, in contrast to the remaining ordinary events (see Spenvis description, [2]).

The JPL model is based on data from solar cycles 20, 21, and part of 22. JPL model produces by J.Feynman with her colleagues [12] does not make any assumption about large and moderate events. The data set used for the JPL model consists of a nearly continuous record of daily average fluxes above the energy thresholds of 1, 4, 10, 30, and 60 MeV. The proton events considered in the JPL models are defined as the total fluence occurring over series of days during which the proton fluence exceeded a selected threshold.

For the JPL model, the statistical properties of the events occurring during active periods of the solar cycle are considered separately from those occurring during the quiet periods. It was assumed that no significant proton fluence exists during quiet periods and that the

only model needed is one for the active periods. Therefore, only data collected during the 7 active years of the cycles were used for this model.

Lognormal distributions which have been used in JPL model gives good description for large event fluences, but deviate from the measured distributions for smaller event fluences [11],[12]. Using a complete list of solar proton event fluences from January 1974 to May 2002 based on measurements from the IMP-8, GOES-7 and GOES-8 spacecrafts, updated values have been proposed in the Rosenqvist model for the fluence specification in the energy ranges >10 MeV and > 30 MeV [15]. The model Rosenqvist et al. implemented in SPENVIS uses these updated values in combination with the JPL-91 parameter values. JPL and Rozenqvist models are also very similar in the energy range 0.1-100 MeV.

Another model which is used for estimation of solar proton fluences in SPENVIS is ESP-PSYCHIC (Prediction of Solar particle Yields for Characterizing Integrated Circuits) model. ESP model developed by Xapsos et al. ([13], [14],) incorporates the whole three cycles of solar activity and produces predicted proton fluences slightly higher than JPL model does. The JPL model only provides fluence estimates up to 60 MeV. The ESP model extends this energy range up to 300 MeV. It has been shown also that long-term solar heavy ion fluxes exceed galactic cosmic ray fluxes during solar maximum and should be taken into account for the years of solar maximum. The PSYCHIC model includes cumulative solar heavy ion fluences during the solar maximum period for nearly all naturally occurring elements from Hydrogen (H) to Uranium (U) with atomic numbers 1-92.

Comparison of the assessment of integrated solar proton fluences by different models are plotted on Figure 31. This plot demonstrates that JPL, King, ESP and Rozenqvist models give similar results in the middle range of energies 5-100 MeV for integral solar proton fluences on Molniya orbit with the magnetic shielding in the form of the IGRF model. The top panel plot of Figure 31with linear scale of integral proton fluxes demonstrates a difference between solar proton fluences estimated by JPL, King, ESP and Rozenqvist models for small energies. The bottom panel plot with logarithmic scale demonstrates a difference between solar proton fluences estimated by these models for large energies.

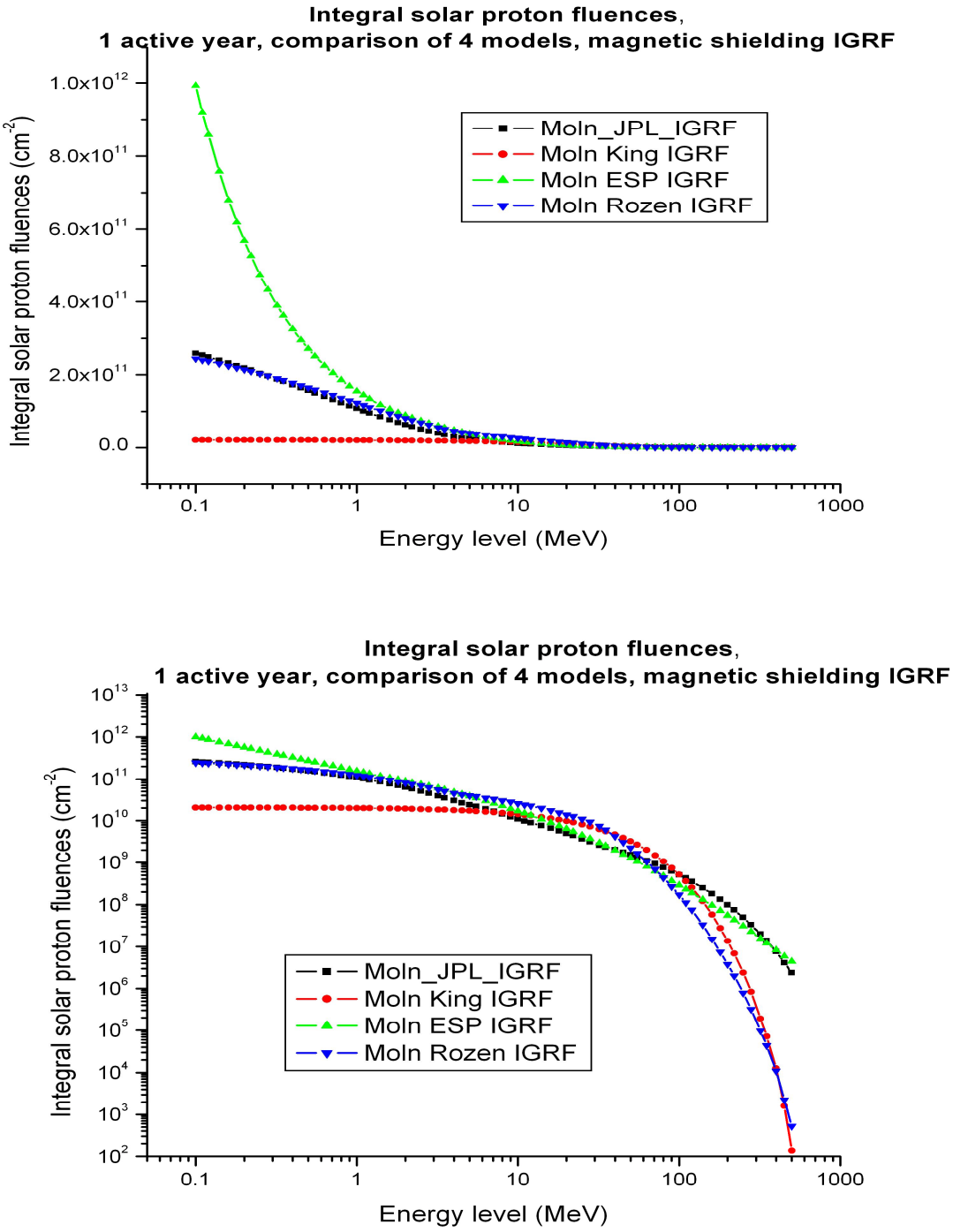

Figure 31. Integral solar proton fluences on Molniya orbit calculated by four models of solar protons JPL model, King model, Rozenqvist model, and ESP model. The top panel plot is with linear scale of integral proton fluxes demonstrates a difference between models for small energies. The bottom panel plot with logarithmic scale demonstrates a difference between models for large energies.

6.2 Influence of the magnetic shielding model on the integrated solar proton fluences

For the considered models (JPL, King, ESP and Rozenqvist models) different magnetic shieldings are implemented in the SPENVIS software. The choices are the IGRF model of geomagnetic field, a Störmer eccentric dipole, or an upgraded Störmer model for the eccentric dipole. The result of calculation of integral solar proton fluences with use of JPL model with different magnetic shieldings are plotted on Figure 32-Figure 34. These plots demonstrate that the magnetic shielding where the geomagnetic field is represented in IGRF form and in the form of an eccentric dipoles give approximately similar results.

Figure 32-Figure 33 demonstrate that for both TAP and Molniya orbits a magnetic shielding partly protects satellites from the solar proton fluences comparing with the unshielded magnetosphere, and different shieldings (the IGRF model, a Störmer eccentric dipole model, an upgraded Störmer eccentric dipole model) provide approximately the same reduction of proton fluences for the orbit. Plots for shielded and unshielded solar proton fluences for Tundra orbit demonstrate that solar proton fluences are approximately the same and do not depend on a magnetic shielding.

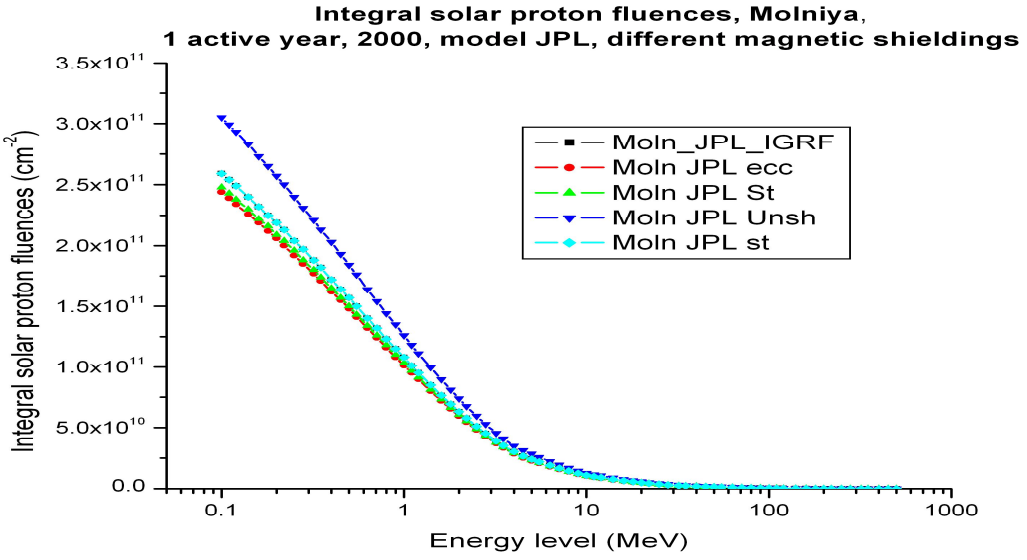

Figure 32. Integral solar proton fluences on Molniya orbit. Model JPL with different magnetic shieldings: IGRF model, Störmer eccentric dipole model, upgraded Störmer model for the eccentric dipole, without shielding, and storm magnetosphere with IGRF shielding.

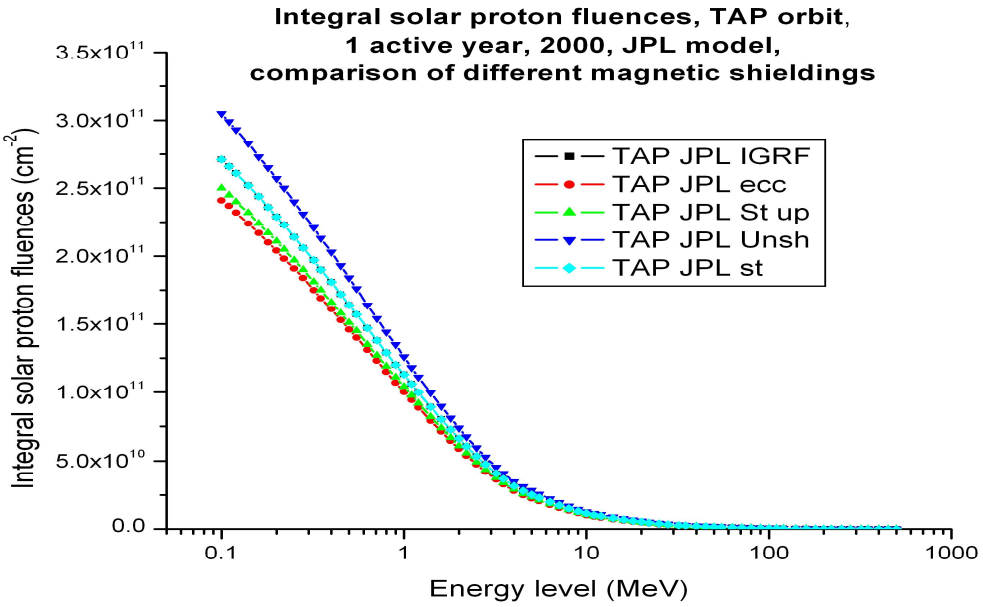

Figure 33. Integral solar proton fluences on TAP orbit. Model JPL with different magnetic shieldings: IGRF model, Störmer eccentric dipole model, upgraded Störmer model for the eccentric dipole, without shielding, and storm magnetosphere with IGRF shielding.

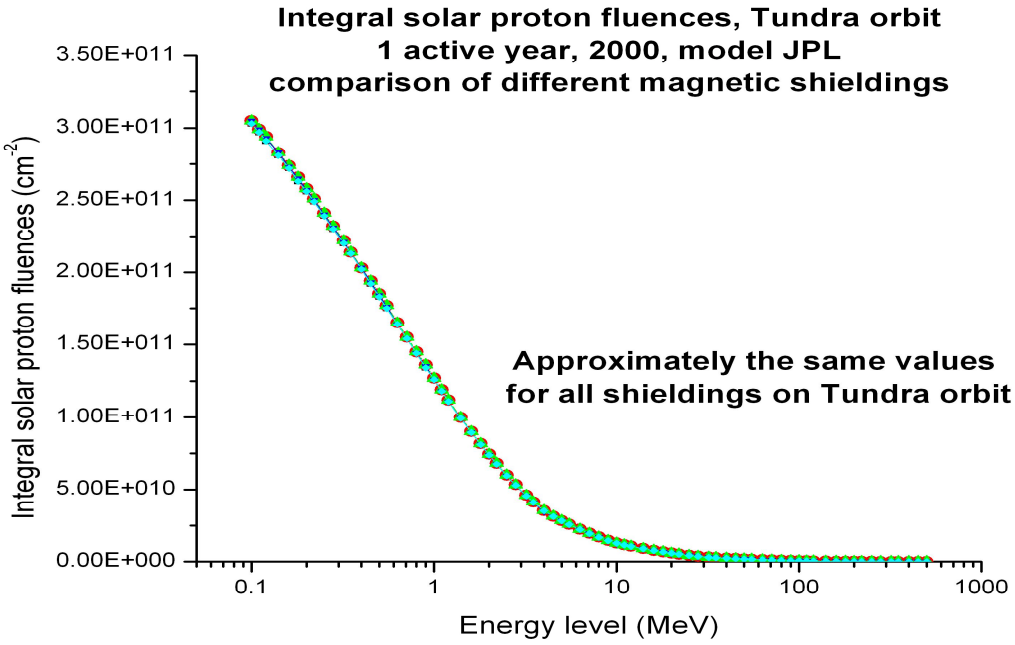

Figure 34. Integral solar proton fluences on Tundra orbit. Model JPL with different magnetic shieldings: IGRF model, Störmer eccentric dipole model, upgraded Störmer model for the eccentric dipole, without shielding, and storm magnetosphere with IGRF shielding.

6.3 Long-term integral solar proton fluences estimated by JPL, King, Rozenqvist, and ESP models

Here we consider the integral solar proton fluences evaluated by using all four models (JPL, King model, Rozenqvist model and ESP-PSYCHIC) implemented in SPENVIS. Plots (Figure 35-Figure 38) provide the integral solar proton fluences evaluated by these models with the magnetic shielding in the form of the IGRF model. These plots demonstrate that solar proton fluences are larger for Tundra orbit because this orbit is further from the Earth than the other two orbits and is not protected by the Earth's magnetic field. These plots show that fluences on TAP orbit are larger than on Molniya orbit but the difference is small, approximately 10% for small energies (E<5 MeV), and this difference is almost negligible for larger energy protons.

Plots for solar proton fluences for JPL, King, Rozenquist and ESP-PSYCHIC models with the magnetic shielding in the form of a Störmer eccentric dipole, an upgraded Störmer eccentric dipole and without magnetic shielding are in Appendix 4. These plots also support the fact that the proton fluences are larger for Tundra orbit, and that the solar proton fluences for TAP and Molniya orbits are similar.

The calculations were made using the assumption of a quiet magnetosphere with unchanged magnetic moment, for all arrival directions. Prediction period was taken as 1 year, corresponding to the solar maximum, 2000, with 90.00% probability of fluences not being exceeded. For ESP-PSYCHIC model which calculates also the heavy ion environment the ion range was taken as H – U (atomic numbers 1-92).

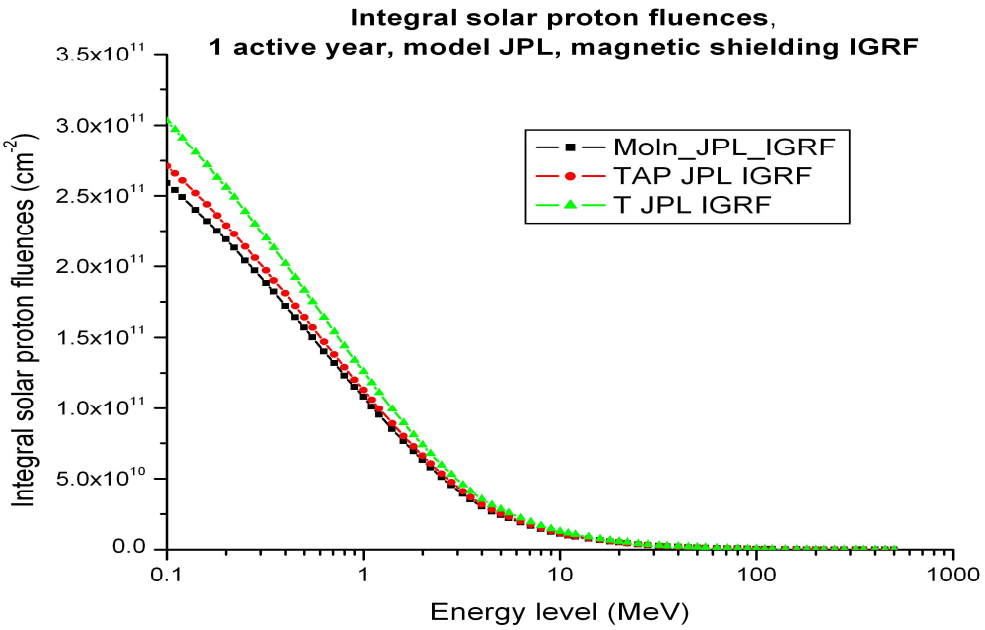

Figure 35. Integral solar proton fluences on HEO orbits. 2000. JPL model.

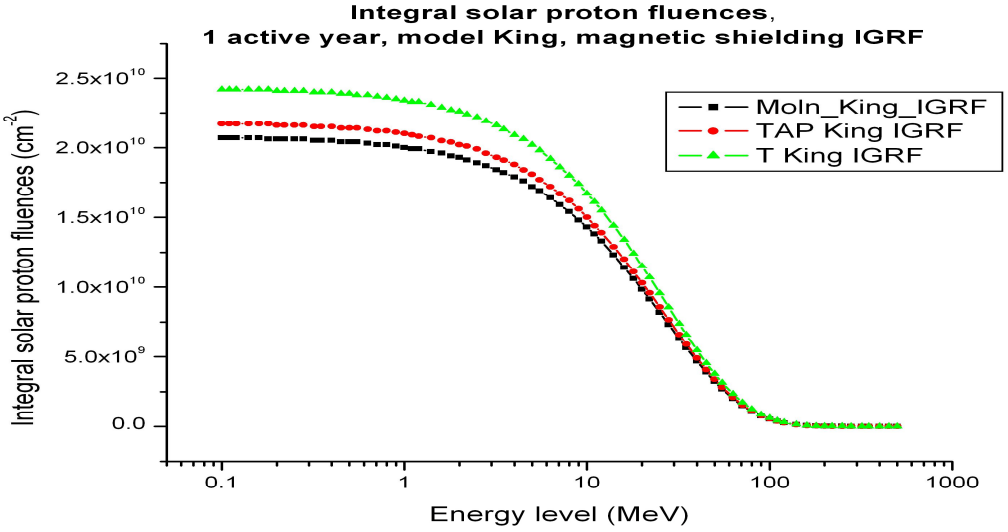

Figure 36. Integral solar proton fluences on HEO orbits. 2000. King model.

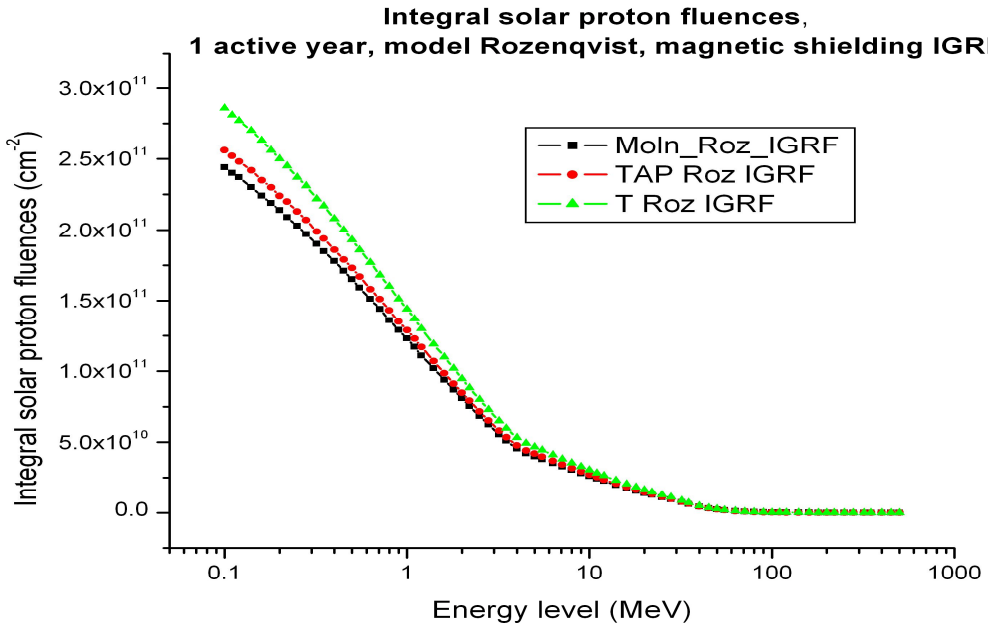

Figure 37. Integral solar proton fluences on HEO orbits. 2000. Rozenqvist model.

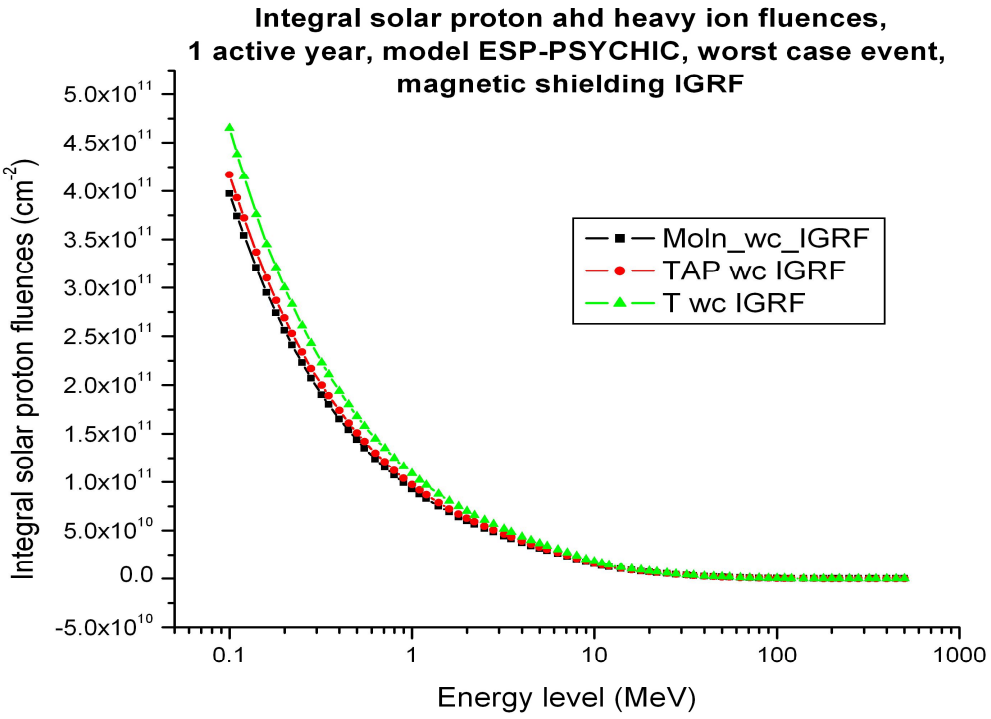

Figure 38. Integral solar proton fluences on HEO orbits. 2000. ESP-PSYCHIC model.

7 Galactic Cosmic Rays spectra (CRÈME-86 model)

To estimate the influence of Galactic Cosmic Rays on the satellite radiation environment, one of the galactic cosmic rays (GCR) models can be used. The CRÈME-86 GCR model in SPENVIS is based on the CRÈME-86 model and CRÈME-96 which include the solar cycle modulation in the cosmic ray environment. Cosmic ray fluxes are anticorrelated with solar activity so the highest cosmic ray fluxes occur at solar minimum.

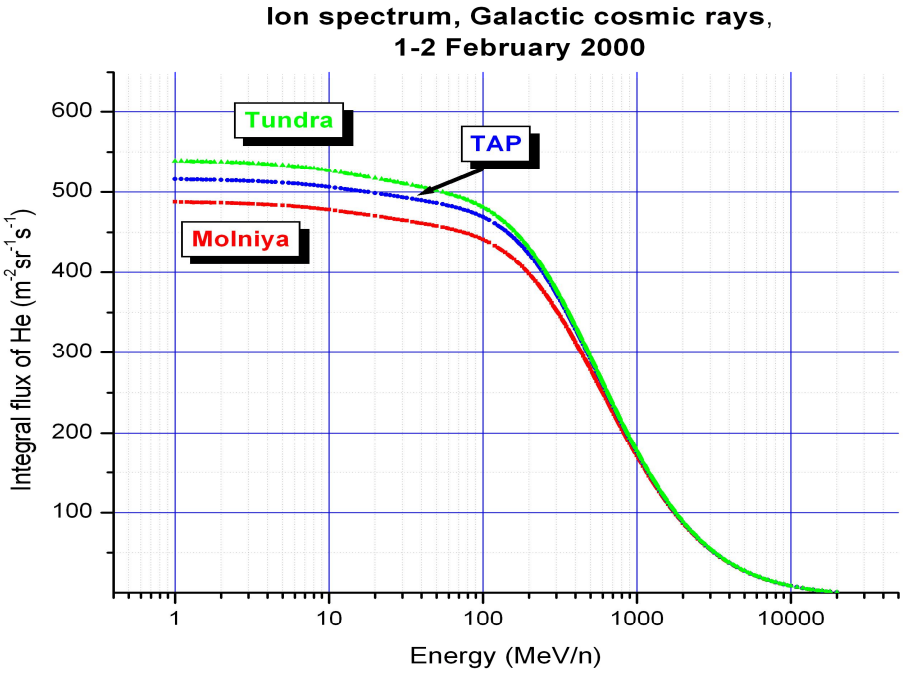

Figure 39. Spectrum of ion flux. Galactic cosmic rays, model CRÈME-86

Plot (Figure 39) demonstrates that Tundra orbit gets more radiation from the galactic cosmic rays than the other two orbits. The integral proton fluxes of galactic cosmic rays are lower for TAP orbit than for Tundra orbit, and lower for Molniya orbit than for TAP orbit.

8 Short-time Solar Particles Fluxes

Solar flare particle flux models are needed for evaluating single-event upset rates. To obtain only solar flare fluxes by use of SPENVIS codes, the cosmic ray component (which is denoted in the CRÈME-86 model as M=1) has been subtracted from the CRÈME-86 environment models and notation for this model is M=5-1 for the ordinary flare flux with the mean composition and M=12-1 for the worst-case flare flux. The solar flare proton fluxes are plotted on Figure 40-Figure 43. The fluxes were calculated for all arrival directions in ion range from H to U (atomic numbers Z=1-92).

Solar proton fluxes which were calculated without magnetic shielding are plotted on Figure 40. On Figure 41-Figure 42 there are plots of solar proton fluxes with the magnetic shieldings in the form of the IGRF model and in the form of an eccentric dipole. The comparison of Figure 40-Figure 43 demonstrates that the magnetic shielding reduces the influence of the galactic cosmic rays on the proton fluxes for TAP and Molniya orbits, but does not protect Tundra orbit.

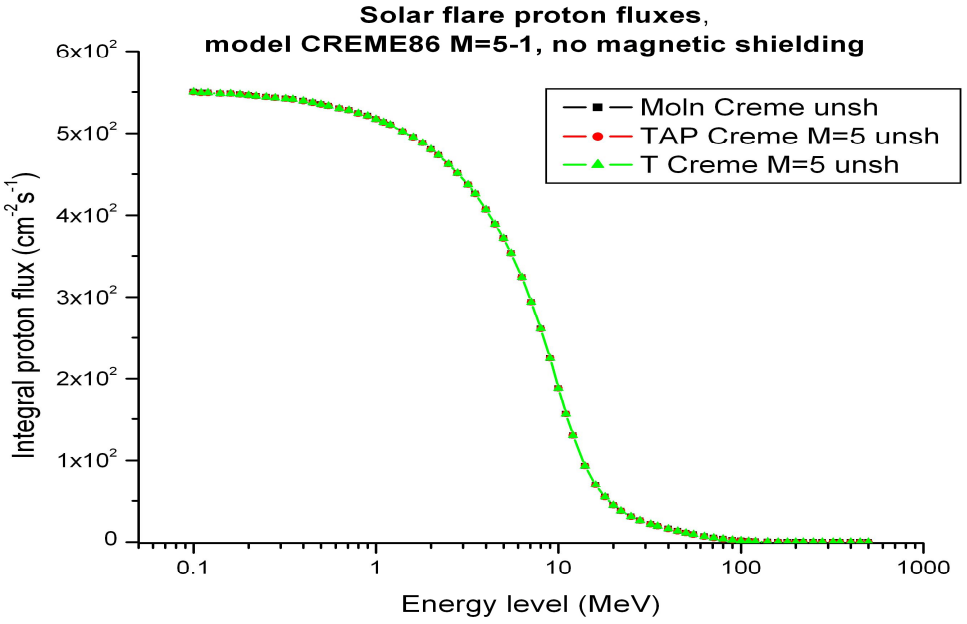

Figure 40. Spectrum of solar proton fluxes of solar flares. Model CRÈME-86, M=5-1. No magnetic shielding

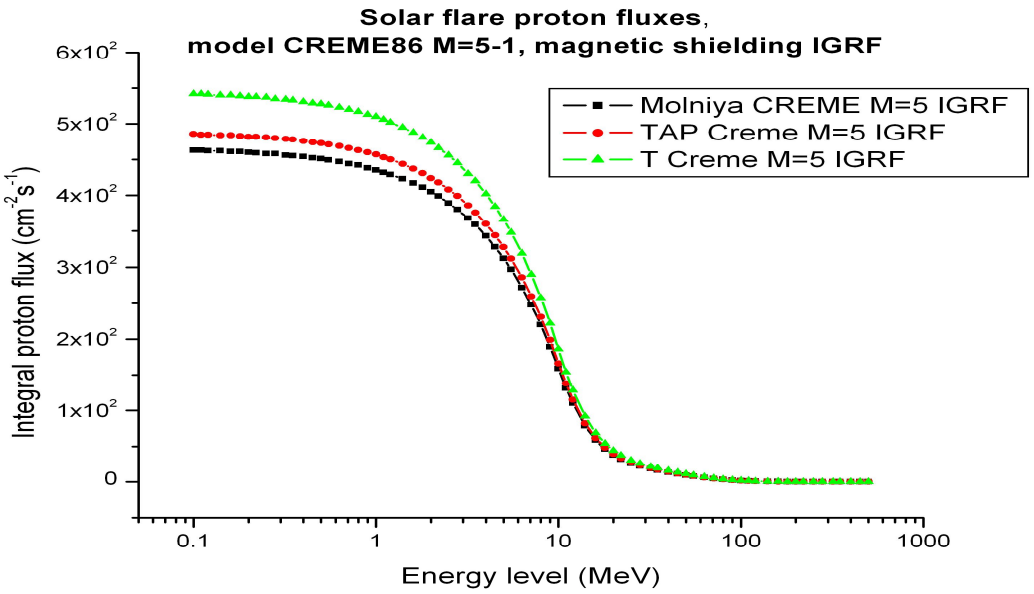

Figure 41. Spectrum of solar proton fluxes of solar flares. Model CRÈME-86, M=5-1. Magnetic shielding IGRF.

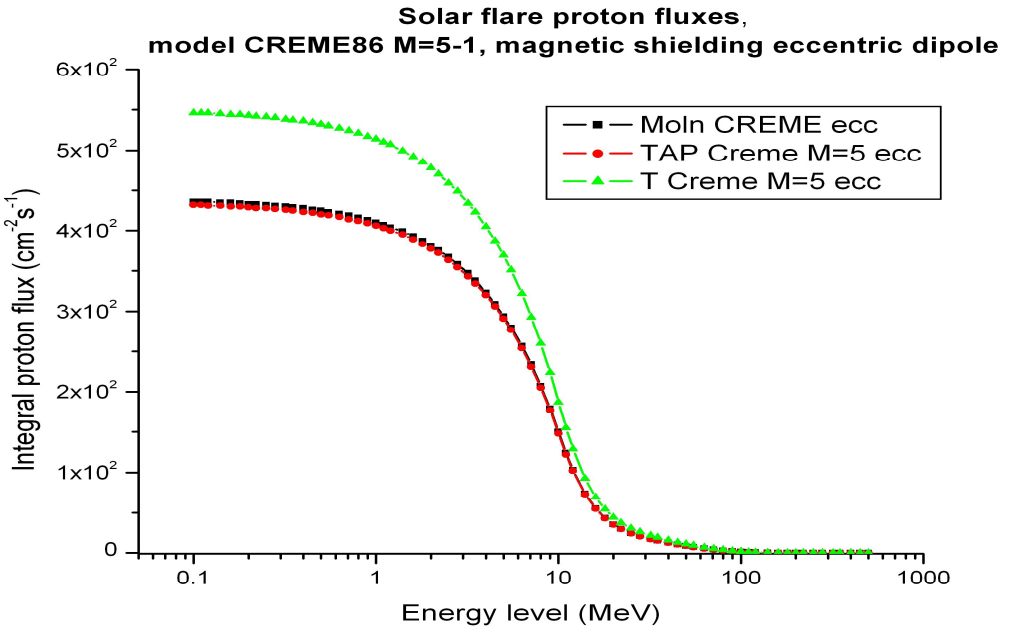

Figure 42. Spectrum of solar proton fluxes of solar flares. Model CRÈME-86, M=5-1. Model for the magnetic shielding is an eccentric dipole.

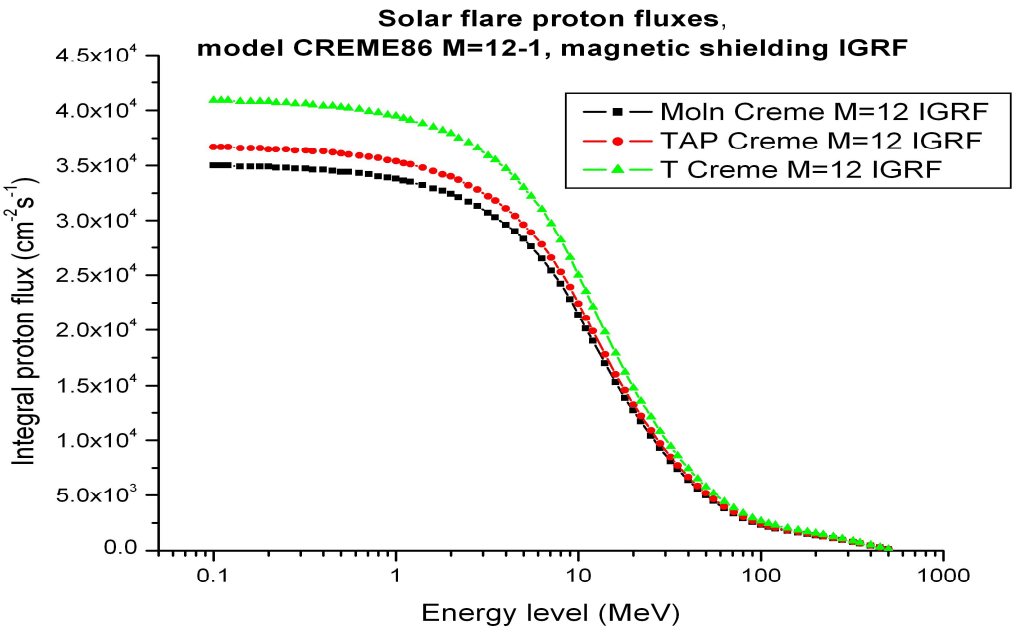

Figure 43. Spectrum of solar proton fluxes of solar flares. Model CRÈME-86, M=12-1.

9 Attenuation factor

The result that Tundra orbit is less protected from galactic cosmic rays and solar protons is also supported by the so-called attenuation factor. The attenuation coefficient is a quantity that characterizes how easily a medium can be penetrated by high-energetic particles. According to the SPENVIS notations, if the attenuation factor is close to 1 it means that the space is transparent for the radiation, and if the attenuation factor is close to 0, it means that flux of radiation is quickly "attenuated" (weakened) as it passes through the medium)

Results for different orbits are presented in Figure 44-Figure 46 .The attenuation factor for all energies from 0.1 MeV to 500 MeV are above 0.79 on Molniya orbit, >0.78 on TAP orbit and >0.99 on Tundra orbit, i.e. natural geomagnetic shielding is low on all orbits and especially on Tundra orbit.

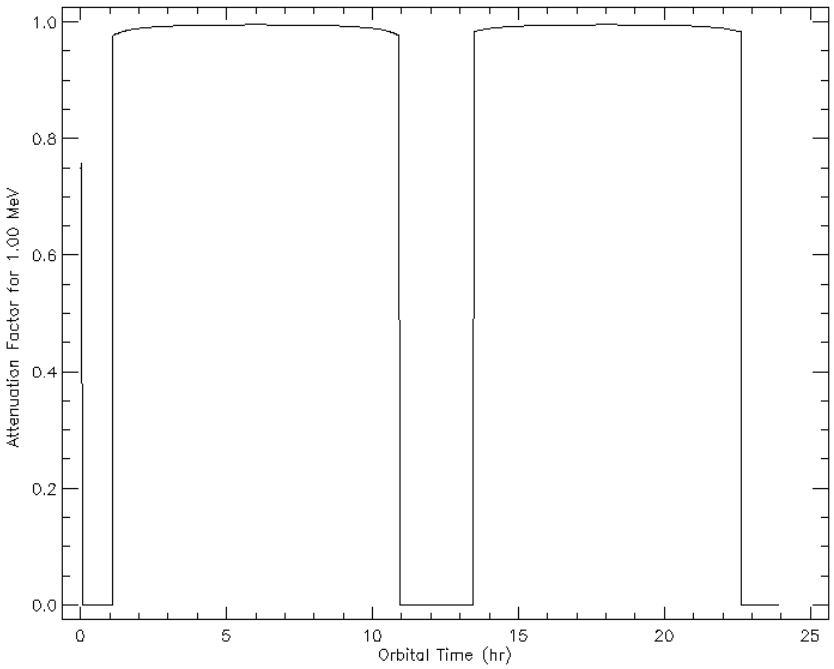

Figure 44. Attenuation factor for 1MeV on Molniya orbit

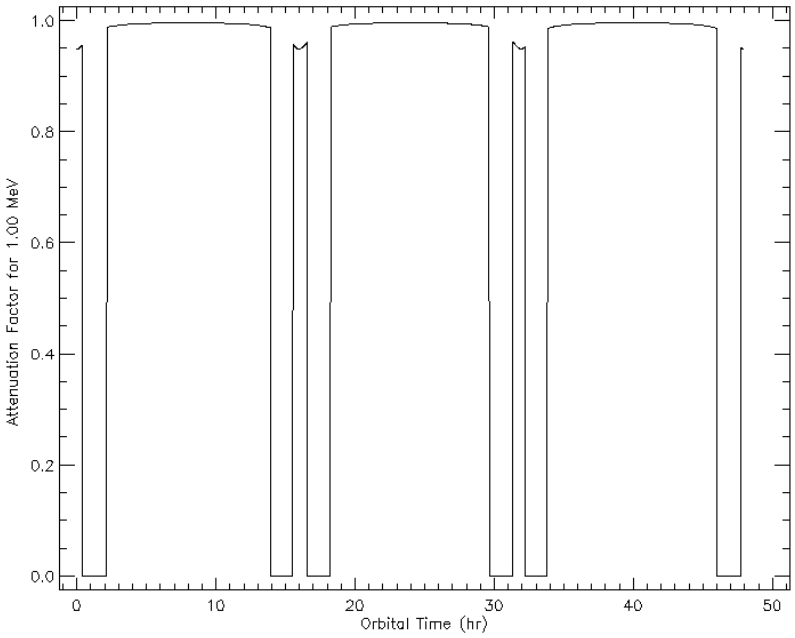

Figure 45. Attenuation factor for 1MeV on TAP Orbit

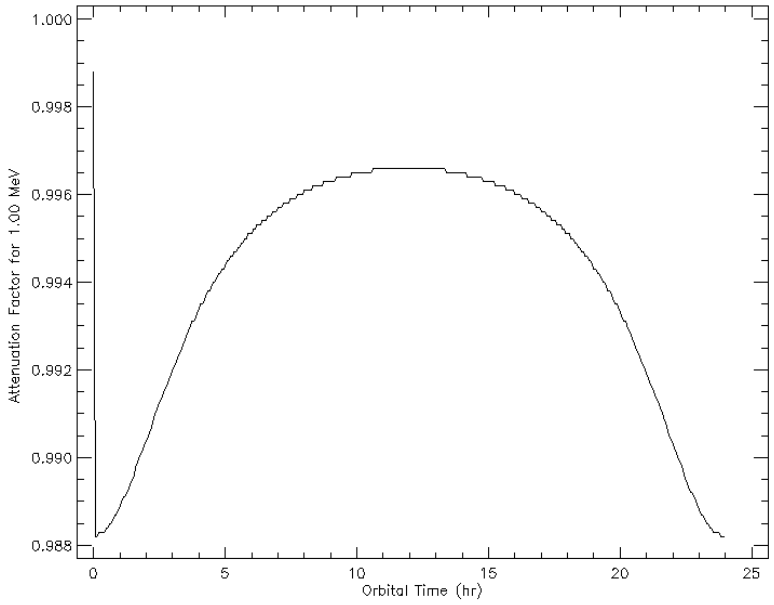

Figure 46. Attenuation factor for 1MeV on Tundra Orbit

10 Solar Cell Damage Equivalent Fluences

To estimate solar cell degradation in space the omnidirectional space radiation is converted to a damage equivalent unidirectional fluence at a normalised energy and in terms of a specific radiation particle. This equivalent fluence will produce the same damage as that produced by omnidirectional space radiation considered if the relative damage coefficient (RDC) is properly defined to allow the conversion. The effective relative damage coefficients allow the conversion of various energy spectra of space electrons and protons into equivalent fluences. The equivalent fluences are based on normal-incidence monoenergetic irradiations for which the degradations of the solar cells of interest are characterized.

Equivalent fluence calculations involve an integration of the omnidirectional fluence times the appropriate damage coefficients. When the equivalent fluence is determined for a given space environment, the parameter degradation can be evaluated in the laboratory by irradiating the solar cell with the calculated fluence level of unidirectional normally incident flux. The equivalent fluence is normally expressed in terms of 1 MeV electrons or 10 MeV protons. The usual practice in the study of solar cell damage has been to represent the experimental data in terms of changes in the cell short circuit current (I_{sc}), open circuit voltage (V_{oc}), and maximum power (P_{max}) [2].

The three basic input elements necessary to perform degradation calculations are:

1. degradation data for solar cells under normal incidence 1 MeV electron irradiation,

2. effective relative damage coefficients for omnidirectional space electrons and protons of various energies for solar cells with various coverglass thicknesses,
3. space radiation environment data for the orbit of interest.

Electron/proton damage ratios which were used in SPENVIS is 3000.0. The electron-to-proton damage ratio is the ratio of the MeV electron fluence required to reduce solar cell maximum power by a certain percentage to those fluences of protons of various energies required to produce the same amount of degradation [16]. Calculations are made for Si, with thickness of shieldings 2.2 g/cm^3

Equivalent fluences for Molniya orbit for the total radiation are higher than for TAP and Tundra orbits (Figure 47-Figure 48). Fluences equivalent to the trapped electrons are larger for TAP orbit than for Molniya and Tundra orbit while trapped protons provide less equivalent fluences for TAP orbit than for Molniya orbit.

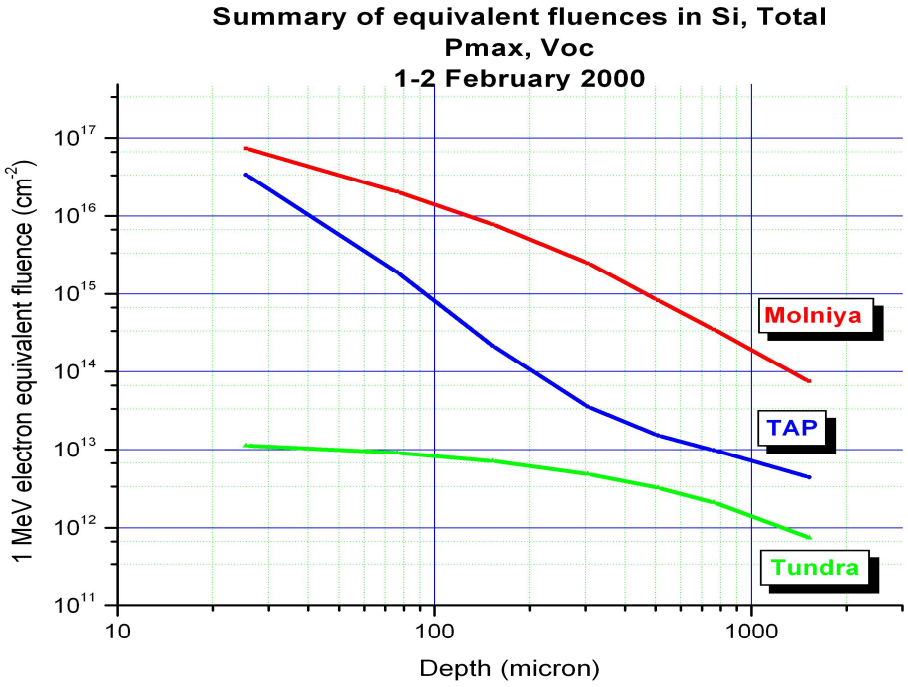

Figure 47. Equivalent fluences of the total trapped radiation for different depths. Maximum power. Open circuit voltage

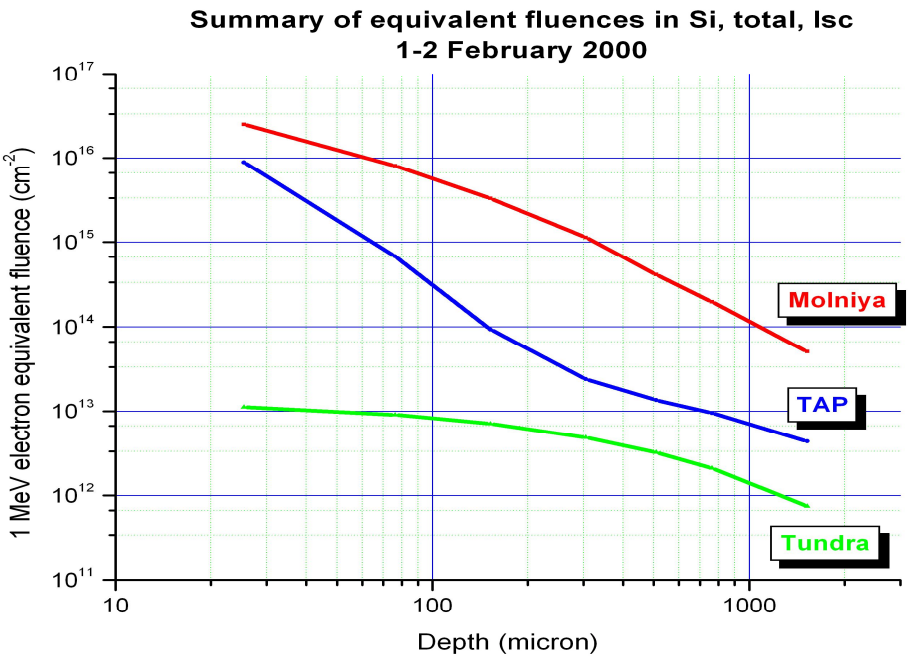

Figure 48. Equivalent fluences of the total trapped radiation for different depths. Circuit current.

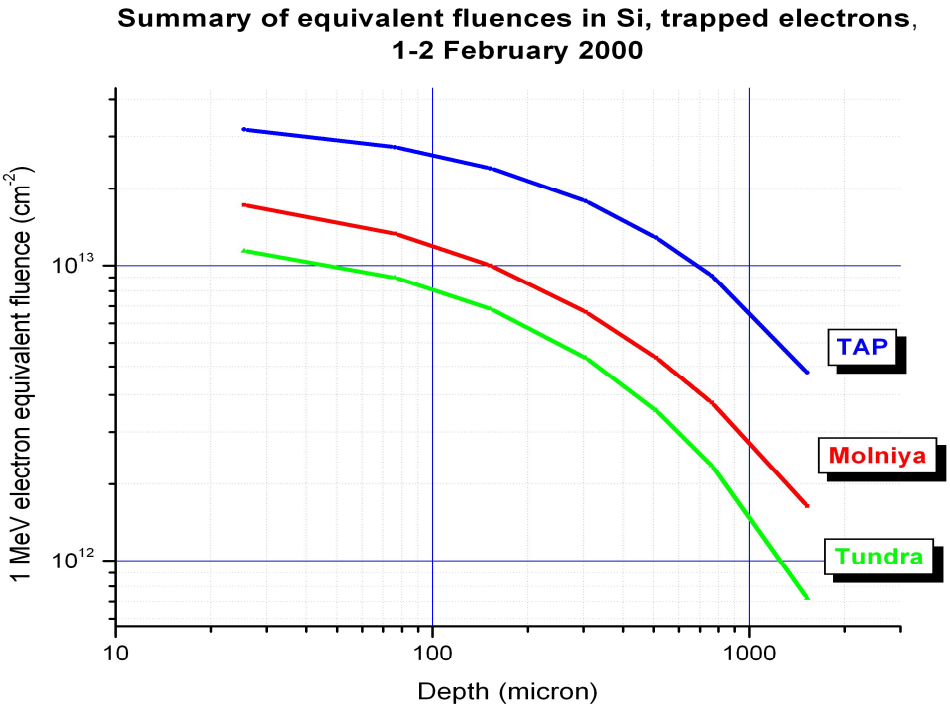

Figure 49. Equivalent fluences of the trapped electrons for different depths. Maximum power. Open circuit voltage. Circuit current.

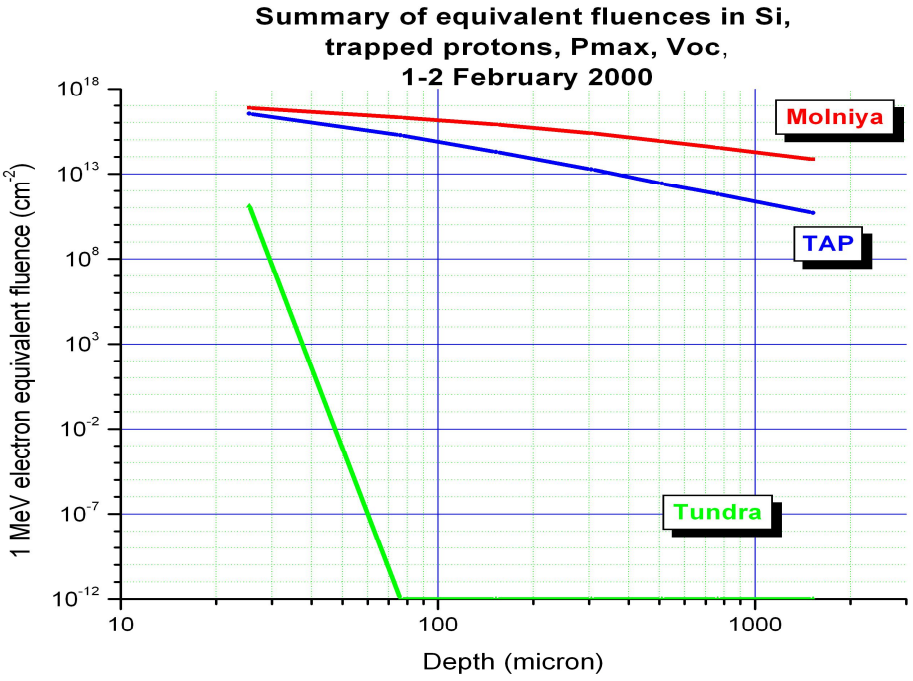

Figure 50. Equivalent fluences of the total trapped radiation for different depths. Maximum power. Open circuit voltage

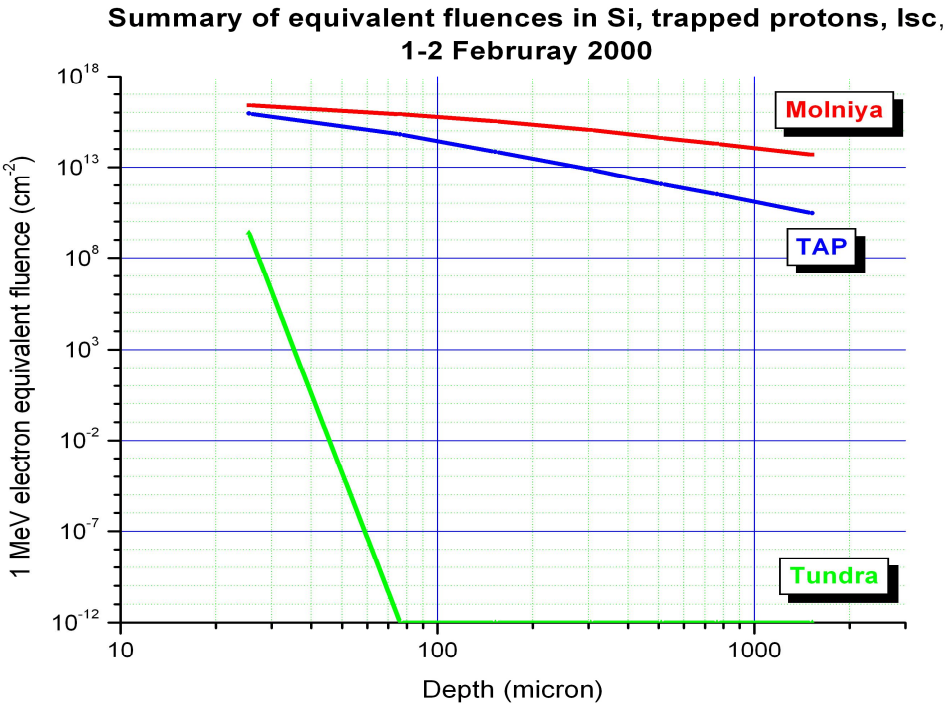

Figure 51. Equivalent fluences of the trapped protons radiation for different depths. Circuit current

11 Single Event Upset Rates

The uninterrupted and progressive miniaturization of microelectronic devices while resulting in more powerful computers, has also made these computers more susceptible to the effects of ionizing radiation. This is of particular concern for space applications due to the radiation fields encountered outside the protective terrestrial atmosphere and magnetosphere. The main type of effects studied are the so called Single Event Upsets (SEUs) where ionization caused by the passage of a single heavy ion produces a bit flip and hence a computer error or a system crash. Such events can also lead to destructive latchups and burnouts. For calculating the single event upset rate the linear energy transfer spectrum is used.

11.1 Linear energy transfer

Linear Energy Transfer is the energy absorbed by the target through which a particle is traveling per unit length of the track of the particle. For the purposes of this calculator, the LET is expressed in units of MeV cm^2/mg [17].

Particle fluxes are defined mainly by trapped protons in the radiation belt as well as by particles of galactic cosmic rays and by protons and ions produced by solar flares. Linear energy transfer is less meaningful for electrons, because of their low mass relative to the atoms they ionize. In SPENVIS tools for LET calculations the following models are used

- AP-8 max model for the trapped radiation,
- CRÈME-86 (M=5-1) for solar particles (ions H-U, with the mass numbers in the range 1-72),
- CRÈME-86 (M=1) for Galactic cosmic rays particles (ions H-U, with the mass numbers in the range 1-72).

Analyses of flux spectra (Figure 52- Figure 55) demonstrate that TAP orbit gets less fluxes of solar flare particles than the other two orbits. Molniya orbit is under stronger influence of the trapped radiation (see Figure 53) than two other orbits. Tundra orbit is under stronger influence of galactic cosmic rays and solar flares particles than the other two orbits (Figure 54-Figure 55). The summation of all three sources for particle fluxes is less for TAP orbit than for the other two orbits for all LET values (Figure 52).

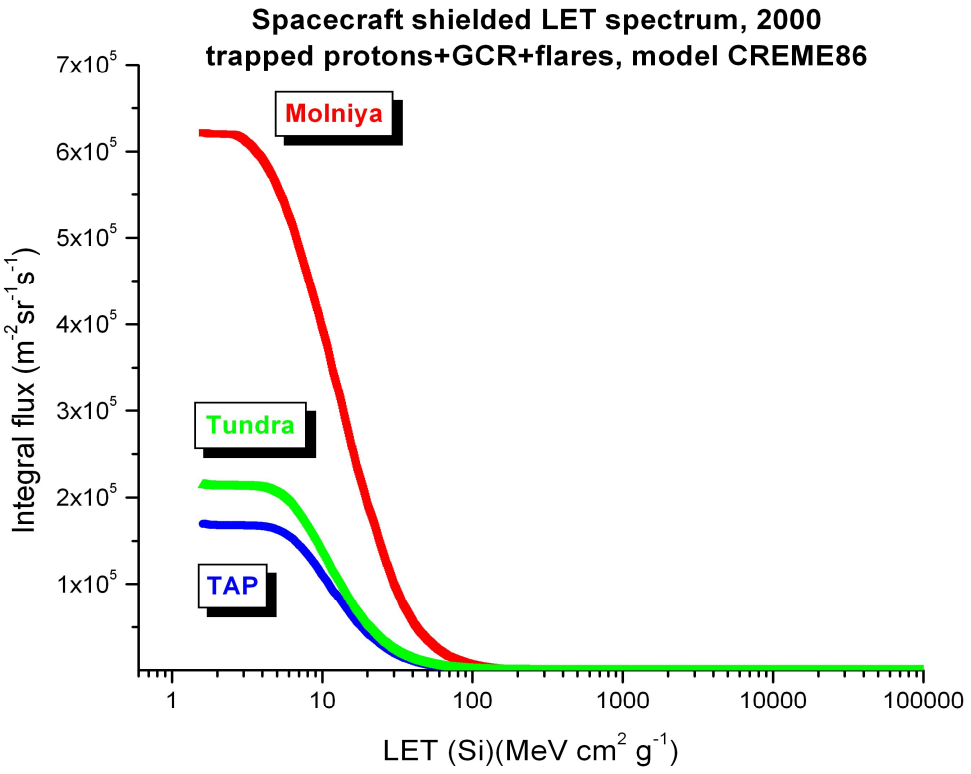

Figure 52. Particle spectra for HEO orbits. Calculations are made for trapped radiation protons in solar maxima, Galactic cosmic rays particles (model M=1), and solar flare particles (model CRÈME-86)

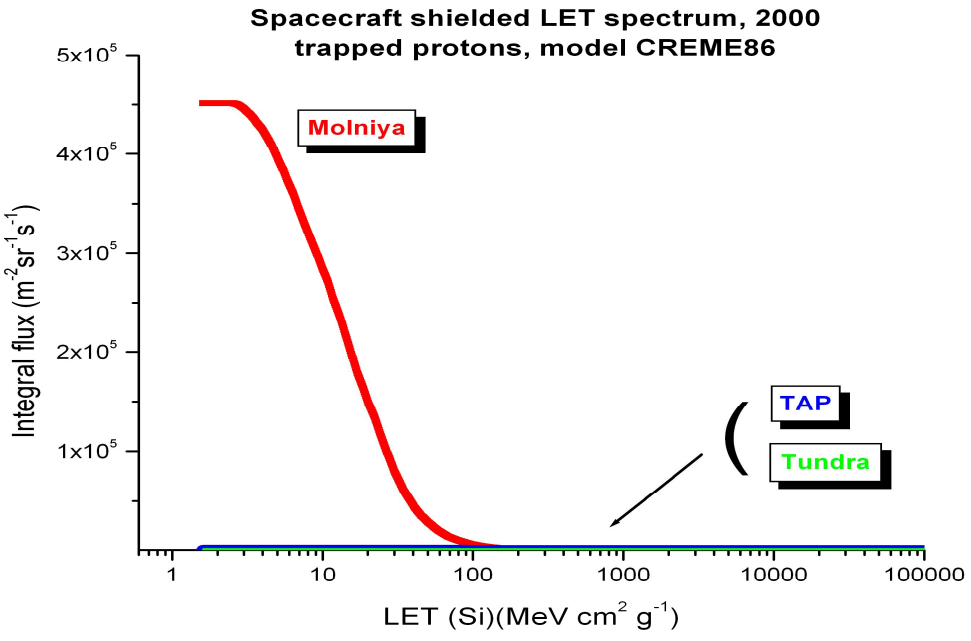

Figure 53. Particle spectra for HEO orbits trapped radiation protons. Calculations are made for solar maxima,

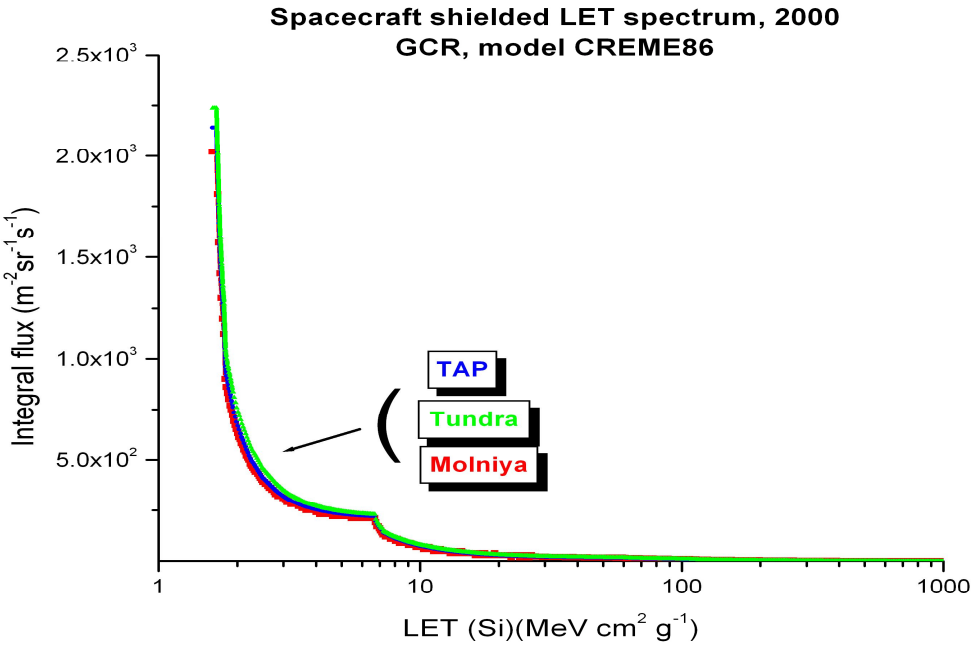

Figure 54. Particle spectra for HEO orbits.
Galactic cosmic rays particles (model M=1)

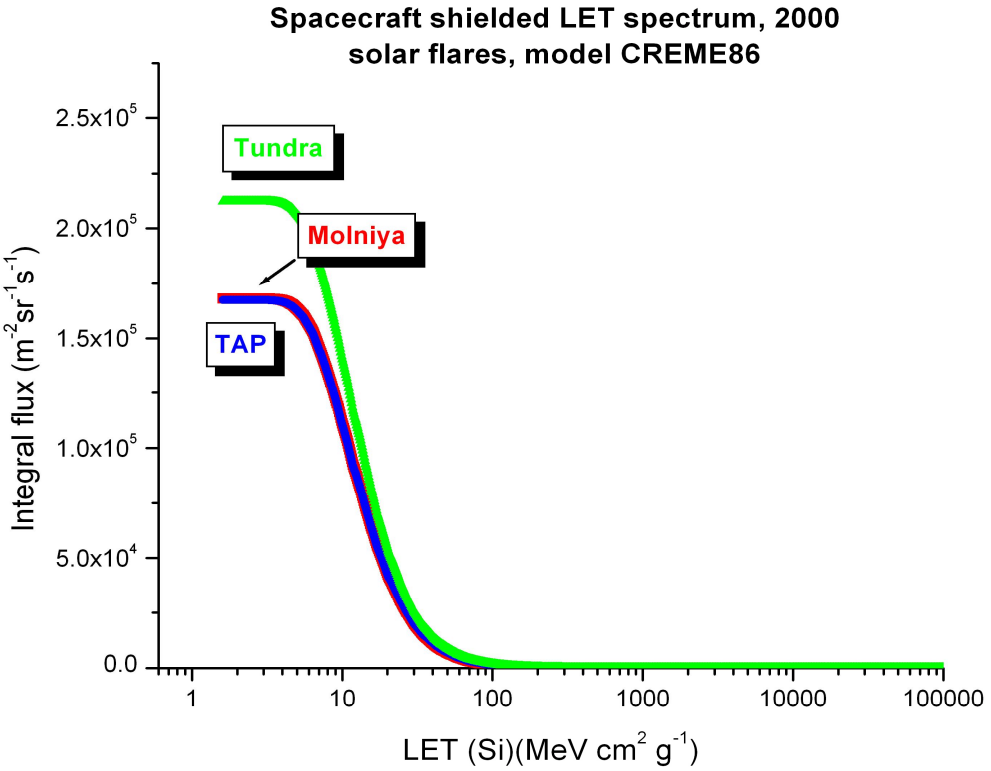

Figure 55. Particle spectra for HEO orbits. Solar flare particles (model CRÈME-86)

11.2 Single event upset rates

Single Event Upset (SEU) occurs when a sufficiently large burst of charge is collected on a critical node in one of the digital microcircuits on a chip. The minimum charge required to produce an SEU is called the critical charge Q_c.

This burst of charge can come from a segment of the ionised trail left by the passage of an intensely ionising particle. It is assumed that each critical node is surrounded by a sensitive volume (idealised as a rectangular parallellopiped = RPP model) and that the charge deposited in this volume is collected. The dimensions of the sensitive volume are related to those of the critical node. The simple model described above predicts that when the critical charge has been collected, an SEU will occur. The amount of charge collected depends linearly on the LET of the ionising particle and the length of its path within the sensitive volume.

SEU rate is calculated based on the flux particle spectra, P(LET)=P(L). Adams (1983) [18] provides the guideline to compute the single event upset rate SEU. The SEU rate U (in $bit^{-1}\ s^{-1}$) is the value of the following integral:

$$U = \pi \cdot A \cdot \left(\frac{X}{e}\right) Q_c \int_{L\,\min}^{L\,\max} \frac{D[p(L)] \cdot F(L)}{L^2} dL ,$$

where

- A is the surface area of the sensitive volume in m^2
- (X/e) the ratio of the energy X that is needed to create one electron-hole pair (3.6 eV in Si) to the elementary charge e (= $1.602 \cdot 10^{-19}$C) that converts pC to MeV
- L the LET in $MeV \cdot cm^2 \cdot g^{-1}$,
- $F(L)$ is the integral LET spectrum in $particles \cdot m^{-2} \cdot s^{-1} \cdot sr^{-1}$,
- $D[p(L)]$ the differential path length distribution in the sensitive volume of each memory cell in $cm^2 \cdot g^{-1}$
- $p(L)=(X/e) \cdot Q_c/L$ is the path length over which an ion of LET L will produce a charge Q_c,
- $L_{min}=(X/e) \cdot Q_c/p_{max}$ the required minimum LET in $MeV \cdot cm^2 \cdot g^{-1}$ for an upset;
- $L_{max}=1.05 \times 10^5$ $MeV \cdot cm^{2} \cdot g^{-1}$ the highest LET any stopping ion can deliver,
- Q_c the minimum charge in pC required to produce an upset,
- p_{max} the largest diameter of the sensitive volume in $g \cdot cm^{-2}$.

SPENVIS provides the minimum charge required to produce an upset, Q_c= 0.0013 pC.

The results of SPENVIS calculation for SEU rate is in Table 2. It demonstrates that SEU rate for TAP orbit is approximately an order of magnitude less than for Molniya orbit and approximately 20% less than for Tundra orbit.

Table 2. SEU based on direct ionization and proton induced ionization on HEO orbits.

Orbit	Direct ionisation $bit^{-1}s^{-1}$	Proton induced ionization $bit^{-1}s^{-1}$	Total ionisation $bit^{-1}s^{-1}$
Molniya	1.1027E-05	7.3407E-09	1.1034-05
TAP	2.7297E-06	1.3598E-08	2.7433E-06
Tundra	3.4470E-06	1.7113E-08	3.4641E-06

12 Total Ionizing Doze

The top-level ionizing dose environment is represented by the dose depth curve. This curve provides a dose as a function of spherical shielding. The dose depth curve can be calculated with the SHIELDOSE model. The SHIELDOSE model is based on a large data set containing the dose per unit of incident fluence as a function of depth of Aluminium shielding and particle energy.

Total ionizing mission dose for HEO orbits was evaluated by application of SHIELDOSE software (SPENVIS) for target material Si with the spherical shielding, in the centre of Al spheres. We compare here the results which were obtained with use of AE8/ AP8 and AE9/AP9 models. Calculation of solar protons were made based on ESP-PSYCHIC model for the total fluence for ions in the range from H to U. The magnetic shielding was taken in the form of IGRF model.

Total mission ionizing dose is plotted on Figure 56-Figure 60. The total ionizing dose consists of the ionizing dose from the trapped electrons (see Figure 61-Figure 65), trapped protons (Figure 66-Figure 70), ionization due to Bremsstrahlung (see Figure 71-Figure 75) and solar protons (Figure 76). Bremsstrahlung is electromagnetic radiation produced by the deceleration of a charged particle such as an electron when it collides with another object.

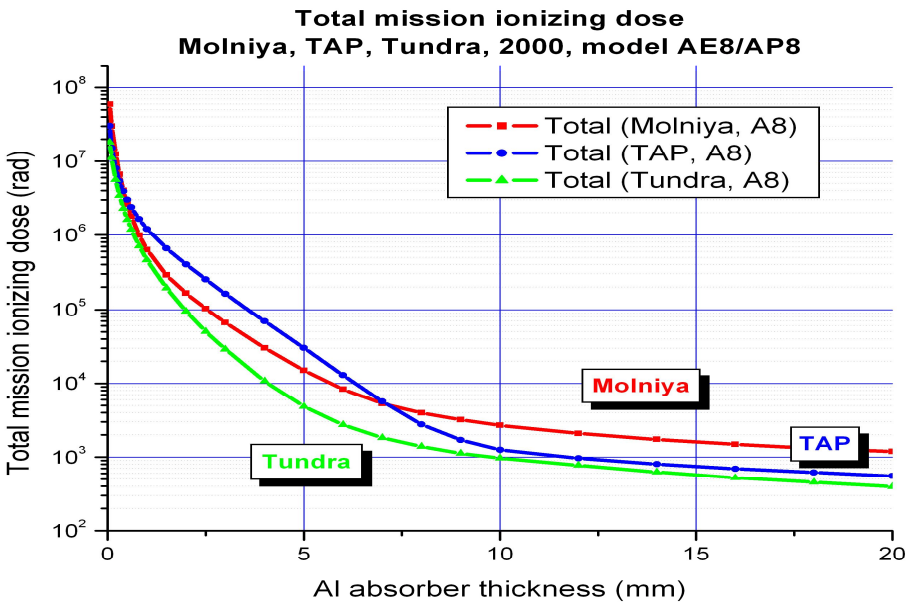

Figure 56. Total mission ionizing dose for different Al shielding thicknesses. HEO orbits, 2000. Model AE8/AP8

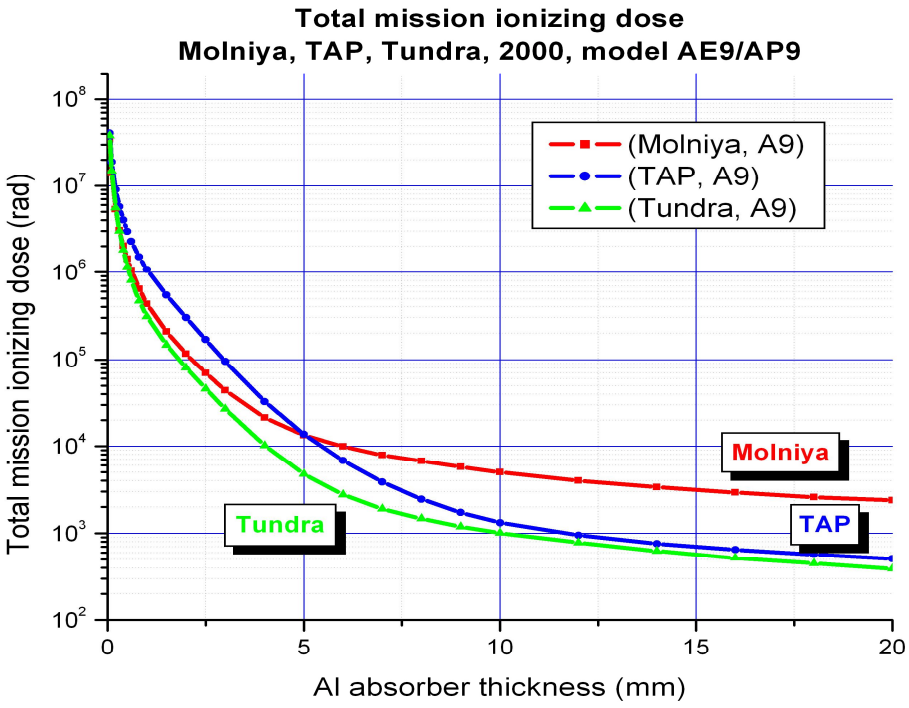

Figure 57. Total mission ionizing dose for different Al shielding thicknesses. HEO orbits, 2000. Model AE9/AP9

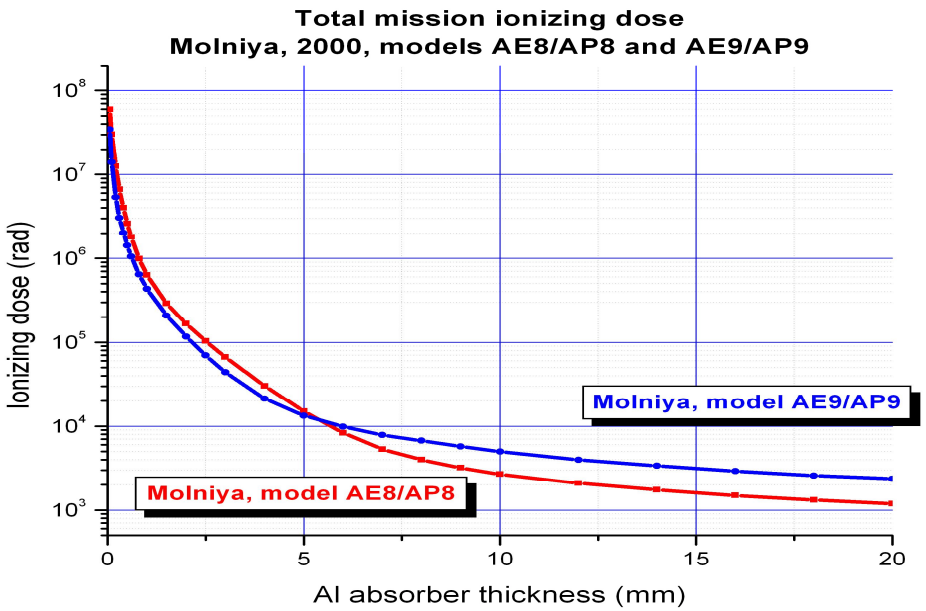

Figure 58. Total mission ionizing dose for different Al shielding thicknesses. Molniya orbit, 2000. Models AE8/AP8 and AE9/AP9.

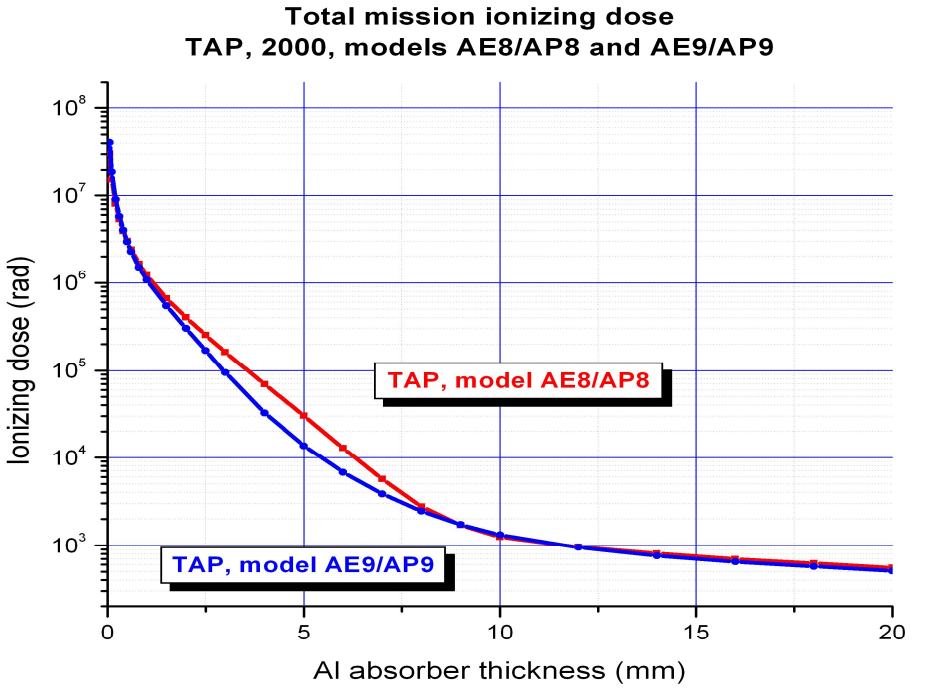

Figure 59. Total mission ionizing dose for different Al shielding thicknesses. TAP, 2000. Models AE8/AP8 and AE9/AP9.

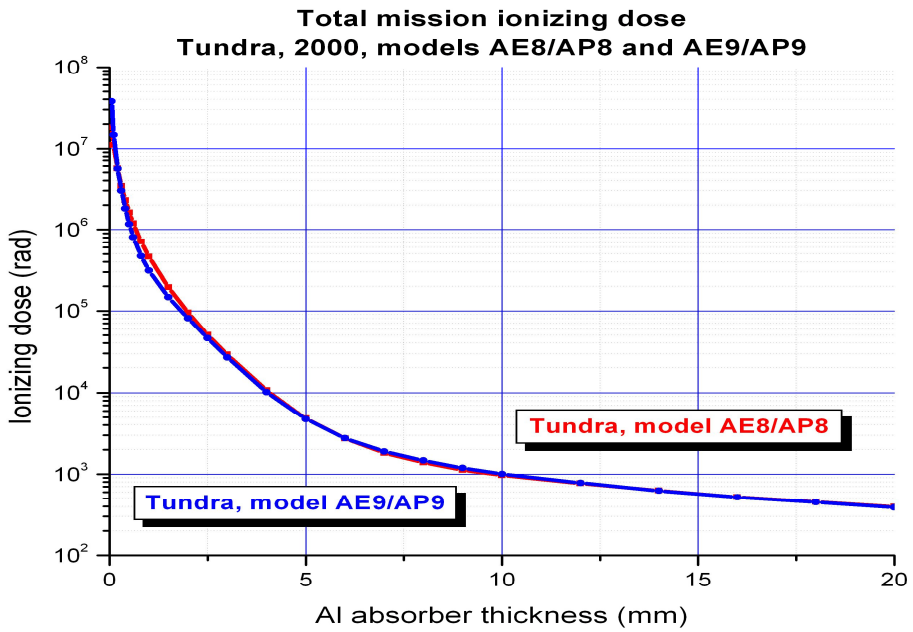

Figure 60. Total mission ionizing dose for different Al shielding thicknesses. Tundra, 2000. Models AE8/AP8 and AE9/AP9.

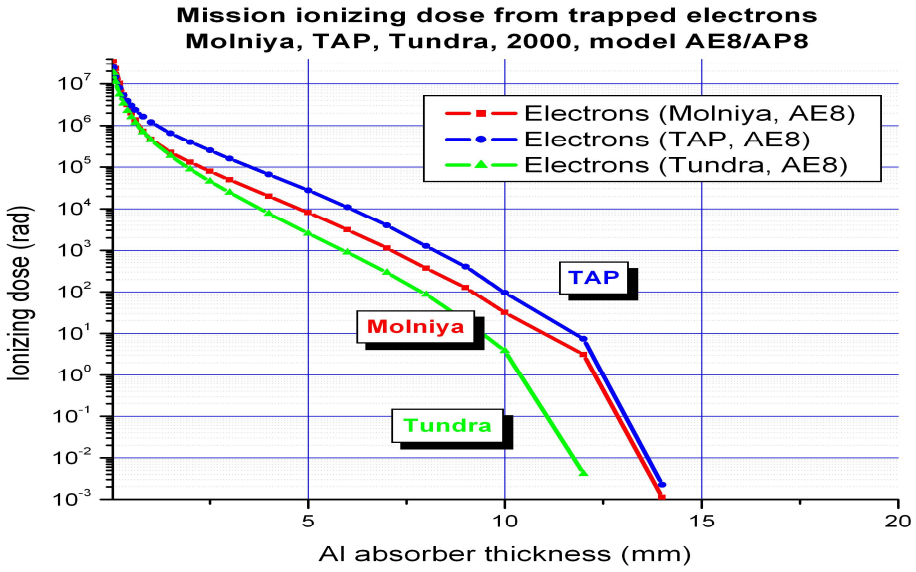

Figure 61. Mission ionizing dose from trapped electrons for different Al shielding thicknesses. HEO orbits, 2000. Model AE8.

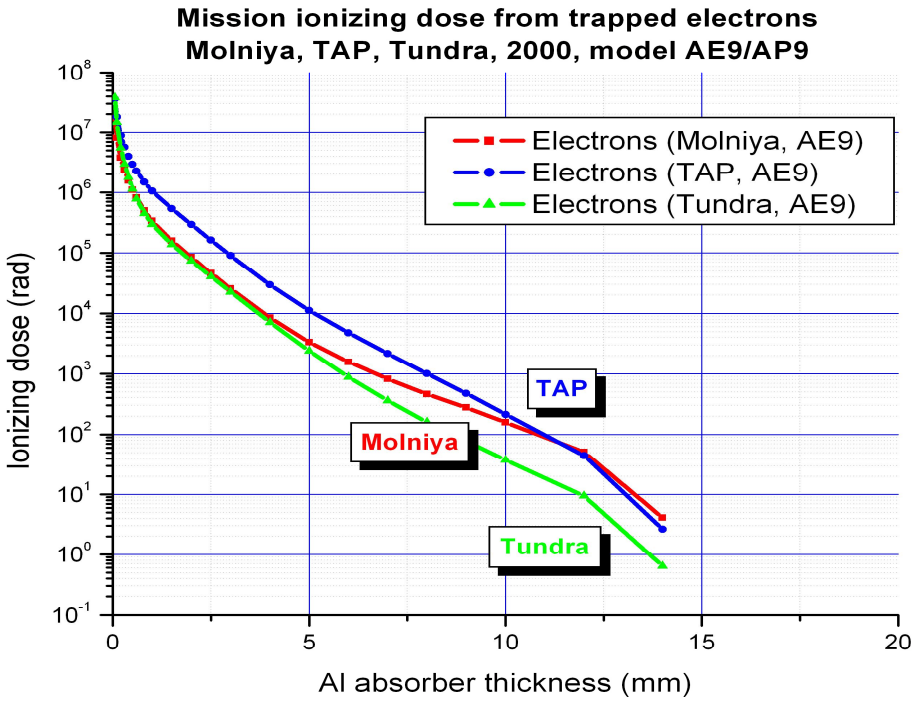

Figure 62. Mission ionizing dose from trapped electrons for different Al shielding thicknesses. HEO orbits, 2000. Model AE9.

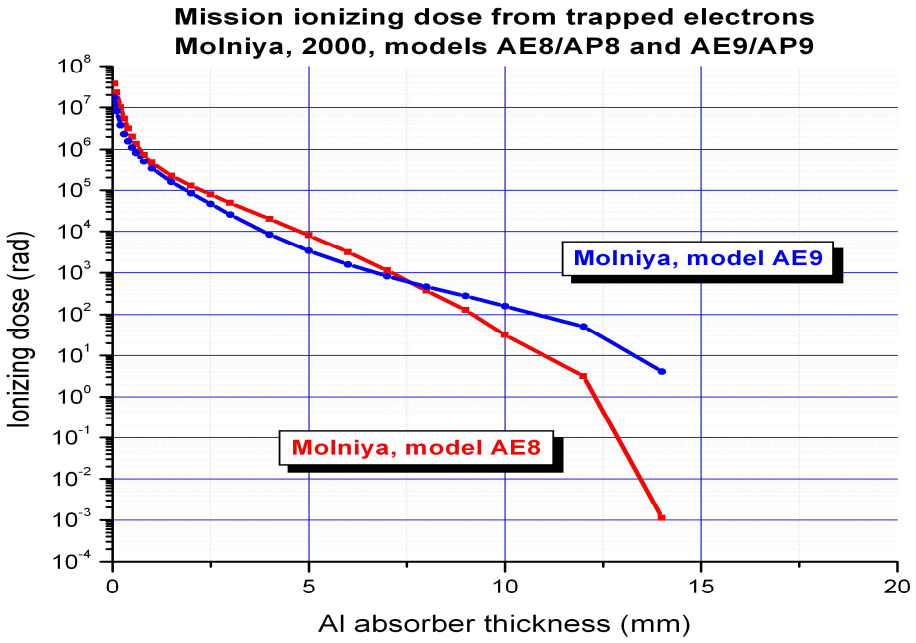

Figure 63. Mission ionizing dose from trapped electrons for different Al shielding thicknesses. Molniya orbit, 2000. Models AE8, AE9.
Models AE8 and AE9.

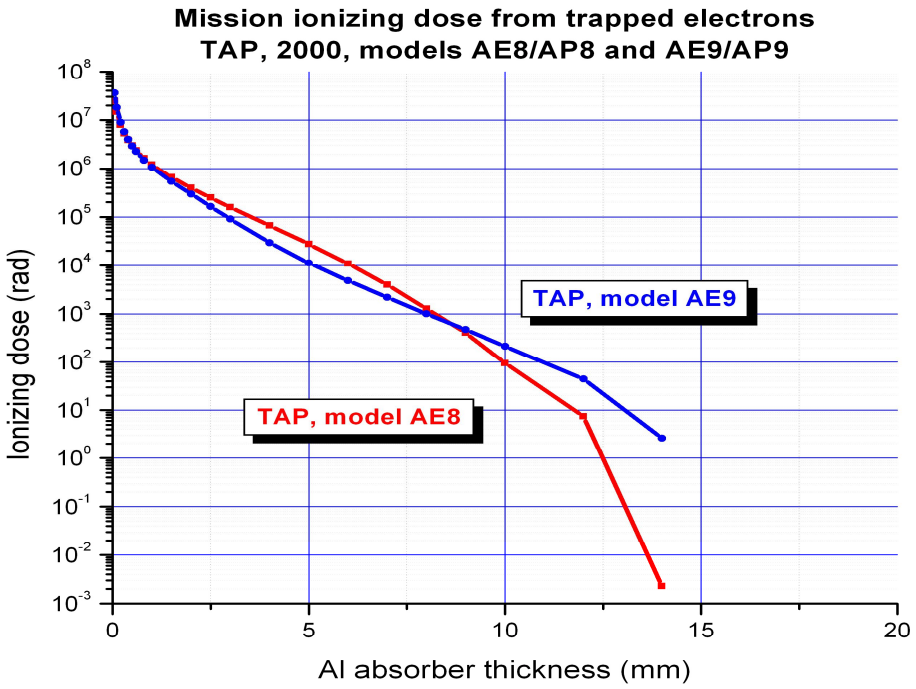

Figure 64. Mission ionizing dose from trapped electrons for different Al shielding thicknesses. TAP, 2000. Models AE8, AE9.

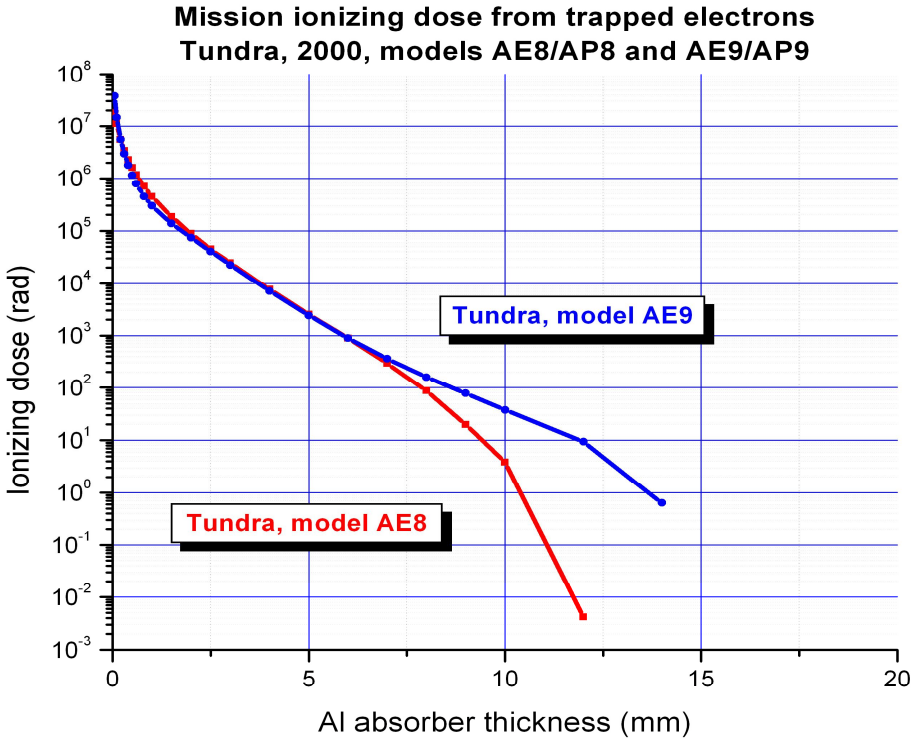

Figure 65. Mission ionizing dose from trapped electrons for different Al shielding thicknesses. Tundra orbit, 2000. Models AE8, AE9.

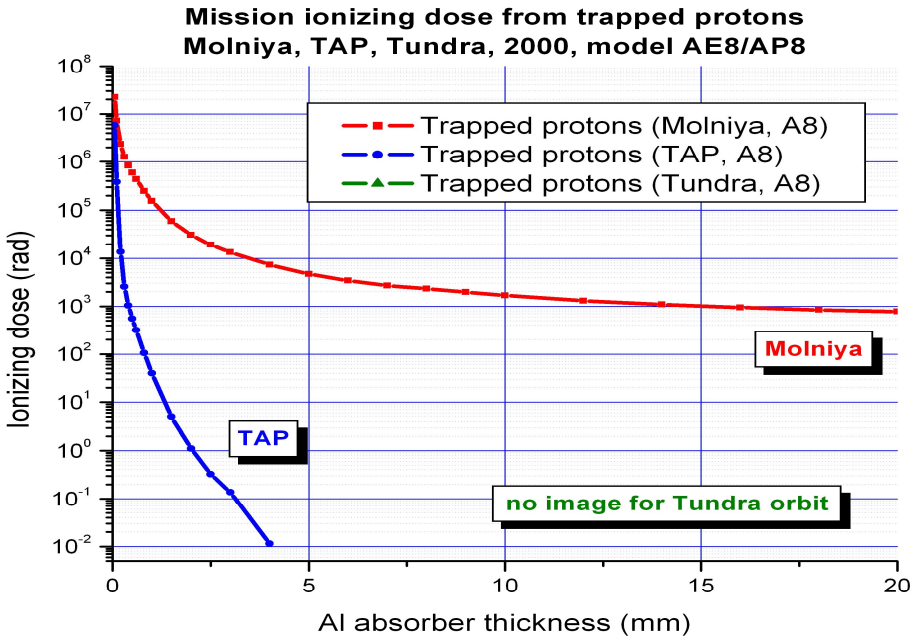

Figure 66. Mission ionizing dose from trapped protons for different Al shielding thicknesses. HEO orbits, 2000. Model AP8.

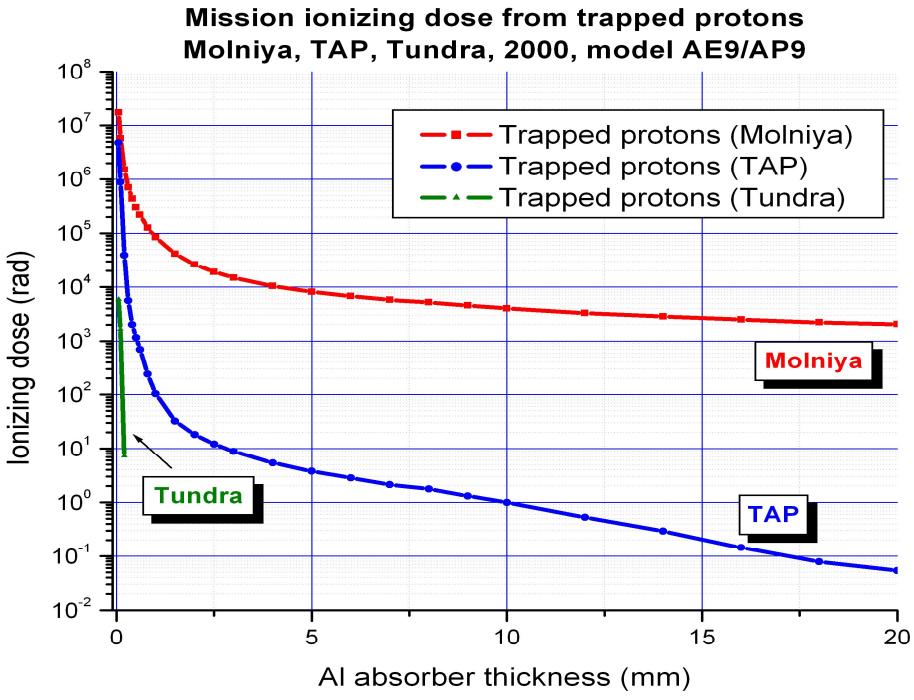

Figure 67. Mission ionizing dose from trapped protons for different Al shielding thicknesses. HEO orbits, 2000. Model AP9.

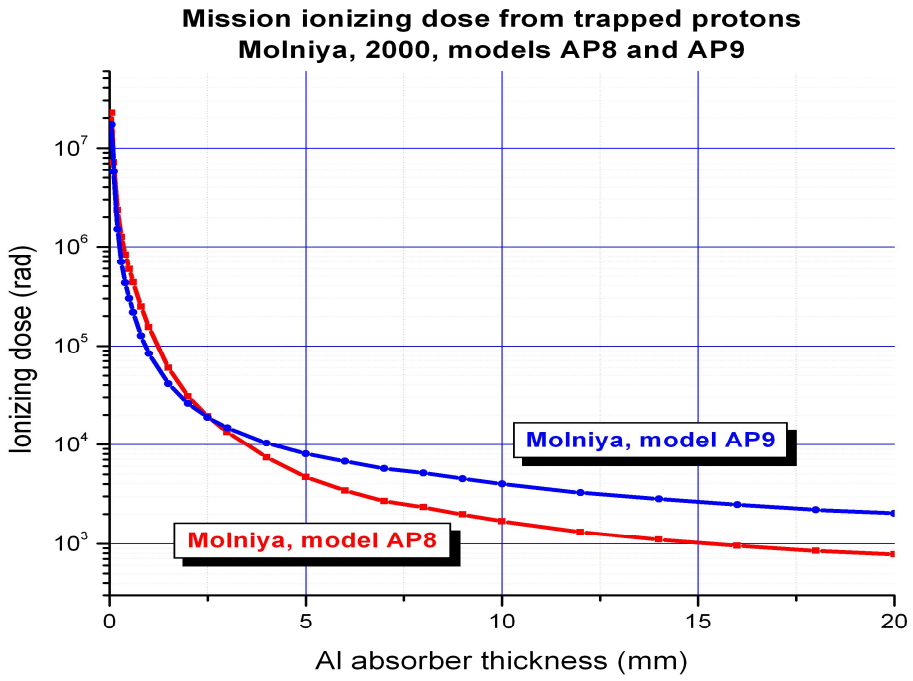

Figure 68. Mission ionizing dose from trapped protons for different Al shielding thicknesses. Molniya, 2000. Models AP8, AP9.

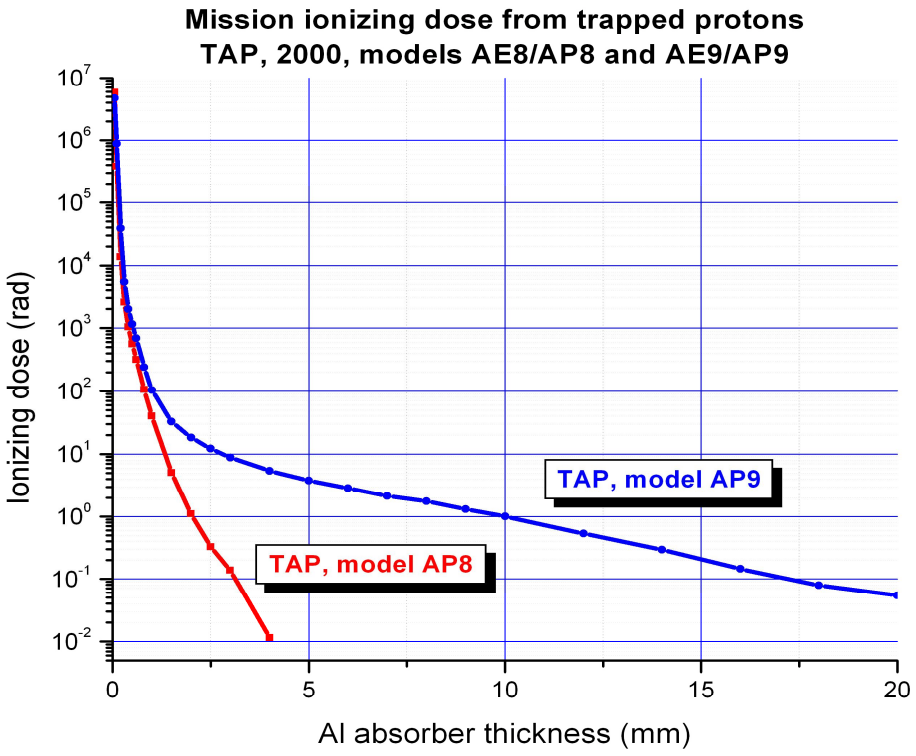

Figure 69. Mission ionizing dose from trapped protons for different Al shielding thicknesses. TAP, 2000. Models AP8, AP9. There are no data for the ionizing dose from trapped protons in AP8 model for Al thickness greater than 4 mm.

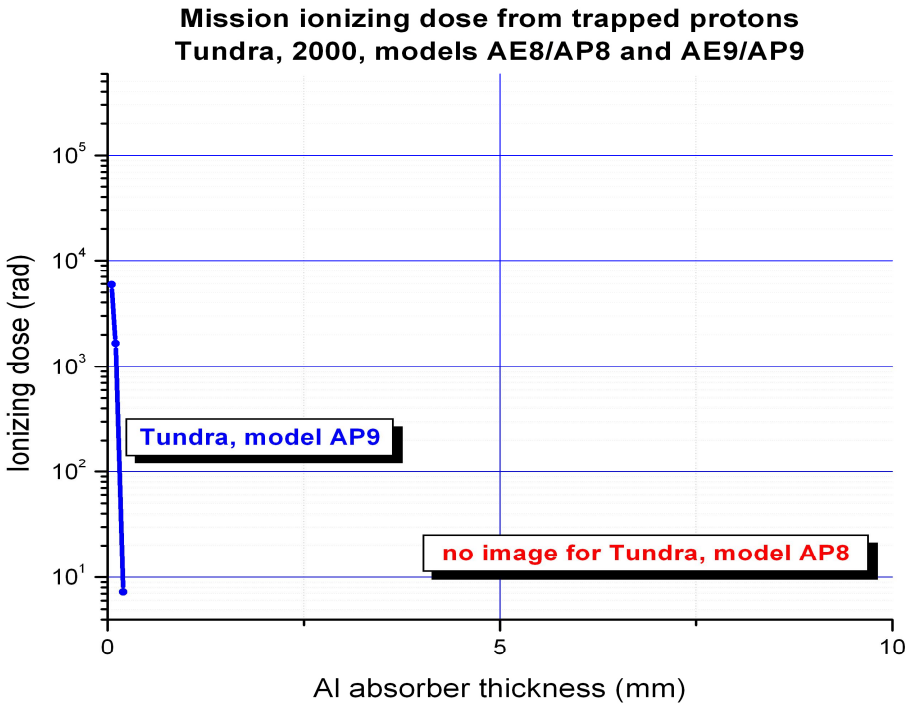

Figure 70. Mission ionizing dose from trapped protons for different Al shielding thicknesses. Tundra, 2000. Models AP8, AP9. There are no data for the ionizing dose from trapped protons in AP8 model for Tundra orbit.

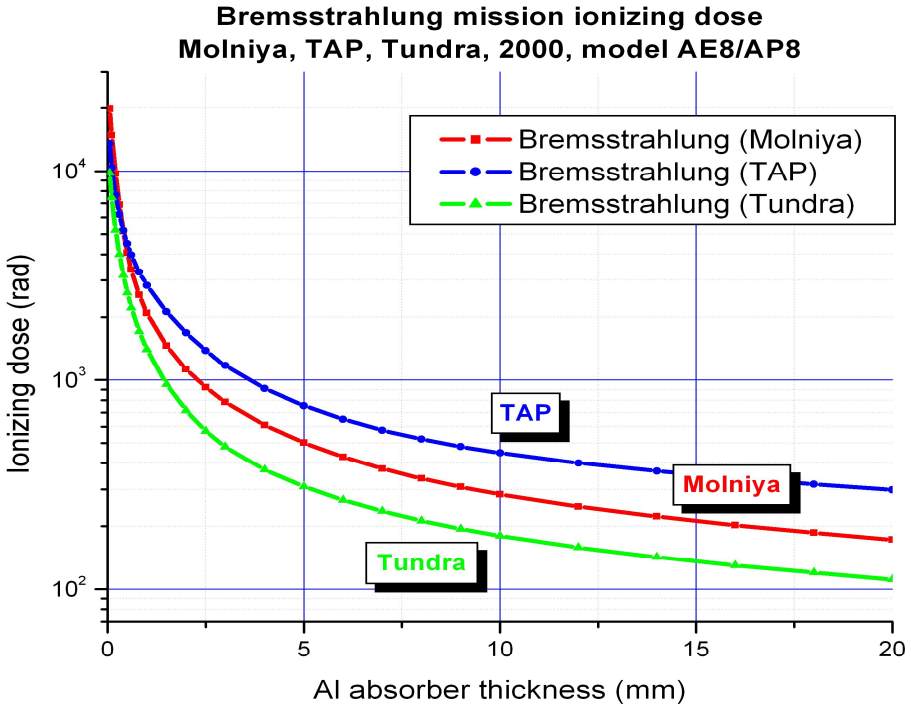

Figure 71. Bremsstrahlung mission ionizing dose for different Al shielding thicknesses. HEO orbits, 2000. Models AE8/AP8.

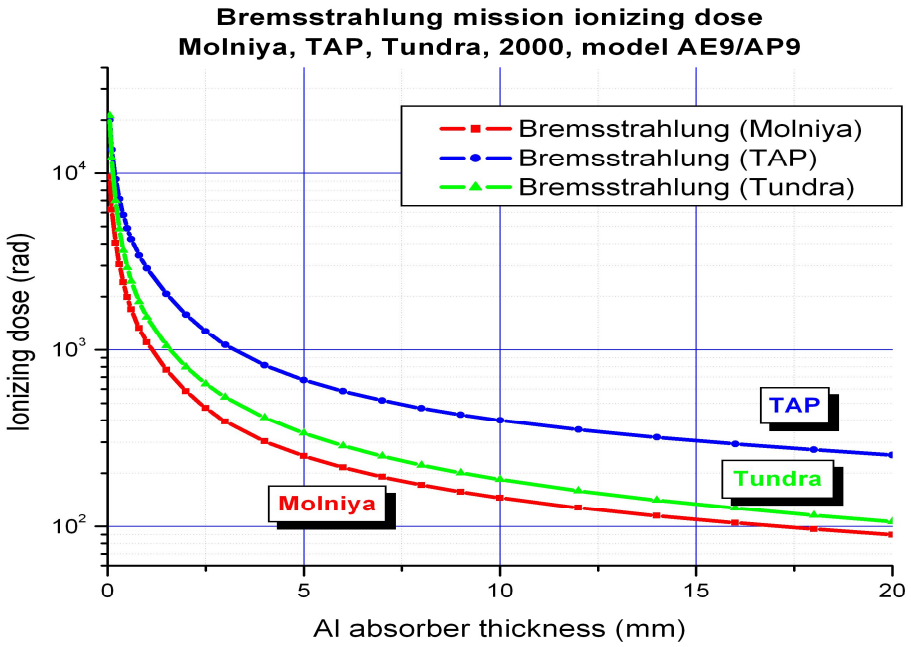

Figure 72. Bremsstrahlung mission ionizing dose for different Al shielding thicknesses. HEO orbits, 2000. Models AE9/AP9.

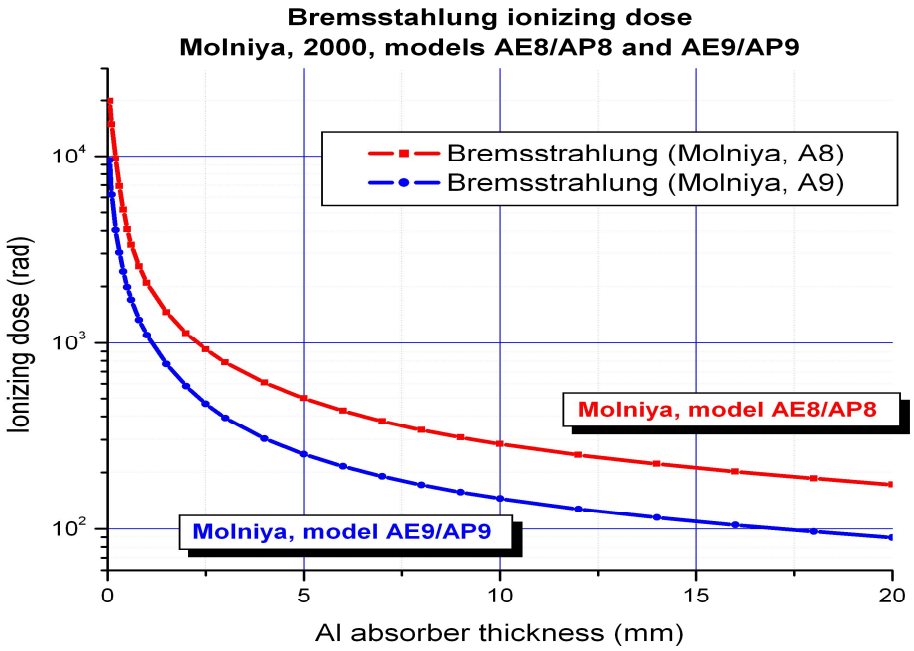

Figure 73. Bremsstrahlung ionizing dose for different Al shielding thicknesses. TAP, 2000. Models AE8/ AP8, AE9/ AP9.

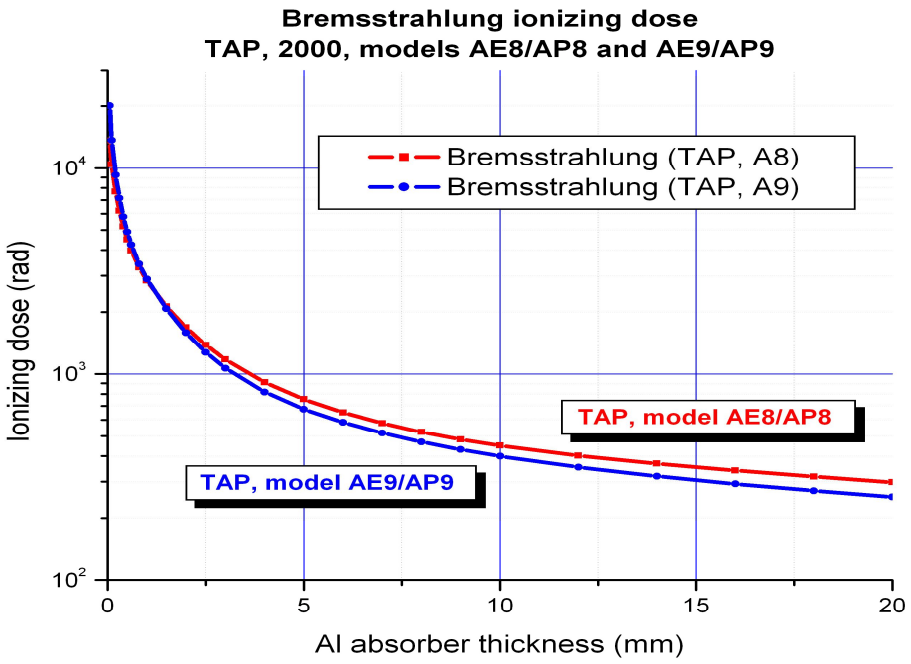

Figure 74. Bremsstrahlung ionizing dose for different Al shielding thicknesses. TAP, 2000. Models AE8/ AP8, AE9/ AP9.

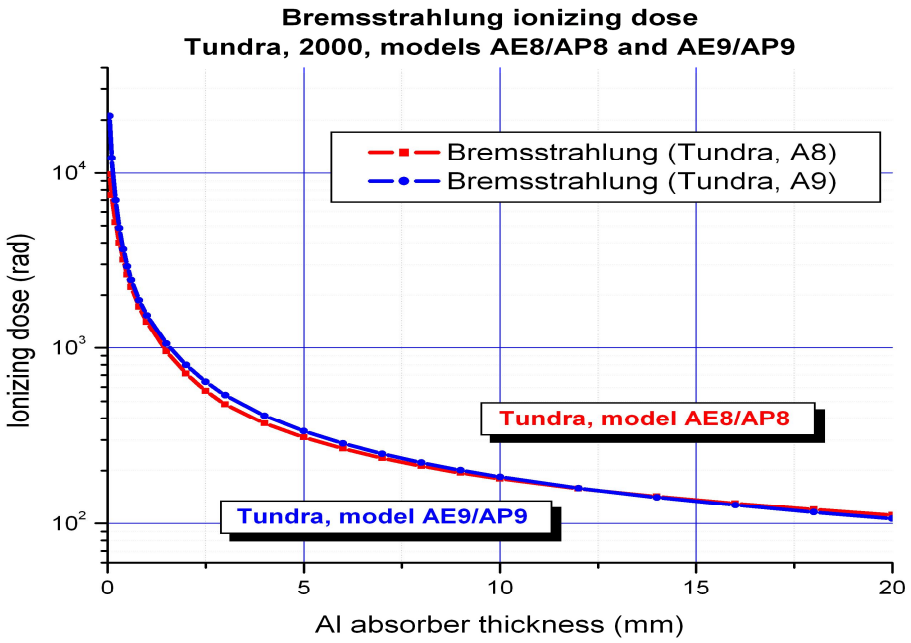

Figure 75. Bremsstrahlung ionizing dose for different Al shielding thicknesses. Tundra orbit, 2000. Models AE8/ AP8, AE9/ AP9.

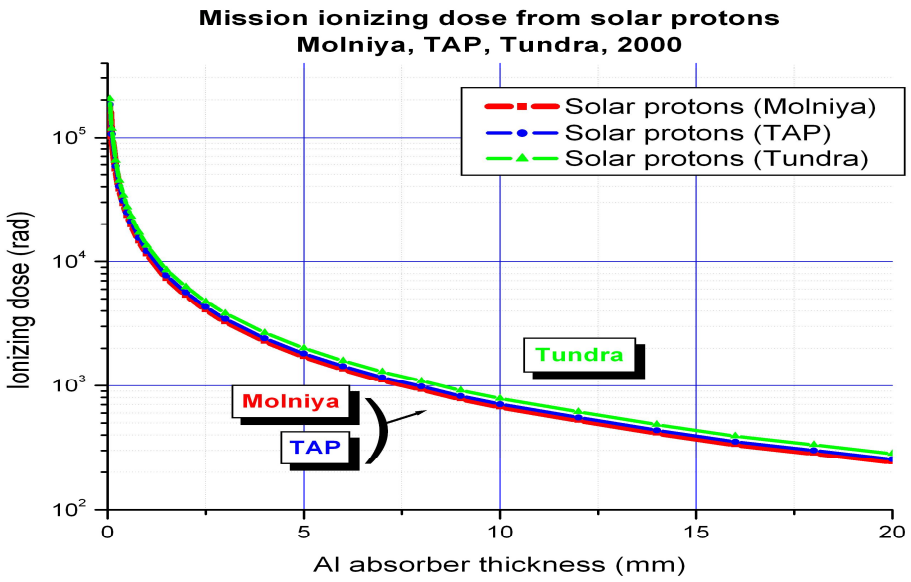

Figure 76. Mission ionizing dose from solar protons for different Al shielding thicknesses. HEO orbits, 2000.

We can conclude that the ionizing dose caused by the trapped electrons and Bremsstahlung is higher for TAP orbit than for Molniya and Tundra orbits, but the ionizing dose caused by trapped protons is less for TAP orbit than for Molniya orbit. The ionizing dose caused by solar protons is the highest for Tundra orbit and approximately the same for both TAP and Molniya orbits.

Overall, the total ionizing dose is less for Tundra orbit than for TAP and Molniya orbits. The ionizing dose for TAP orbit is less than the dose for Molniya orbit for larger energies, when the Aluminium absorbing shielding is > 7 mm (for models AE8/AP8) and > 5mm (for models AE9/AP9).

13 Discussion

In this study different available models for the radiation environment in HEO orbits were used. For the trapped radiation we used both the old models AE8/AP8 which has been used for several decades and the new models AE9/AP9 which has just become available. This comparison was made for three orbits which are under consideration for the Polar Communication Mission.

We also made an assessment of different models of solar energetic particles and galactic cosmic rays which are available in SPENVIS software to know how application of different models can change the result of the radiation assessment.

The comparison of these models in application to HEO orbits gives us a better understanding of the radiation environment on these orbits.

Acknowledgements

We acknowledge the AE9/AP9/SPM development team: the Air Force Research Laboratory and the National Reconnaissance Office in partnership with MIT Lincoln Laboratory, Aerospace Corporation, Los Alamos National Laboratory, Boston College Institute for Scientific Research, and Atmospheric and Environmental Research, Incorporated.

References:

1. Trichtchenko, L. Radiation environment analysis for Canadian Polar Communication and Weather mission; Geological Survey of Canada, Open File 7252, 2012; 139 pages, doi:10.4095/291813
2. Spenvis software, http://www.spenvis.oma.be
3. Trishchenko, A., and Garand,L., Spatial and Temporal Sampling of Polar Regions from Two-Satellite System on Molniya Orbit, Journ. Of Atmospheric and Oceanic Technology, V 28, pp. 977-992, 2011.
4. Trishchenko, A.P., Garand, L., and Trichtchenko, L.D. Three apogee 16-h highly elliptical orbit as optimal choice for continuous meteorological imaging of polar regions, *Journal of Atmospheric and Oceanic Technology*. Vol. 28, No. 11. pp.1407-1422, 2011.
5. Capderou M., *Satellites: Orbits and Missions,* Vol. 1, ISBN 2-287-21317-1, Springer-Verlag France 2005, Chapter 5.
6. Ginet, G.P., O'Brien, T.P., Huston, S.L., Johnston, W.R., Guild, T.B., Friedel, R., Lindstrom, C.D., Roth, C.J., Whelan, P., Quinn, R.A., Madden, D., Morley, S., Yi-Jiun Su, AE9, AP9 and SPM : New models for specifying the trapped energetic particle and Space Plasma Environment, *Space Sc. Rev*, 2013
7. http://lws-set.gsfc.nasa.gov/documents/AE9-AP9_Requirements_v4.pdf AE-9/AP-9 Trapped Radiation and Plasma Models. Requirements Specification. 31 Mar 2009. G. P. Ginet, Air Force Research Laboratory, T. P. O'Brien, The Aerospace Corporation
8. Trichtchenko,L., Nikitina,L., Harrison, M. Statistical analysis of space environment on highly elliptical orbits. HEO1 and HEO3 missions data, , Geological Survey of Canada, Open File 7389, 2013, 144 pages, doi:10.4095/292717
9. Space engineeringg. Space environment. European cooperation for space standardization. ECSS-E-10-04A. 21 January 2000.
10. Program of Radiation hardness assurance for space systems by Christian Poivey (SGT-Inc, NASA GSFC)
11. King, J. H., Solar Proton Fluences for 1977-1983 Space Missions, *J. Spacecraft Rockets, 11*, 401, 1974.

12. Feynman, J., G. Spitale, J. Wang, and S. Gabriel, Interplanetary Proton Fluence Model: JPL 1991, *J. Geophys. Res., 98*, 13,281-13,294, 1993.
13. Xapsos, M. A., Summers, G.P., Barth, J.L., Stassinopoulos, E.G. and Burke, E.A. Probability Model for Cumulative Solar Proton Event Fluences, *IEEE Trans. Nucl. Sci., 47*, 486-490, 2000.
14. Xapsos, M. A., Summers, G.P., Barth, J.L., Stassinopoulos, E.G. and Burke, E.A. Probability Model for Worst Case Solar Proton Event Fluences, *IEEE Trans. Nucl. Sci., 46*, 1481-1485, 1999.
15. Rosenqvist, L., Hilgers, A., Evans, H., Daly, E.A., Hapgood, M., Stamper, R., Zwickl, R., Bourdarie, S. and Boscher, D. : Toolkit for Updating Interplanetary Proton-Cumulated Fluence Models, *Journal of Spacecraft and Rockets*, Vol. 42, No. 6, 2005.
16. Walkden, M.V., 1980, Proton-to-electron damage ratios for some modern types of solar cells, *Solar cells*, V.2, Issue 1, p.25-29.
17. Xapsos, M.A., Stauffer, C., Jordan, T., Barth, J.L. and Mewaldt, R.A. Model for Cumulative Solar Heavy Ion Energy and Linear Energy Transfer Spectra, *IEEE Trans. Nucl. Sci., 54, No. 6*, December 2007.
18. Adams, J. H., Jr., The Variability of Single Event Upset Rates in the Natural Environment, *IEEE Trans. Nucl. Sci., 30*, 4475-4480, 1983.

Appendix 1. Time distribution of the trapped radiation. Electron fluxes and fluences

Molniya. 1 February 2000, electron fluxes and fluences.

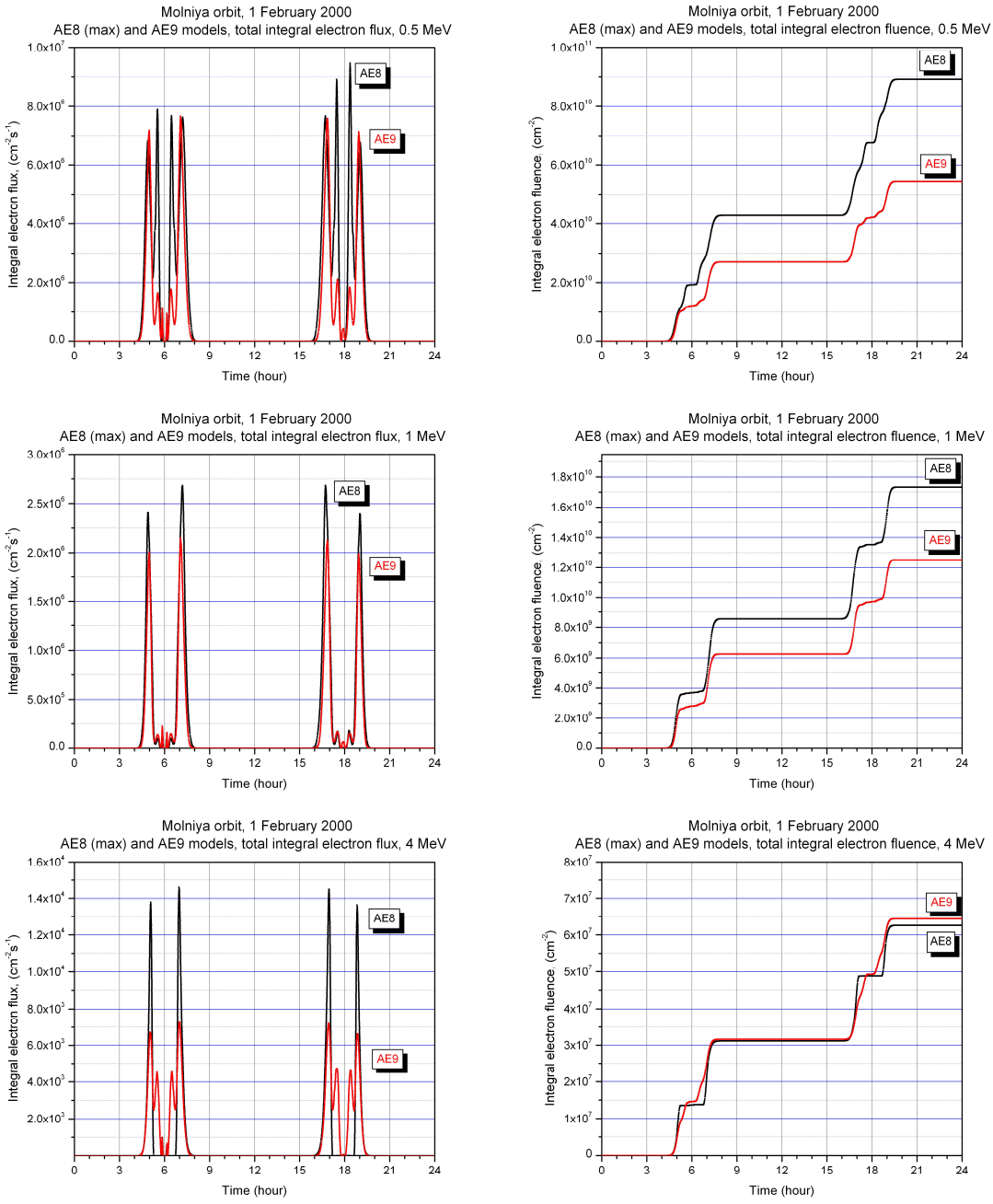

Figure 77. Electron flux variations along Molniya orbit and the total integral electron fluence (energy 0.5MeV, 1MeV, 4MeV)

TAP orbit, 1-2 February 2000, electron fluxes and fluences

.

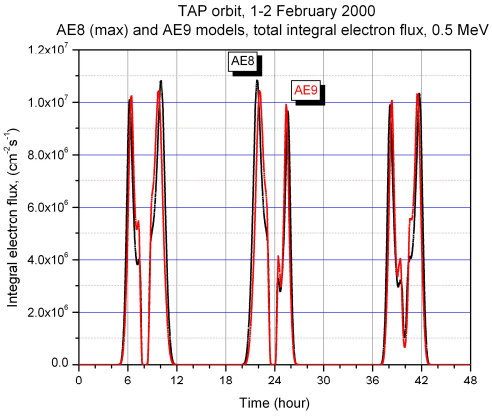
TAP orbit, 1-2 February 2000
AE8 (max) and AE9 models, total integral electron flux, 0.5 MeV
AE8
AE9
Integral electron flux, (cm-2s-1)
Time (hour)

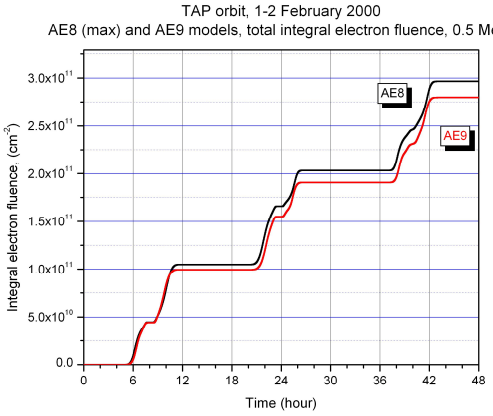
TAP orbit, 1-2 February 2000
AE8 (max) and AE9 models, total integral electron fluence, 0.5 MeV
AE8
AE9
Integral electron fluence, (cm-2)
Time (hour)

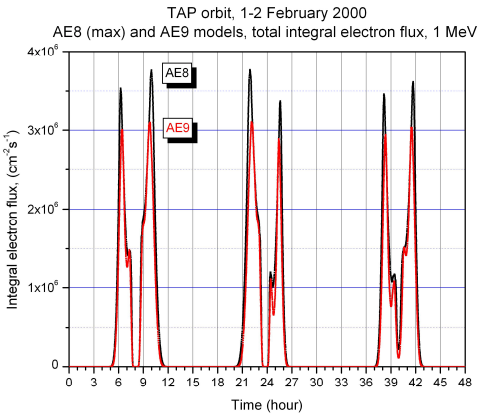
TAP orbit, 1-2 February 2000
AE8 (max) and AE9 models, total integral electron flux, 1 MeV
AE8
AE9
Integral electron flux, (cm-2s-1)
Time (hour)

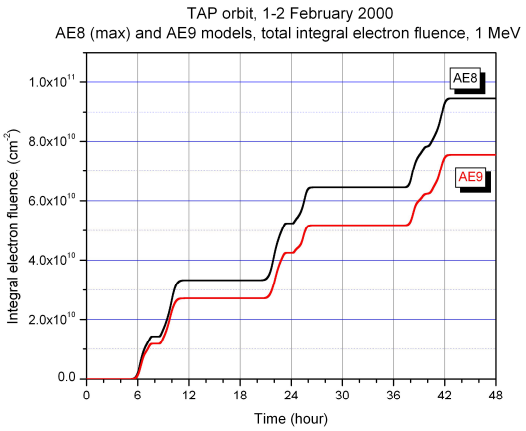
TAP orbit, 1-2 February 2000
AE8 (max) and AE9 models, total integral electron fluence, 1 MeV
AE8
AE9
Integral electron fluence, (cm-2)
Time (hour)

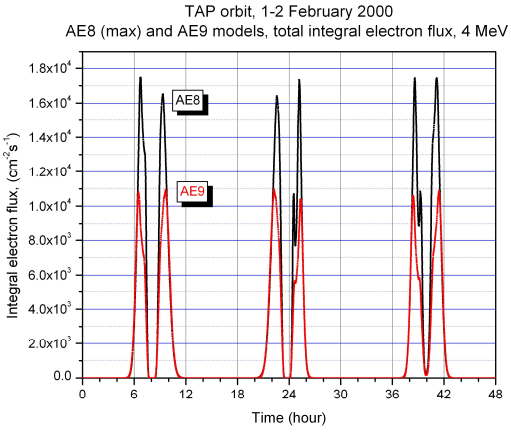
TAP orbit, 1-2 February 2000
AE8 (max) and AE9 models, total integral electron flux, 4 MeV
AE8
AE9
Integral electron flux, (cm-2s-1)
Time (hour)

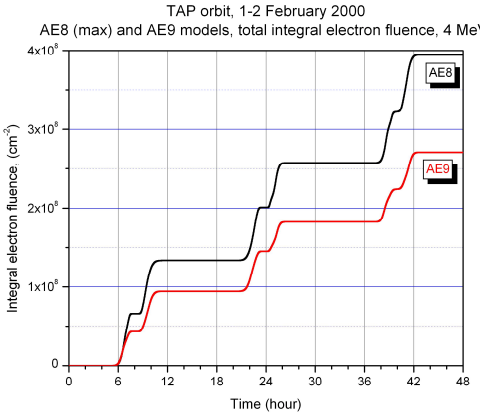
TAP orbit, 1-2 February 2000
AE8 (max) and AE9 models, total integral electron fluence, 4 MeV
AE8
AE9
Integral electron fluence, (cm-2)
Time (hour)

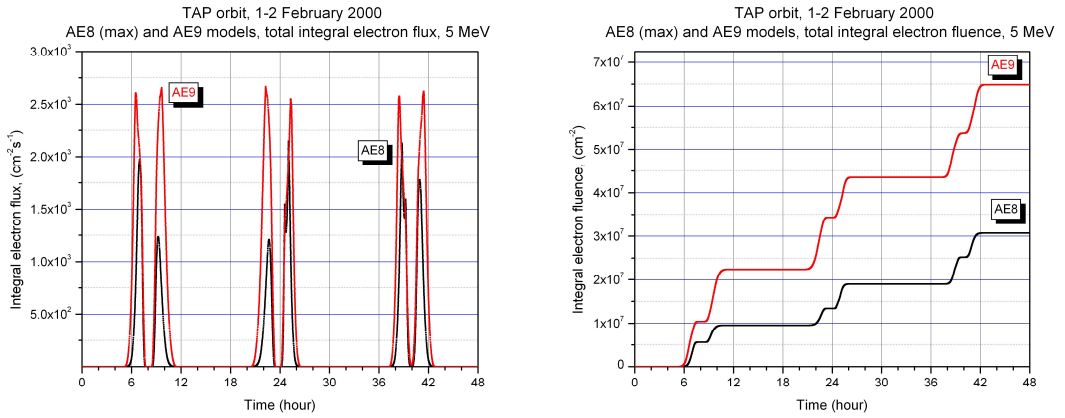

Figure 78. Electron flux variations along TAP orbit and the total integral electron fluence (energy 0.5MeV, 1MeV, 4MeV, 5 MeV)

Tundra orbit, 1 February 2000, electron fluxes and fluences.

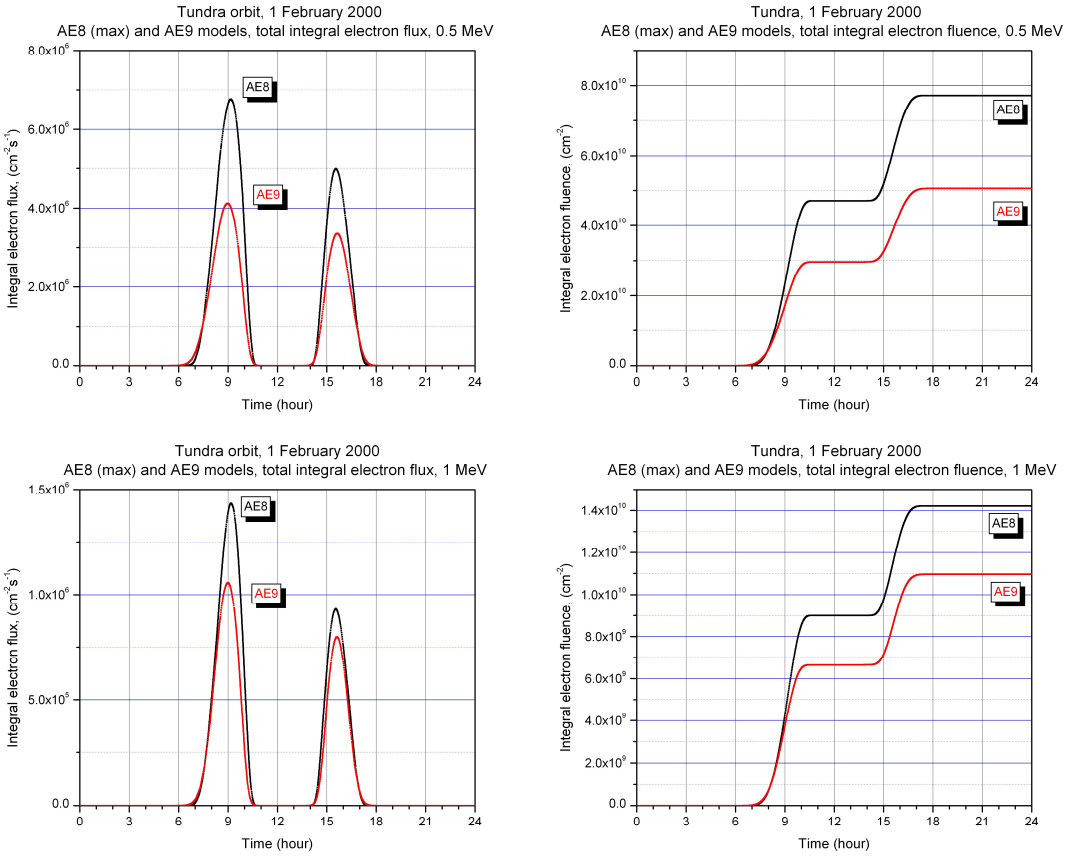

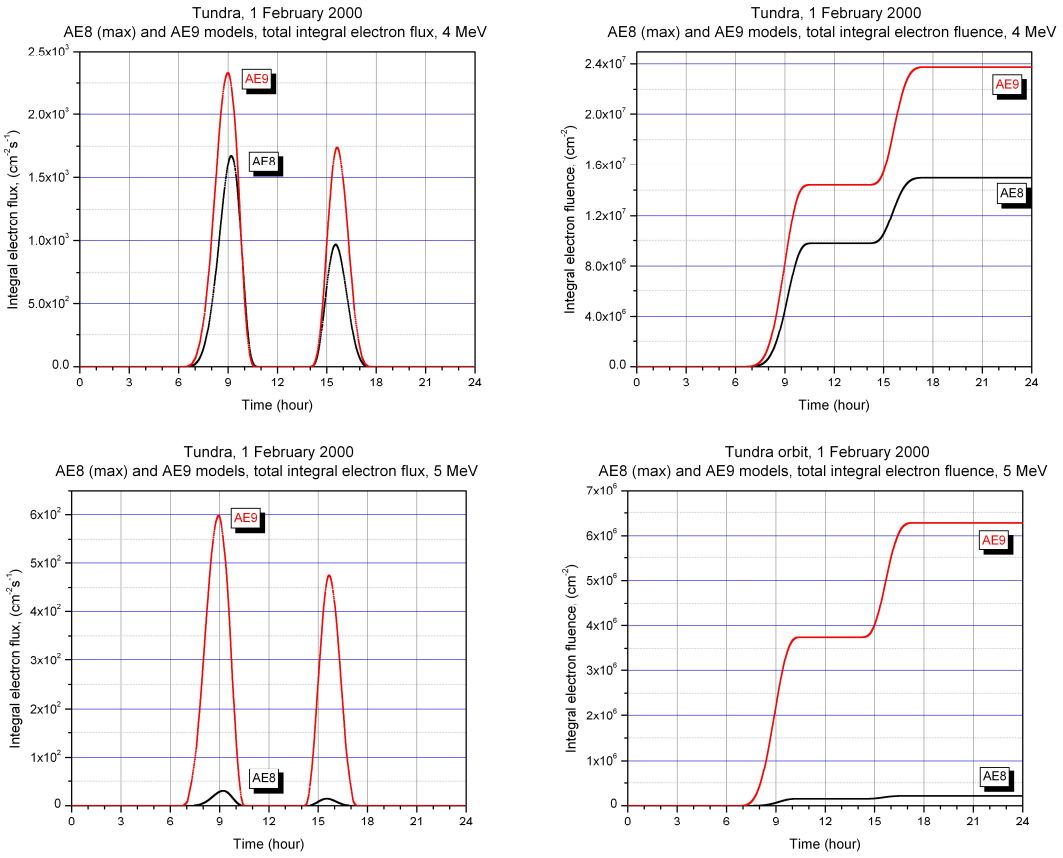

Figure 79. Electron flux variations along Tundra orbit and the total integral electron fluence (energy 0.5MeV, 1MeV, 4MeV, 5MeV)

Appendix2. Time distribution of the trapped radiation. Proton fluxes and fluences.

We considered the proton environments on three orbits, Molniya, TAP, and Tundra orbit for 1 February 2000.

Molniya 1 February 2000, protons

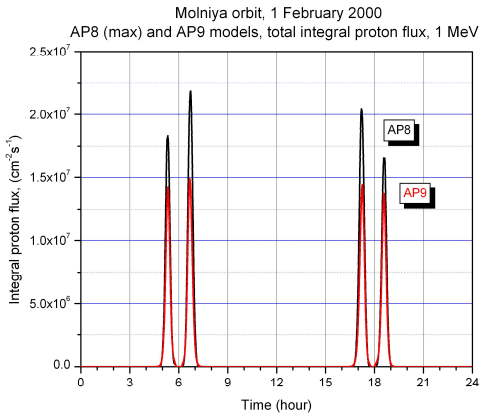

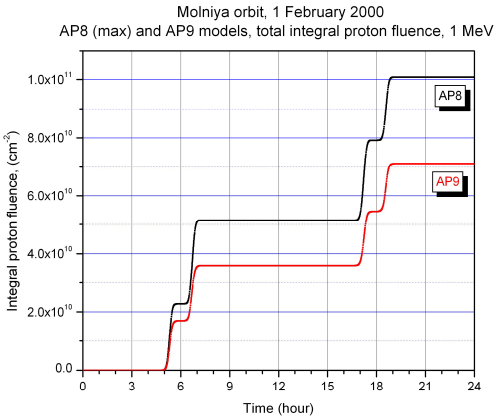

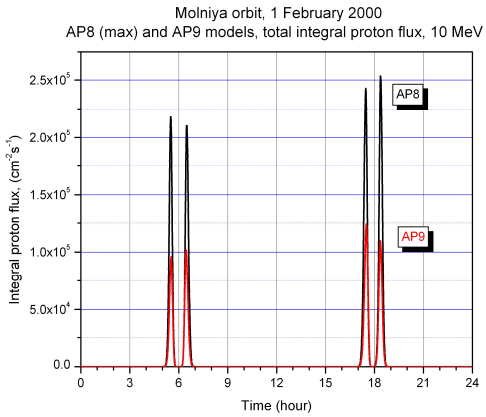

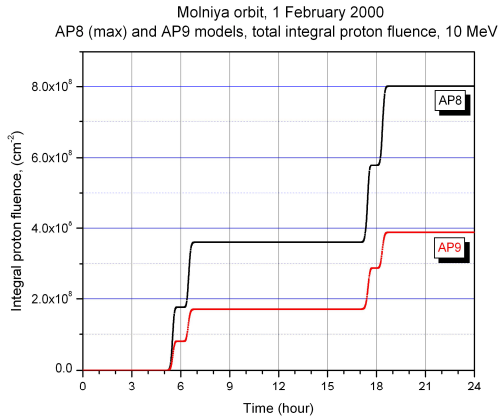

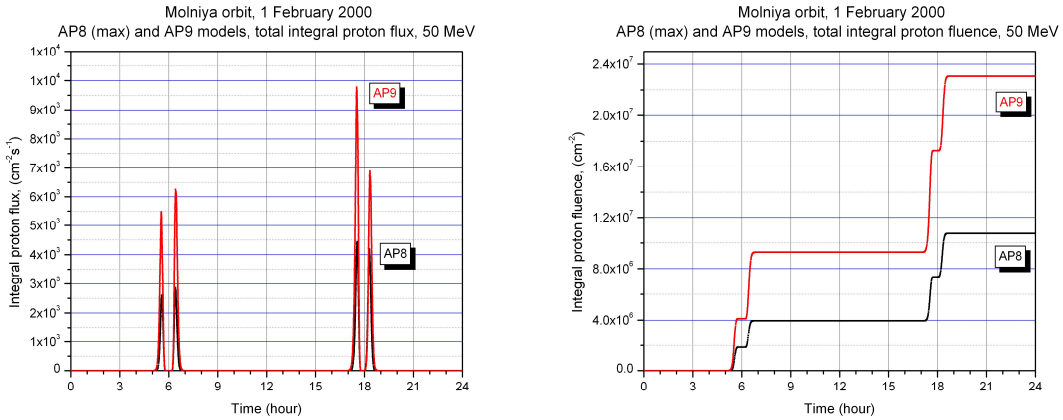

Figure 80. Proton flux variations along Molniya orbit and the total integral proton fluence (energy 1MeV, 10MeV, 50MeV)

TAP orbit, 1-2 February 2000, protons

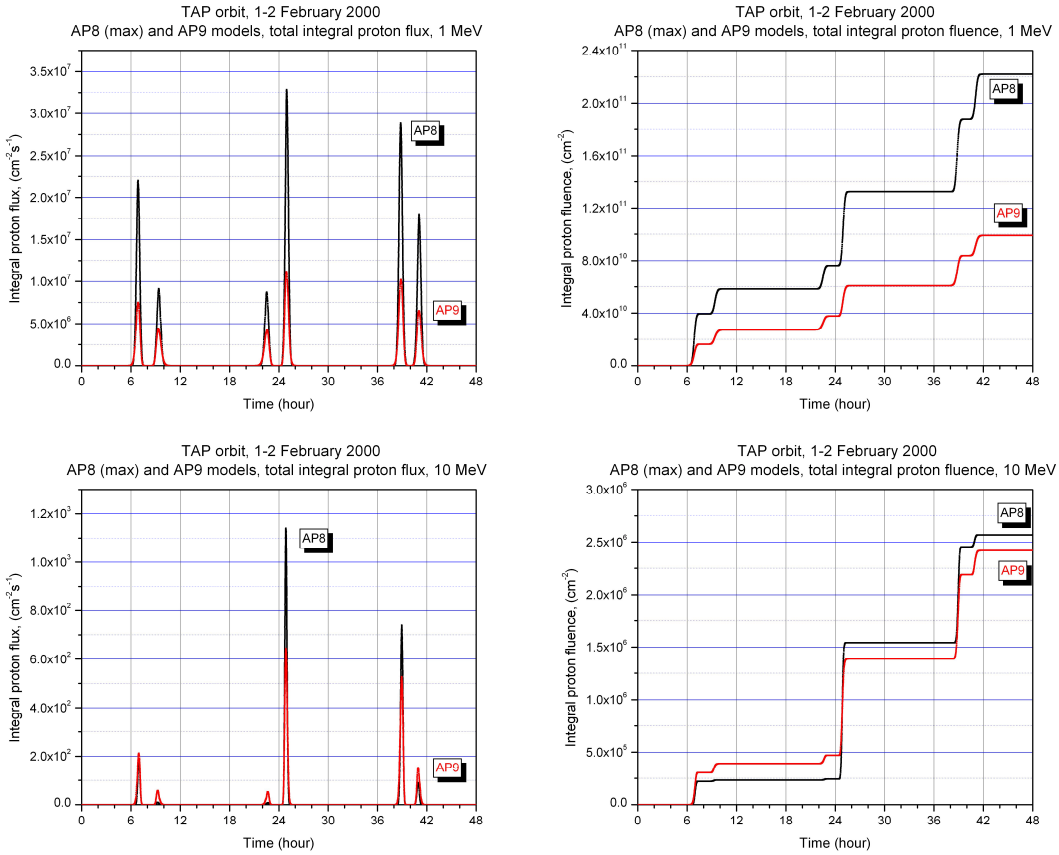

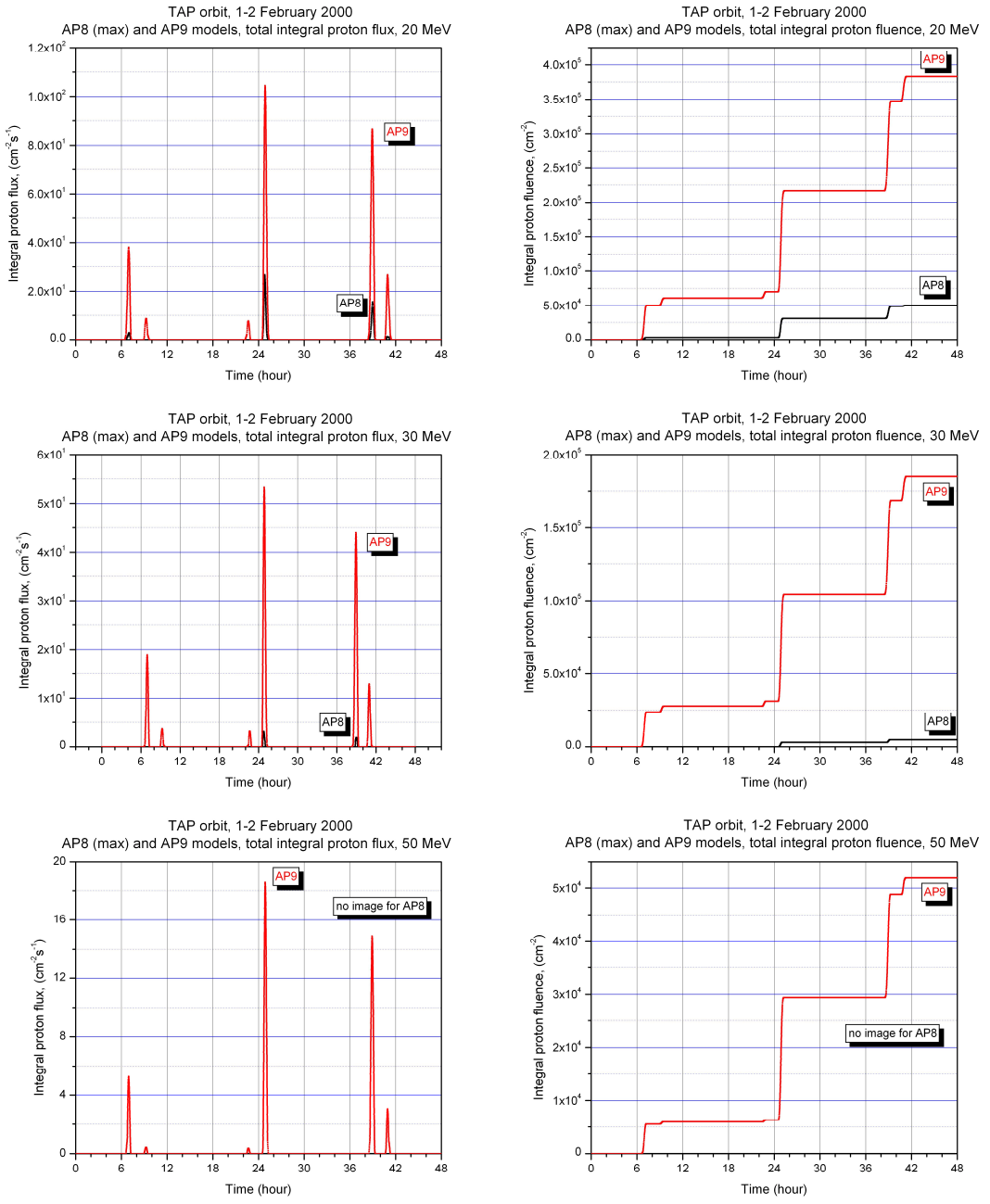

Figure 81. Proton flux variations along TAP orbit and the total integral proton fluence (energy 1MeV, 10MeV, 20 MeV, 50MeV)

Tundra orbit, 1 February 2000, protons

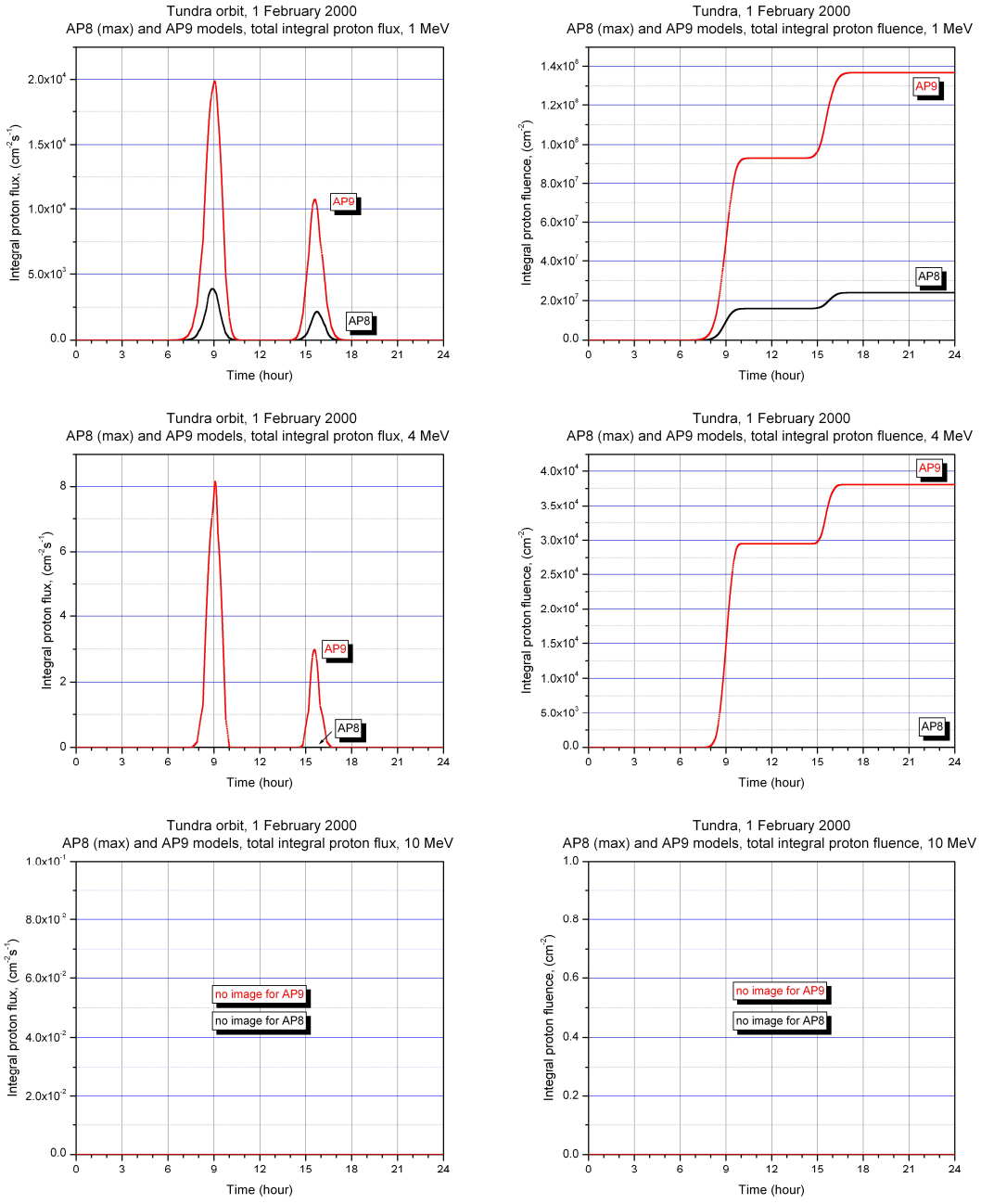

Figure 82. Proton flux variations along Tundra orbit and the total integral proton fluence (energy 1MeV, 4 MeV, 10MeV)

Appendix 3. Annual radiation dose for HEO orbits

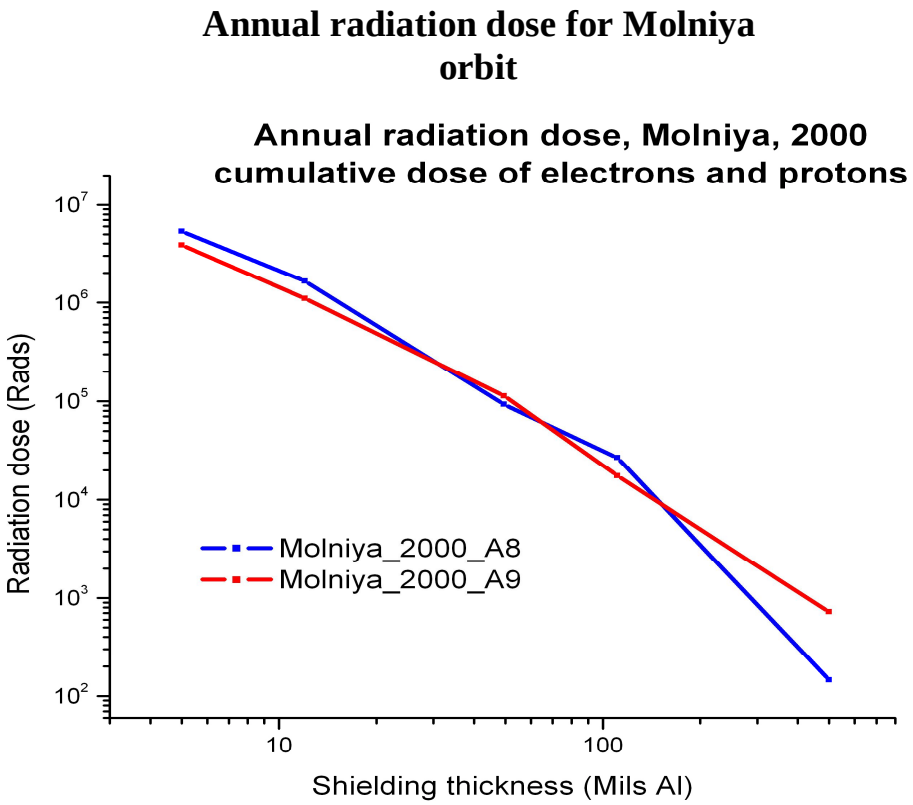

Figure 83. Annual radiation dose for Molniya orbit provided by two models A8 and A9 including both proton and electron radiation. 2000.

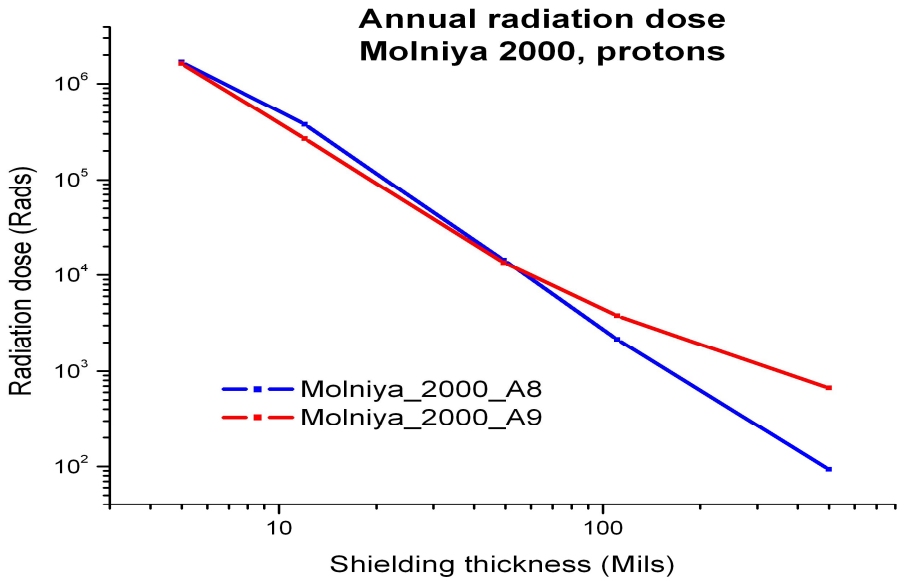

Figure 84. Annual radiation dose for Molniya orbit provided by two models A8 and A9. 2000.

Proton radiation.

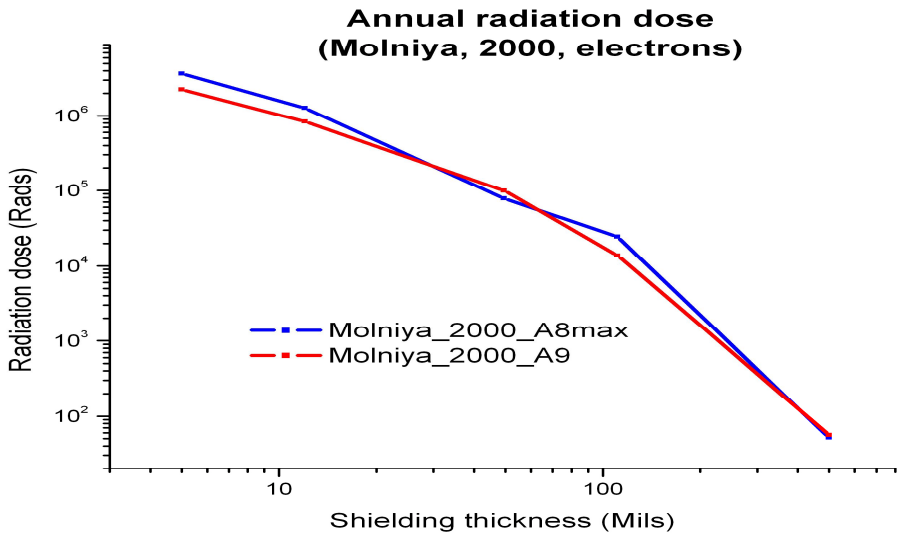

Figure 85. Annual radiation dose for Molniya orbit provided by two models A8 and A9. 2000. Electron radiation.

Annual radiation dose for TAP orbit

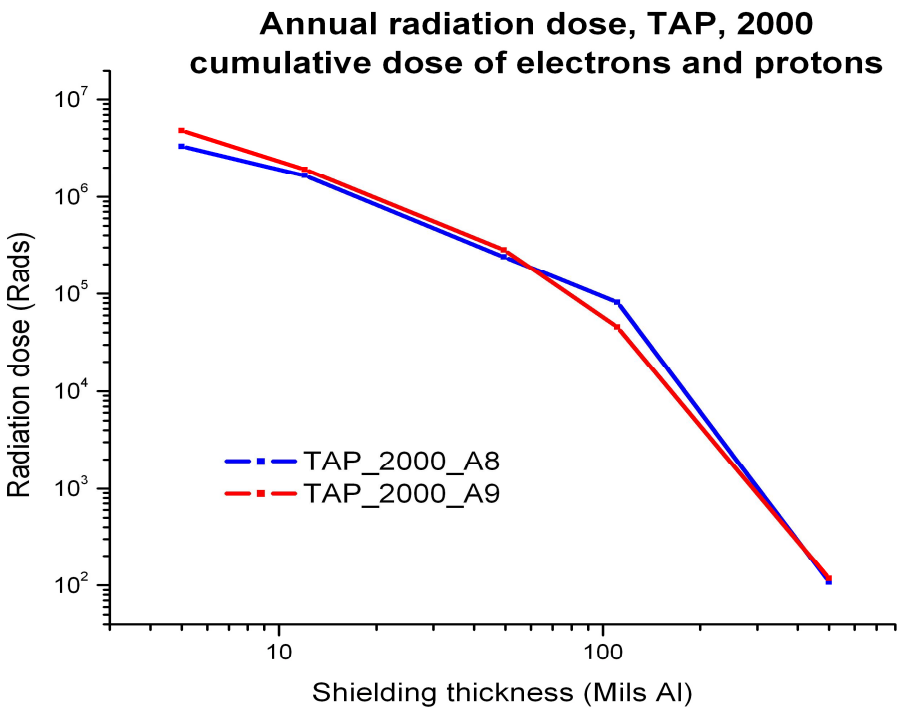

Figure 86. Annual radiation dose for TAP orbit provided by two models A8 and A9 including both proton and electron radiation. 2000.

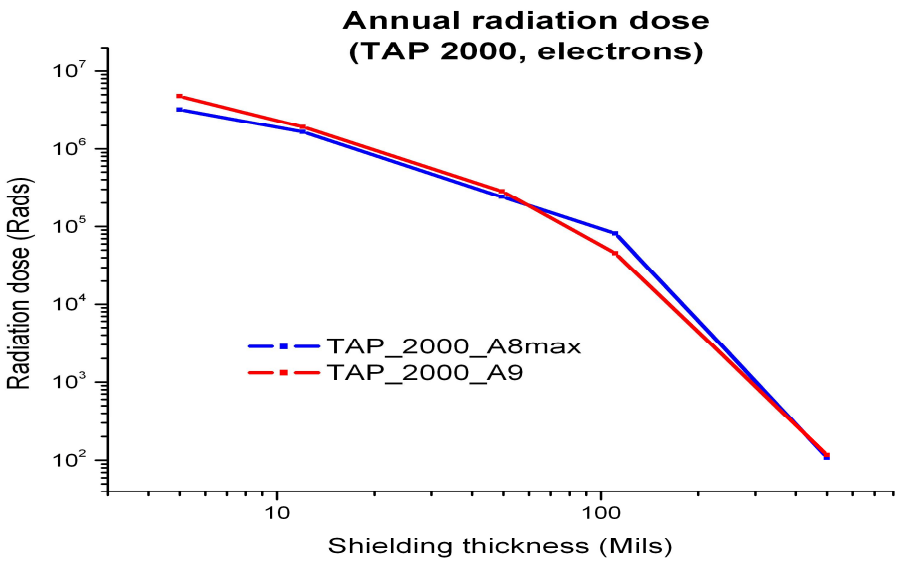

Figure 87. Annual radiation dose for TAP orbit provided by two models A8 and A9. 2000. Electron radiation

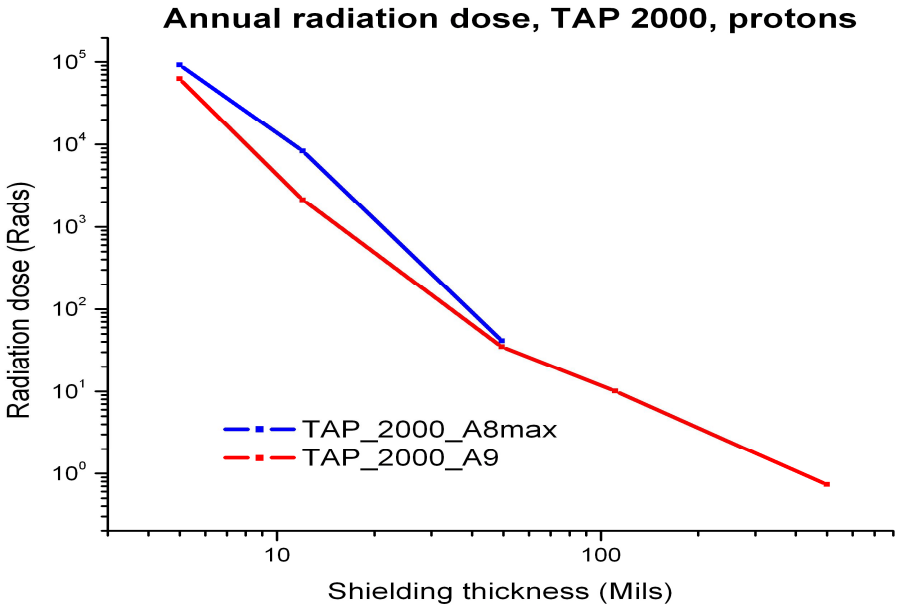

Figure 88. Annual radiation dose for Molniya orbit provided by two models A8 and A9. 2000. Proton radiation

Annual radiation dose for Tundra orbit

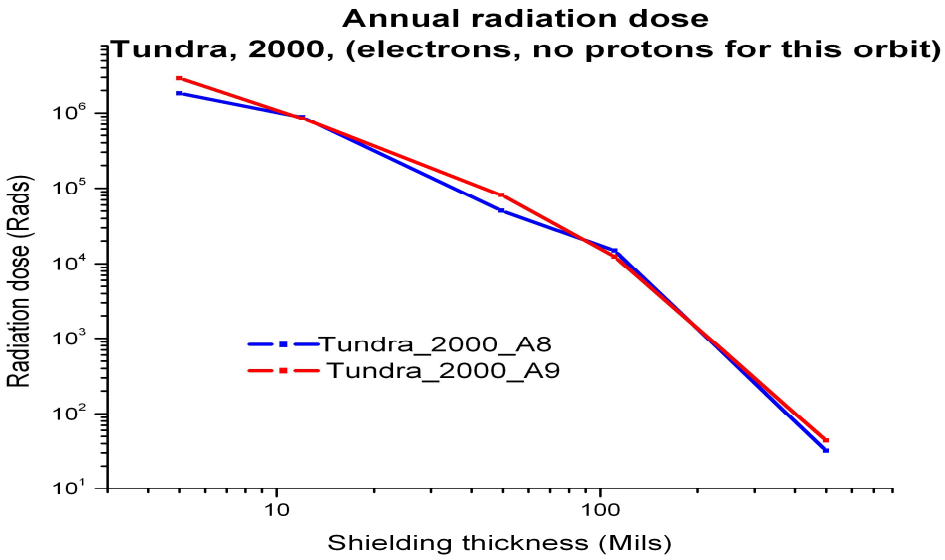

Figure 89. Annual radiation dose for Tundra orbit provided by two models A8 and A9. Electron radiation. 2000.

Appendix 4. Integral solar proton fluences estimated by JPL, King, Rozenqvist and ESP-PSYCHIC models with different magnetic shieldings

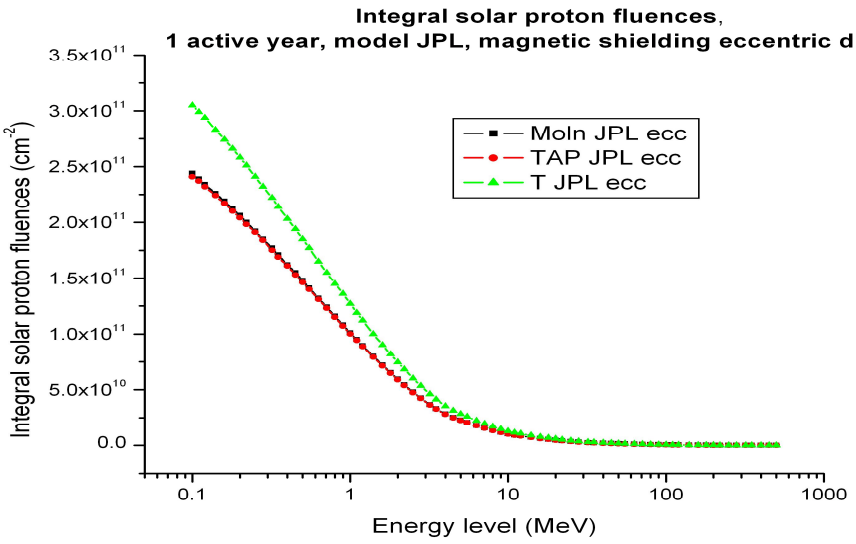

Figure 90. Integral solar proton fluences, 2000, JPL model, magnetic shielding in the form of a Störmer eccentric dipole

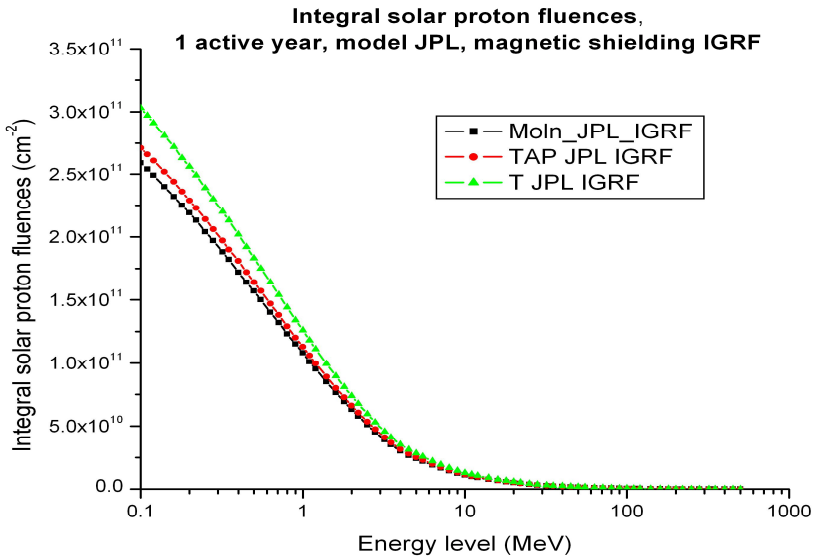

Figure 91. Integral solar proton fluences, 2000, JPL model, magnetic shielding in the form of IGRF model

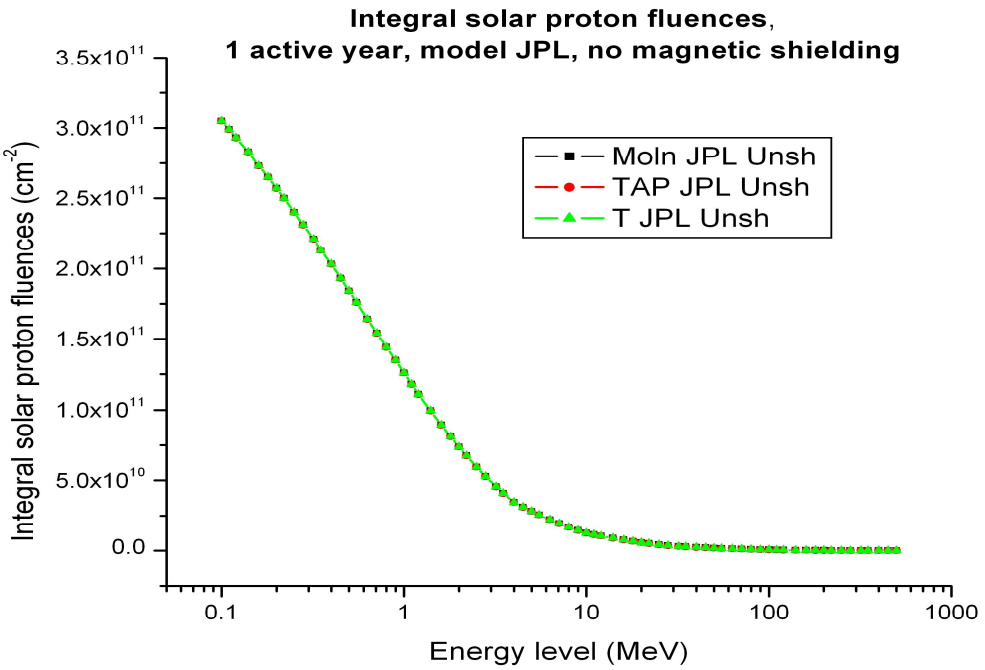

Figure 92. Integral solar proton fluences, 2000, JPL model, no magnetic shielding

King model with different magnetic shieldings

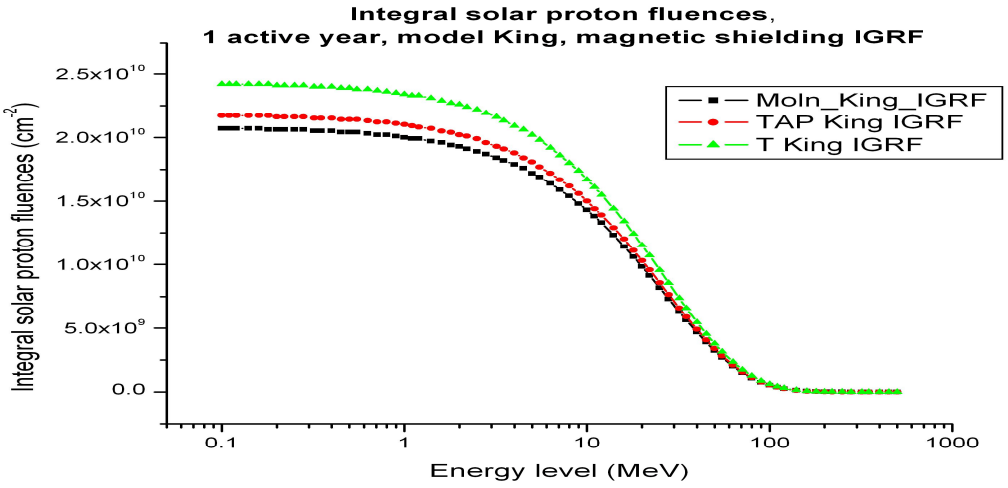

Figure 93. Integral solar proton fluences, 2000, King model, magnetic shielding in the form of IGRF model

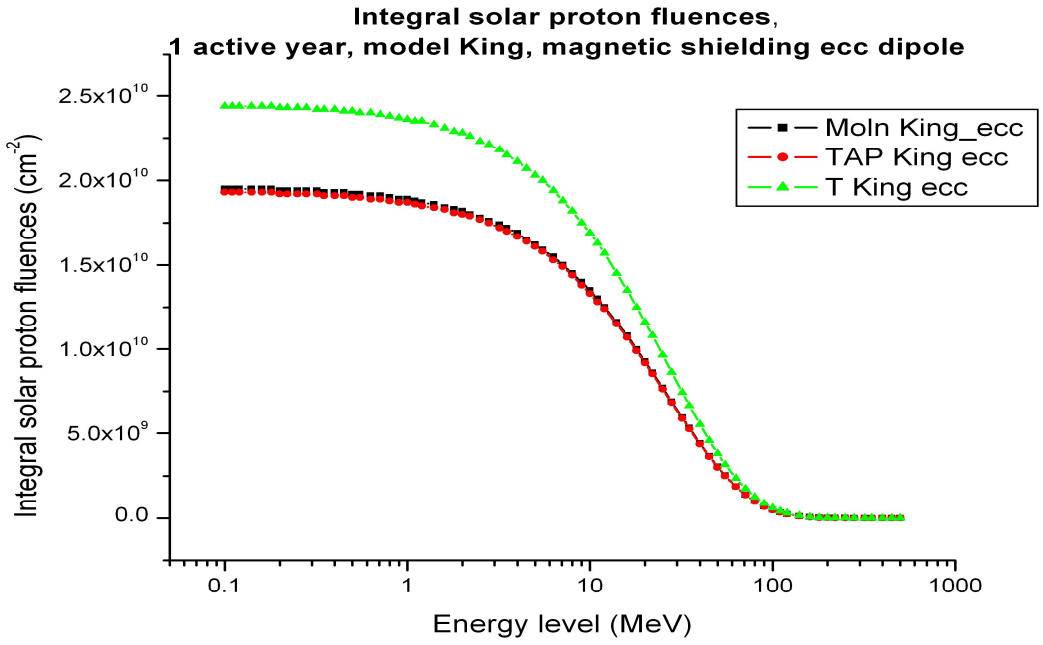

Figure 94. Integral solar proton fluences, 2000, King model, magnetic shielding in the form of a Störmer eccentric dipole

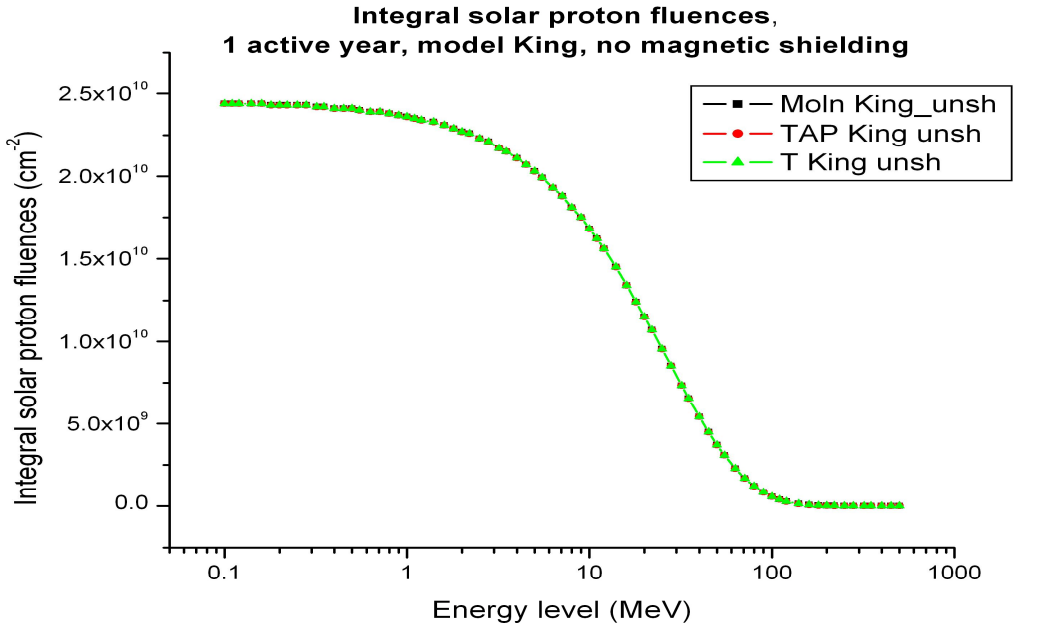

Figure 95. Integral solar proton fluences, 2000, King model, no magnetic shielding

Rozenqvist model with different magnetic shieldings

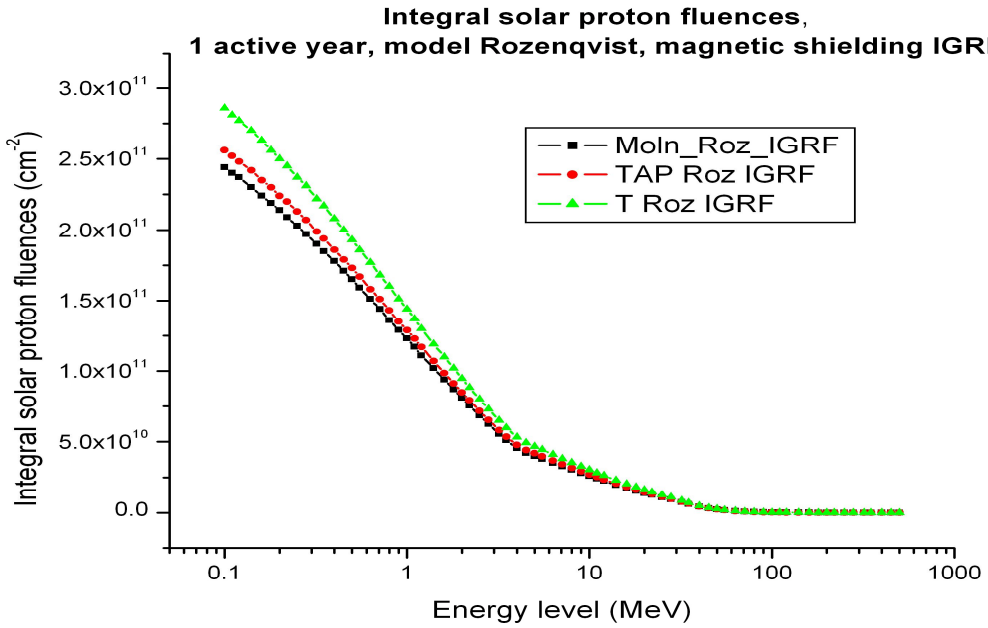

Figure 96. Integral solar proton fluences, 2000, Rozenqvist model, magnetic shielding in the form of IGRF model

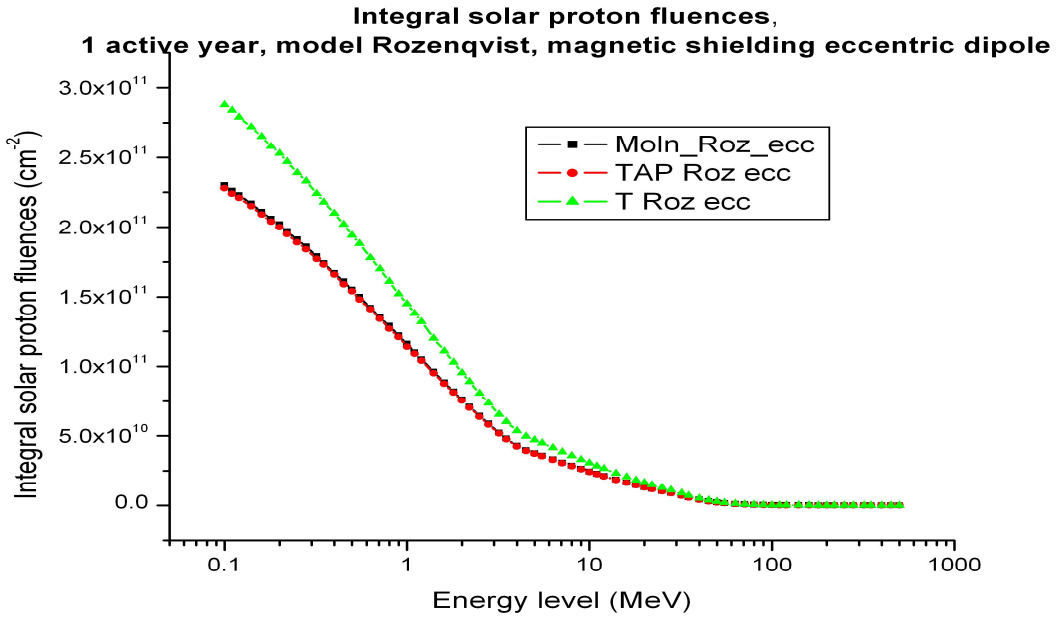

Figure 97. Integral solar proton fluences, 2000, Rozenqvist model, magnetic shielding in the form of a Störmer eccentric dipole

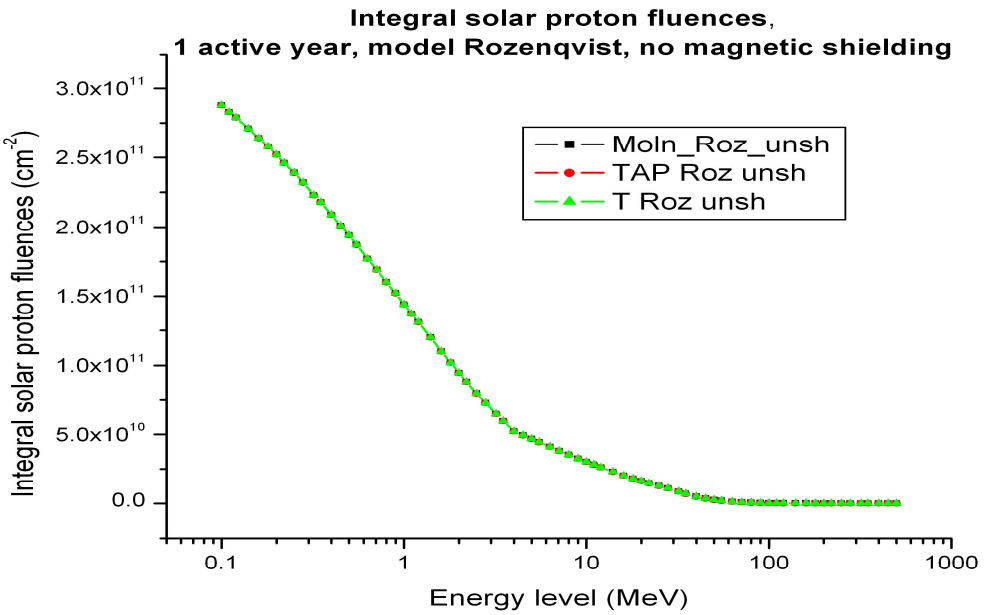

Figure 98. Integral solar proton fluences, 2000, Rozenqvist model, no magnetic shielding

ESP-PSYCHIC model with different magnetic shieldings

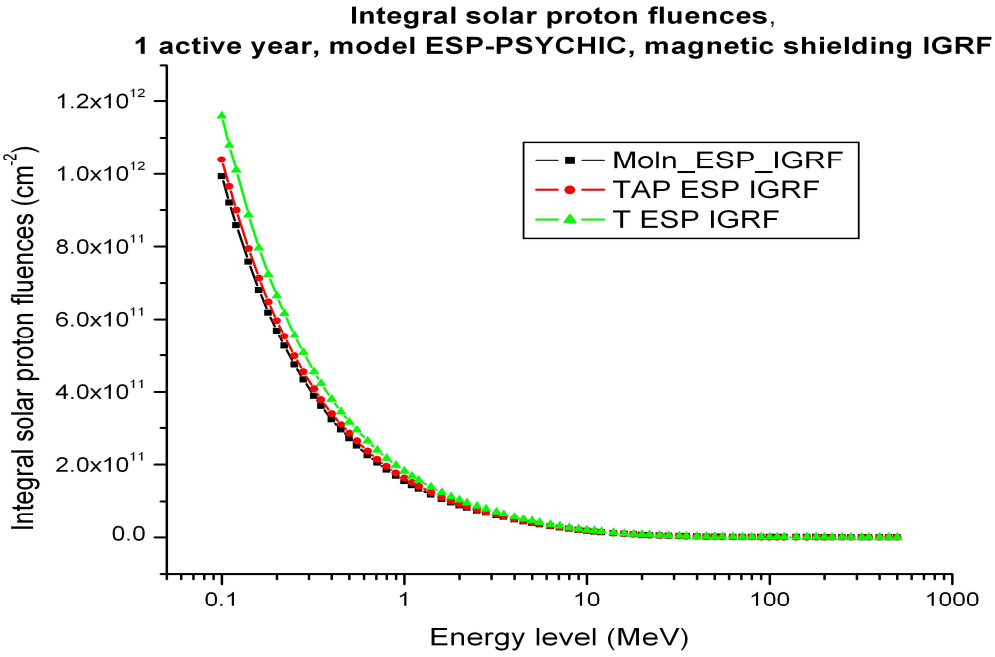

Figure 99. Integral solar proton fluences, 2000, ESP-PSYCHIC model, magnetic shielding in the form of IGRF model

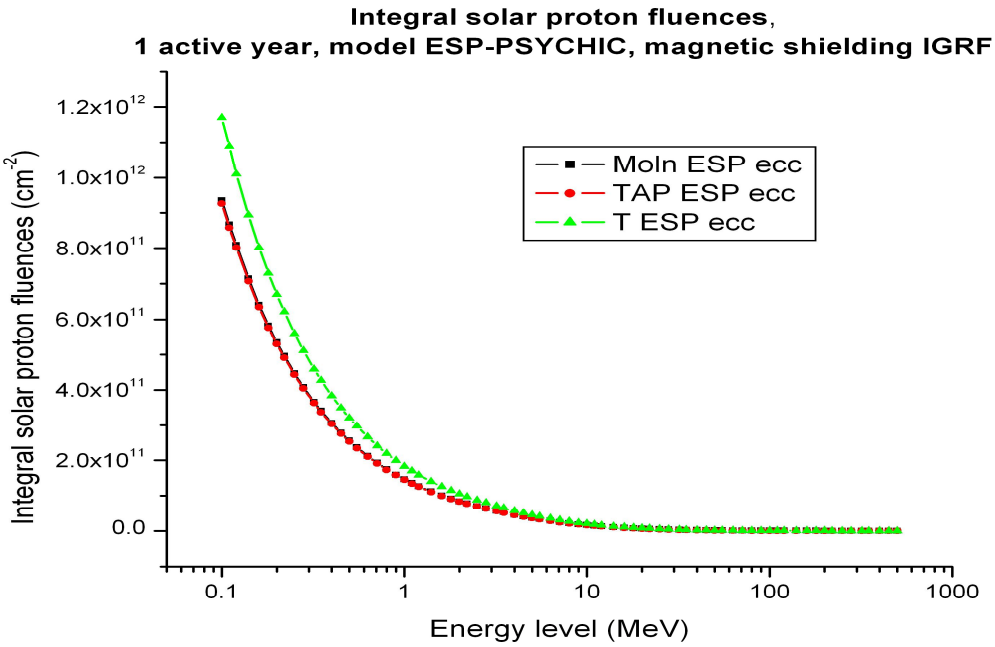

Figure 100. Integral solar proton fluences, 2000, ESP-PSYCHIC model, magnetic shielding in the form of a Störmer eccentric dipole

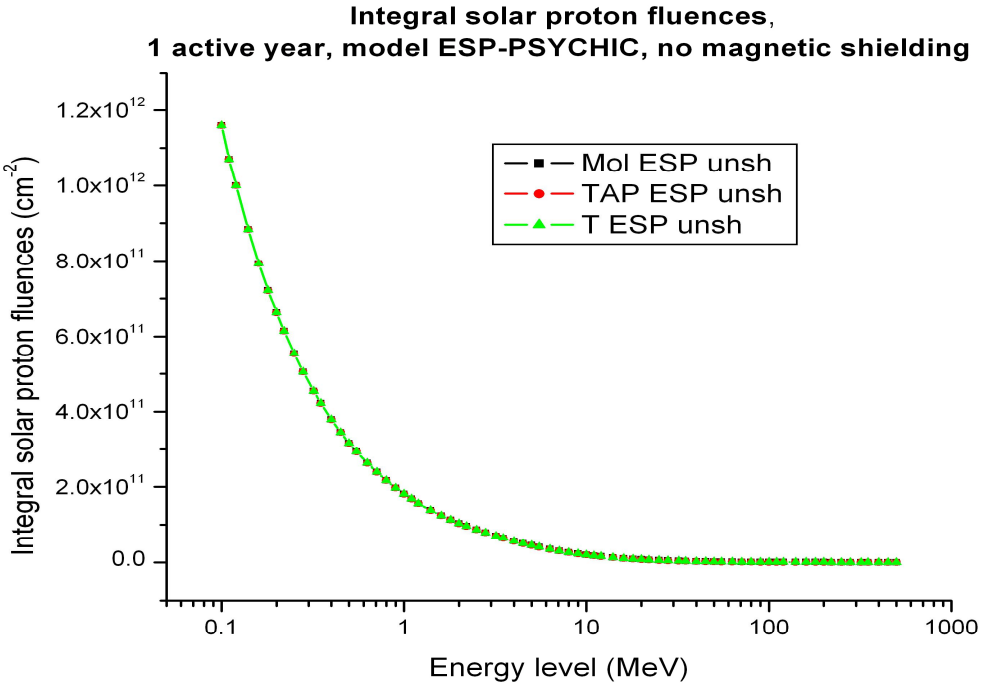

Figure 101. Integral solar proton fluences, 2000, ESP-PSYCHIC model, no magnetic shielding

ESP-PSYCHIC model, worst case scenario, with different magnetic shieldings

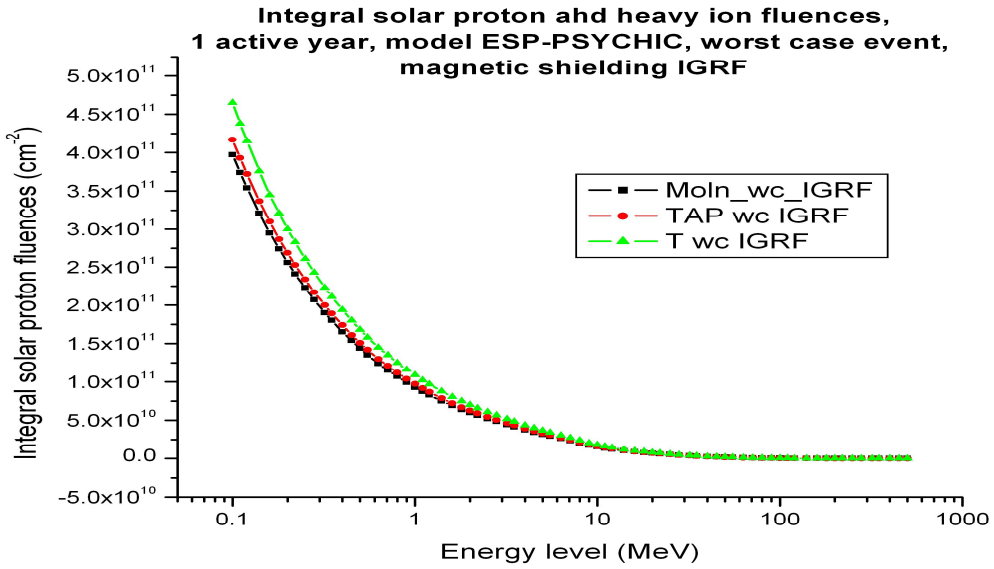

Figure 102. Integral solar proton and heavy ion fluences, 2000, ESP-PSYCHIC model, worst case event, IGRF model for the geomagnetic shielding.

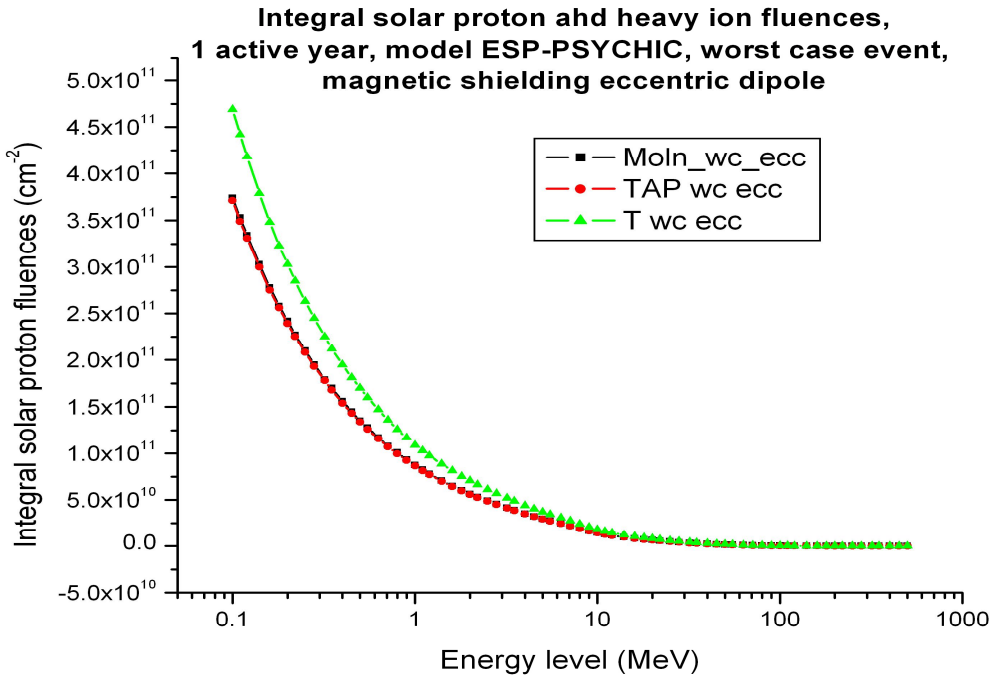

Figure 103. Integral solar proton and heavy ion fluences, 2000, ESP-PSYCHIC model, worst case event, magnetic shielding in the form of a Störmer eccentric dipole.

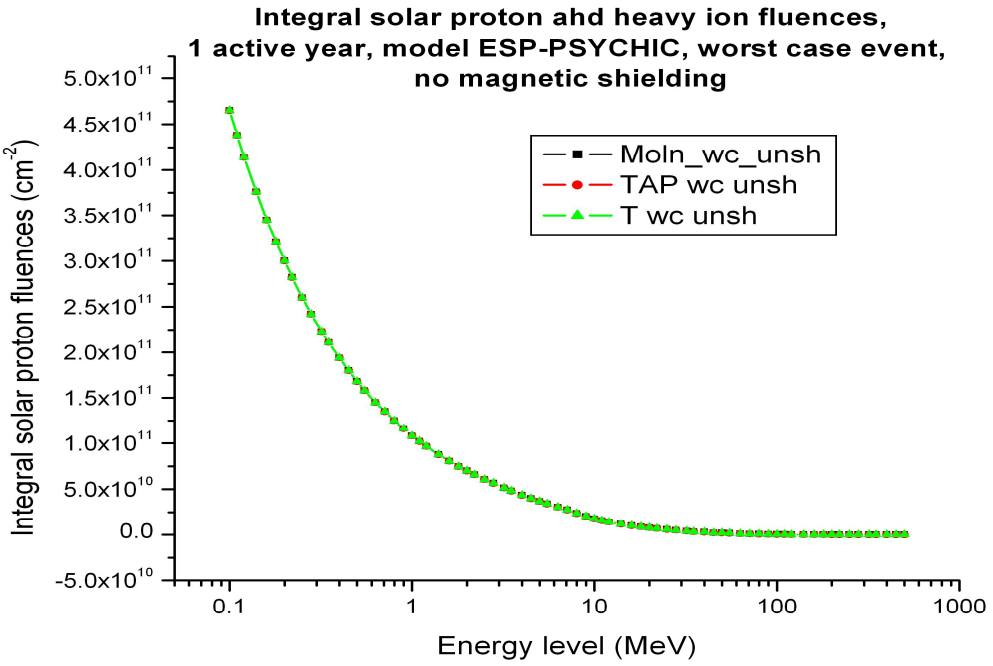

Figure 104. Integral solar proton and heavy ion fluences, 2000, ESP-PSYCHIC model, worst case event, without magnetic shielding.

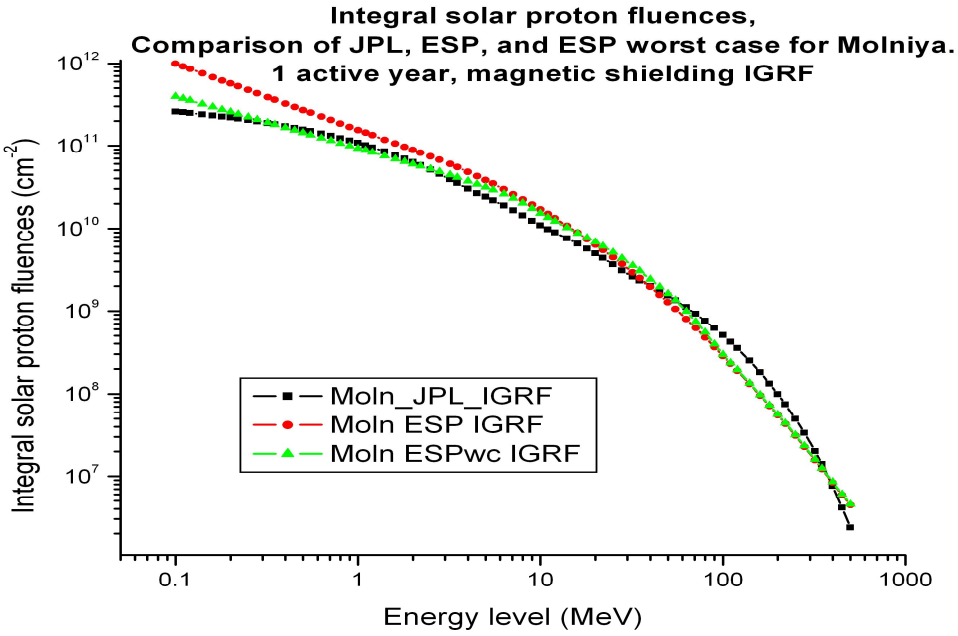

Figure 105. Integral solar proton fluences on Molniya orbit calculated by three models of solar protons